Mechanistic studies of membrane protein biogenesis at the ER and mitochondria

Thesis by

Masami Hazu

In Partial Fulfillment of the Requirements for

the degree of

Doctor of Philosophy

CALIFORNIA INSTITUTE OF TECHNOLOGY

Pasadena, California

2025

Defended December 4, 2024

Masami Hazu
ORCID: 0000-0002-6527-9597

ACKNOWLEDGEMENTS

This thesis is a product of the many people who have helped me get to where I am. I want to acknowledge each and every one of you. This thesis is dedicated to you all.

I would like to first thank my advisor, Rebecca Voorhees. I joined the lab at the height of the pandemic, but even in such times of uncertainty, you welcomed me into your lab. You provided me with a space where I was able to grow as a researcher through your mentorship and guidance. I would also like to thank my committee, Paul Sternberg, Bruce Hay, and Shu-ou Shan for their support and feedback through the years.

I would like to express my deepest gratitude to the members of the Voorhees lab, past and present. I want to start off with thanking those I worked closely with. Tino Pleiner, thank you for being such a great mentor and friend; you taught me everything when I first joined the lab and I am lucky to have been able to work with you. A huge thank you to my EMC subgroup family, Gio Pinton Tomaleri, Kurt Januszyk, and Vy Nguyen, who made working on this project so fun and made it all possible. I also want to thank the MTCH2 subgroup, Taylor Go-Stevens, Erini Galatis, and Alina Guna, for adopting me this past year and a half. I have been lucky to overlap with nearly every person who has stepped foot in the lab. I thank you all for creating a fun working environment: Katie Page, Akshaye Pal, Alison Inglis, Ángel Galvez Merchan, Rob Oania, Maxine Wang, Charlene DeKalb, Natalie Chen, Gina Mawla, Lena Böegeholz, Melanie Ernst, Camryn Lee, Zhilin Luo, Jichen Zhang, Aline Milach Teixeira, and Dina Malounda.

I would like to thank Liz Ayala, Kenya Zeigler, and Lauren Breeyear for all that you do for the division. You are always there to support us with your love and care, and it is truly appreciated.

I have been so lucky to have met so many wonderful people during my time at Caltech. The community I built here has been there to celebrate the good times and support me through the difficult times. To each and every one of you, I thank you from the bottom of my heart. To Maxine Wang, Jonathan Kenny, Kate Radford, Forte Shinko, Victor Garcia, Shawn Yoshida, Cai Ng Tong, Tess Marlin, Maria Derda, Kevin Le, Morgan Foley, and Jolena Zhou, I thank you for your friendship and memories. To quote a special someone you are “the warmest, bravest, kindest, most wonderful human beings I have ever met.”

I would like to thank my family. I would not have come this far in life without the support from you all and I am truly grateful.

Finally, Nathan Hikaru Faialaga, my best friend and life-long partner. There are not enough words to convey how grateful I am to have you in my life. Your unwavering support and love knows no bounds. You credit me for the reason you pursued a PhD. Well, you are the reason that I continued to pursue mine to the end. Thank you.

ABSTRACT

Eukaryotic cells are organized into membrane-enclosed compartments with elaborate networks of integral membrane proteins. From synthesis, localization, and insertion into designated cellular membranes, to proper folding and assembly of the membrane proteins, the successful biogenesis of membrane proteins is crucial for defining the organellar compartments and for overall proteostasis. Recent advances in the field of membrane protein biogenesis in both the endoplasmic reticulum (ER) and the mitochondria have identified novel machineries involved in the membrane insertion step. These are the ER membrane protein complex (EMC) at the ER and the mitochondrial carrier homolog 2 (MTCH2) at the outer mitochondrial membrane (OMM). In this thesis, we employ a combination of biochemical, cell biological, structural, and genetic techniques to explore in mechanistic detail the insertase function of the EMC and MTCH2 at the molecular level. In the first part of the thesis, our work on the EMC maps out the pathway of a tail-anchored (TA) protein through the insertase and revealed a selectivity filter that provides the biochemical basis for how the EMC protects compartment integrity. The selectivity filter of the EMC limits TA protein mislocalization and prevents topological errors of multi-pass membrane proteins. In the second part, ongoing work on MTCH2 reveals the absence of a prominent selectivity mechanism and provides insight into a regulatory mechanism of MTCH2, which seems to be conserved across metazoan MTCH2 homologs.

PUBLISHED CONTENT AND CONTRIBUTIONS

Chapter 2:

Pleiner, T.*, **Hazu, M.***, Tomaleri, G.P.*, Nguyen, V.N., Januszyk K., Voorhees, R.M. (2023) "A selectivity filter in the ER membrane protein complex limits protein misinsertion at the ER" Journal of Cell Biology, 222(8); doi: 10.1083/jcb.202212007

* denotes equal contribution

Contributions: M.H. participated in the conceptual design of the project, performed experiments and data analysis, and helped assemble the manuscript. Specific experimental contributions include *in vitro* biochemistry assays, in cell reporter assays, and crosslinking assays.

Chapter 3:

Hazu, M., Guna, A., Stevens, T.A., Voorhees, R.M., (2024) “Monitoring alpha-helical membrane protein insertion into the outer mitochondrial membrane in mammalian cells” Methods in Enzymology, 707, 63-99; doi: 10.1016/bs.mie.2024.07.054

Contributions: M.H. prepared the figures and wrote the manuscript.

Other contributions:

Pleiner, T.*, Pinton Tomaleri, G.*, Januszyk, K.*, Inglis, A.J., **Hazu, M.**, Voorhees, R.M. (2020) "Structural basis for membrane insertion by the human ER membrane protein complex" Science, 369(6502); 433-436. doi: 10.1126/science.abb5008.

* denotes equal contribution

Contributions: M.H. performed experiments, analyzed data, and helped edit the manuscript. Specific experimental contributions include *in vitro* photocrosslinking assay.

Pleiner, T., **Hazu, M.**, Tomaleri, G.P., Januszyk, K., Oania, R.S., Sweredoski, M.J., Moradian, A., Guna, A., Voorhees, R.M. (2021) "WNK1 is an assembly factor for the human ER membrane protein complex." Molecular Cell, 81(13): 2693-2704.e12.; doi: 10.1016/j.molcel.2021.04.013

Contributions: M.H. performed experiments, analyzed data, and helped edit and revise the manuscript. Specific experimental contributions include expression and purification of proteins for *in vitro* assays, *in vitro* photocrosslinking assay, and radioactive pulse-chase assay.

Guna, A., **Hazu, M.**, Tomaleri, G.P., Voorhees, R.M. (2022) "A TAle of Two Pathways: Tail-Anchored Protein Insertion at the Endoplasmic Reticulum" Cold Spring Harbor Perspectives in Biology; doi: 10.1101/cshperspect.a041252

Contributions: M.H. prepared the figures, and helped edit and revise the manuscript.

Stevens, T.A., Tomaleri, G.P., **Hazu, M.**, Wei, S., Nguyen, V.N., DeKalb, C., Voorhees, R.M., Pleiner, T. (2024) "A nanobody-based strategy for rapid and scalable purification of native human protein complexes" Nature Protocols, 19, 127-158; doi: 10.1038/s41596-023-00904-w

Contributions: M.H. performed experiments. Specific experimental contribution include establishing and optimizing the nanobody expression and purification protocol.

Page, K.R., Nguyen, V.N., Pleiner, T., Tomaleri, G.P., Wang, M.L., Guna, A., **Hazu, M.**, Wang, T., Chou, T., Voorhees, R.M., (2024) "Role of a holo-insertase complex in the biogenesis of biophysically diverse ER membrane proteins" Molecular Cell 84(17): 3302-3319.e11; https://doi.org/10.1016/j.molcel.2024.08.005

Contributions: M.H. participated in the design, analysis, and interpretation of the photocrosslinking assays.

TABLE OF CONTENTS

LIST OF ILLUSTRATIONS AND/OR TABLES

Page

Chapter 1

INTRODUCTION

1.1 Overview

Eukaryotic cells are organized into many distinct subcellular compartments, each with a unique biochemical environment and dedicated machinery to carry out its specialized function within the cell. The evolution of discrete and functionalized compartments led to complex and interdependent but mutually cooperative environments (Sommer & Schleiff, 2014) that led to the emergence of the multicellular organism. The increasing complexity of cellular organization provided enormous benefits but introduced a new challenge, as proteins now needed to localize to their respective subcellular compartments. This necessitated the development of highly selective targeting mechanisms, and the translocation of proteins into or across cellular membranes. One key class of protein that relies on their accurate sorting to carry out their functions is membrane proteins.

Membrane proteins comprise approximately one quarter of the eukaryotic proteome and are essential in a range of functions including intracellular trafficking, signal transduction, and neuronal signaling (Wallin & Von Heijne, 1995; Boyd et al., 1998; Krogh et al., 2001). Consequently, defects in membrane protein biogenesis and quality control underlie a myriad of human diseases (Sanders & Myers, 2004; Ng et al., 2012; Marinko et al., 2019), and more than half of all current therapeutic drugs target a membrane protein (Overington et al., 2006; Rask-Andersen et al., 2014). Considering the essential role these proteins play and the consequence of their failed biogenesis, understanding the general principles of their biogenesis is physiologically important and has overarching implications across many fields.

Integral membrane proteins are characterized by the presence of at least one hydrophobic transmembrane domain (TMD) which must be recognized, targeted, and inserted into the hydrophobic lipid bilayer of the correct subcellular compartment and in the correct orientation. There are about 5000 integral membrane proteins predicted in the human proteome (Dobson et al., 2015) and they have highly diverse characteristics, from the number of TMDs they contain, to the topological orientation across the bilayer, and to the biophysical properties within the TMDs (von Heijne, 2007). The hydrophobic TMDs of integral membrane proteins pose a significant challenge as

all membrane proteins throughout the cell are initially synthesized on ribosomes in the aqueous environment of the cytosol where they are prone to aggregation. The TMDs must, therefore, be shielded by specialized factors and this requires the efficient recognition, targeting, and insertion of the TMDs into the lipid bilayer (Keenan et al., 2001; Shao & Hegde, 2011a; Borgese & Fasana, 2011). These steps are crucial to preventing non-productive interactions of TMDs that could lead to aggregation before they reach their correct subcellular compartment for protein folding and assembly into multi-subunit complexes (Shao & Hegde, 2011b; Cymer et al., 2015; Juszkiewicz & Hegde, 2018). An additional challenge is the accurate sorting of integral membrane proteins from their site of synthesis in the cytosol, to their specific destination which can occur co- or post-translationally (Shan & Walter, 2005; Guna, et al., 2023; Vögtle et al., 2009; Jores et al., 2016). Failure in any step of the biogenesis pathway or mislocalization to the wrong compartment can lead to cellular stress, requiring a host of quality control pathways to maintain cellular homeostasis (Meusser et al., 2005; Hegde & Ploegh, 2010).

1.2 Membrane protein biogenesis at the ER

The endoplasmic reticulum (ER) is the largest site of membrane protein synthesis in the cell. Approximately one third of the human proteome matures at the ER, including membrane proteins and secretory proteins. The membrane proteins at the ER are a diverse group of proteins which are targeted to the ER via one of two principal mechanisms; the co-translational targeting directly into the membrane or the post-translational targeting of pre-made proteins. Co-translationally targeted membrane proteins vary in the number and topology of their TMDs. Single-pass (containing a single TMD) and multi-pass (containing two or more TMDs) membrane proteins are further categorized based on the presence of a signal peptide and their topology in the membrane. Type I membrane proteins contain a cleavable signal peptide and adopt the N_{exo} topology, where the N-termini is translocated across into the ER lumen and may localize to the extracellular matrix of a cell. Type II membrane proteins do not contain a signal peptide and adopt the N_{cyt} topology, where the N-termini is localized to the cytosol. And finally, Type III membrane proteins also lack a classical signal peptide but adopt the N_{exo} topology. The Type II and III membrane proteins are also referred to as signal-anchored (SA) proteins as their first and/or only TMD is sufficient for recognition for ER targeting (Hartmann et al., 1989; Wallin & von Heijne, 1995; The UniProt Consortium, 2017). For multi-pass membrane proteins subsequent TMD topology is influenced by the topology of the first TMD. In contrast, the tail-anchored (TA) proteins are characterized by a single TMD followed by a short

soluble C-terminal domain of up to 30-40 amino acids that is translocated across the ER membrane. This topology necessitates a post-translational targeting as the TMD only emerges from the ribosomal exit tunnel after translation is terminated and the nascent chain is released (Kutay et al, 1993; Guna et al., 2023).

A single mechanism alone is insufficient to address the complexities of recognition, targeting, and insertion of such a diverse array of membrane proteins at the ER. Over decades, several membrane protein biogenesis pathways at the ER have been described (Hegde & Keenan, 2022). Of these pathways, perhaps the most well studied is the signal recognition particle (SRP)-dependent recognition and co-translational delivery to the ER membrane for subsequent insertion by the Sec61 translocon (Shao & Hegde, 2011b). In this pathway, the universally conserved SRP recognizes nascent TMDs of membrane proteins as they emerge from the ribosome, shielding them from the aqueous cytosolic environment (Halic & Beckmann, 2005; Shan & Walter, 2005). The SRP also recognizes the cleavable signal peptide of nascent polypeptide chains (Walter & Blobel, 1981; Walter et al. 1981). SRP then directs the ribosome-nascent chain (RNC) complex to the ER membrane by binding to the SRP receptor (SR) (Connelly & Gilmore 1993; Akopian et al., 2013), where it is delivered to the Sec61 translocation channel. The Sec61 translocon is formed from three subunits, Sec61α, Sec61β, and Sec61γ, that create a protein-conducting channel. The Sec61α subunit forms the aqueous central pore through which the soluble domains can translocate across into the ER lumen and the TMDs can insert into the lipid bilayer via the lateral gate of Sec61 (Van den Berg et al., 2004; Rapoport et al., 2017; Park & Rapoport, 2012).

For decades, the above was the gold standard of membrane protein insertion into the ER and it was believed that most membrane proteins were inserted through this pathway. However, not all TMDs are hydrophobic enough to trigger the Sec61 lateral gate opening (Enquist et al., 2009), and consequently directed studies towards identifying and characterizing additional protein machinery that may be involved at the ER. A recent study defined a group of membrane proteins as the Oxa1 superfamily, which includes the bacterial YidC insertase, the archael Ylp1 proteins, and three ER resident proteins; GET1, EMC3, and TMCO1 (Anghel et al., 2017). Members of the superfamily are functional insertases (Kumazaki et al., 2014; Borowska et al., 2015; Pleiner et al., 2020; McGilvray et al., 2020; McDowell et al., 2020), which catalyze the insertion of membrane proteins into the lipid bilayer, and play key roles in membrane protein biogenesis. A major focus of recent research has

been to understand how these insertases work in concert with other ER biogenesis machinery, such as Sec61, to mediate the proper topogenesis, folding, and assembly of membrane proteins.

Recent studies have revealed the existence of a number of "super-complexes" that dynamically interact with one another to facilitate the biogenesis of multi-pass membrane proteins at the ER (McGilvray et al., 2020; Page et al., 2024). The multi-pass translocon (MPT) comprised of the Sec61 translocon, the PAT complex, the BOS complex, and the GEL complex, function co-translationally during the biogenesis of multi-pass membrane proteins (McGilvray et al., 2020). The ER membrane protein complex (EMC) has also been reported to be involved in multi-pass membrane protein biogenesis (Chitwood et al., 2018), and recently been demonstrated to directly interact with the BOS complex and form the EMC-BOS holo-insertase complex. The EMC-BOS holocomplex facilitates insertion of the first TMD of multi-pass membrane proteins or hands over those the EMC cannot insert to the GEL (TMCO1 is a subunit) or Sec61 complexes for insertion, after which the MPT takes over in inserting the remaining TMDs (Page et al., 2024).

These new findings have furthered our understanding surrounding the general principles of co-translational membrane protein biogenesis and highlights the complexity of coordinated biogenesis pathways. However, for the aforementioned TA proteins that require post-translational targeting, alternative pathways are required for their targeting and insertion into the ER membrane.

1.3 TA protein biogenesis at the ER and the EMC

TA proteins are found in all cellular membranes and regulate essential processes such as vesicular transport (SNARE proteins), cholesterol homeostasis at the ER (squalene synthase; SQS), and apoptosis at the mitochondria (BCL-2, Bak). At the ER, TA proteins are primarily inserted through two pathways: (1) the guided entry of TA proteins (GET) pathway that utilizes the GET1/2 complex for insertion at the membrane, and (2) the ER membrane protein complex (EMC) that inserts a subset of ER-destined TA proteins.

The GET pathway is a highly coordinated insertion pathway mediated by several cytosolic proteins and the GET1/2 complex at the ER membrane. In mammalian cells it begins with the cytosolic chaperone SGTA, which recognizes and captures the TMD of the TA protein as it is released from the ribosome. The TA protein is transferred from SGTA onto the ATPase GET3 (formerly TRC40) through the coordinated interactions of the factors GET5 (formerly TRC35), Bag6, and GET4

(formerly UBL4A). The TA protein loaded GET3 is then targeted to the ER membrane where it binds to the GET1/2 complex. Binding to GET1/2 dislodges the TA protein from GET3, releasing it for insertion into the lipid bilayer through the GET1/2 insertase. GET3 is recycled back into the cytosol to initiate the following round of TA protein trafficking to the ER membrane (Shao & Hegde, 2011b; Stefanovic & Hegde, 2007; Schuldiner et al., 2008; McDowell et al., 2020).

The second pathway of TA protein insertion at the ER utilizes the EMC as an insertase. Studies have reported that TA proteins with relatively low hydrophobicity TMDs cannot bind the GET3 chaperone well. Instead, these TA proteins are targeted to the ER by the chaperone calmodulin (CaM) and inserted into the lipid bilayer by the EMC (Shao & Hegde, 2011a; Guna et al., 2018). However, how the CaM bound TA protein is targeted to and handed off to the EMC is unclear, much less the precise molecular mechanism of how the EMC inserts the TMD into the lipid bilayer.

The EMC is a widely conserved, highly abundant complex in all eukaryotes that plays a crucial role in the biogenesis of a diverse set of eukaryotic membrane proteins (Wideman, 2015; Chitwood & Hegde, 2019; Volkmar & Christianson, 2020). First identified in a yeast genetic screen for protein folding factors in the ER (Jonikas et al., 2009), the EMC is essential in all multi-cellular organisms and mutations in humans are linked to severe developmental disorders (Harel et al., 2016; Geetha et al., 2017; Shao et al., 2021). The mammalian EMC was identified as a 9-subunit complex with 7 integral membrane subunits and 2 soluble subunits. The subunits are numbered EMC1-10, where EMC8 and 9 are functional paralogs and a single EMC complex will only have one or the other (Christianson et al., 2012; Wideman, 2015).

After the initial discovery the biochemical function of the EMC was unknown; however, it had been implicated in membrane protein homeostasis due to its epistatic relationships and demonstrated to be involved in membrane protein biogenesis (Bircham et al., 2011; Richard et al., 2013; Satoh et al., 2015; Lahiri et al., 2014; Shurtleff et al., 2018). Only recently has the EMC been demonstrated to function as an insertase for both co- and post-translationally targeted membrane proteins including low-to-moderate hydrophobicity TMD containing TA proteins (Guna et al., 2018,), as well as the first TMD of N_{exo} multi-pass membrane proteins (Chitwood et al., 2018).

It was crucial to obtain a structure of the EMC to be able to dissect the molecular mechanism of its insertase activity. Biochemical studies have demonstrated that the EMC must be assembled with the correct stoichiometry of the nine subunits, as loss of a single “core” subunit (EMC 1, 2, 3, 5, 6) will

result in the degradation of the entire complex (Volkmar et al., 2019). Several structures of the yeast and human EMC were solved in the past few years, including one from our lab (Pleiner et al., 2020; Bai et al., 2020; O'Donnell et al., 2020; Miller-Vedam et al., 2020). The series of structures and accompanying mutagenesis experiments were crucial for proposing explanations of known function but provided surprisingly few new insights into the mechanism.

Given the central role the EMC plays in the biogenesis of a host of membrane proteins, understanding the mechanism of its function is a key area of focus. With the structures of the EMC now in hand, it is possible to carefully dissect the EMC biochemically to uncover the molecular mechanism. Additionally, as a member of the Oxa1 superfamily of insertases, the mechanistic studies of the EMC will further define the general principles of membrane protein biogenesis across all domains of life.

1.4 Membrane protein biogenesis at the mitochondria

The mitochondria are eukaryotic organelles of bacterial ancestry (Roger et al., 2017) and therefore face significantly different challenges to membrane protein biogenesis compared to at the ER. Mitochondria have kept their bacterial predecessor's morphology and contain two membranes, the outer mitochondrial membrane (OMM) and the inner mitochondrial membrane (IMM), which enclose the intermembrane space (IMS) and the mitochondrial matrix respectively. While the mitochondria have retained part of their own genome, only 13 genes in the mitochondrial genome encode for proteins found in the electron transport chain. The vast majority of mitochondrial proteins are nuclear encoded, requiring translation on cytosolic ribosomes, and subsequent targeting and import into the mitochondria (Busch et al., 2023; Pfanner et al., 2019).

Similar to membrane proteins at the ER, membrane proteins in the OMM and IMM are diverse in nature and can be both co- and post-translationally targeted to the mitochondria. However, unique to the mitochondria is the classification of two types of membrane proteins: the β-barrel proteins and the α-helical proteins. The mitochondrial β-barrel proteins are a remnant of the bacterial ancestor and are only found in the OMM, whilst the α-helical membrane proteins are present in both the OMM and IMM. β-barrel proteins are a circular porous structure enclosed by β-sheets with hydrophobic residues facing the lipid bilayer on the outside and hydrophilic residues facing the interior of the pore. α-helical membrane proteins are characterized by the presence of one (single-pass) or more (multi-pass) TMDs embedded into the lipid bilayer. Single spanning α-helical membrane proteins can be categorized into three types based on the position of the TMD: i) signal-anchored (SA) proteins

contain a TMD at their N-terminus with the short N-terminal soluble domain crossing the lipid bilayer, ii) TA proteins with a TMD at the C-terminus followed by a small domain that must be translocated, and iii) membrane proteins with the TMD acting as an internal membrane anchor.

The vast diversity of membrane proteins in the mitochondria resulting from differences in the genome of expression (nuclear vs mitochondrial), site of translation (cytosolic vs mitochondrial matrix ribosomes), and the type of membrane protein (β-barrel vs α-helical proteins) have necessitated a variety of protein targeting and insertion pathways into the mitochondrial membranes. The small number of membrane proteins encoded in the mitochondrial genome are inserted into the IMM by the Oxa1 insertase, a member of the Oxa1 superfamily of insertases (Ott & Hermann, 2010). For nuclear encoded mitochondrial proteins, about 60-70% carry a cleavable N-terminal presequence (Vögtle et al., 2009). The presequence, an amphipathic helix enriched with positively charged residues, is recognized by the translocase of the outer membrane (TOM) complex which translocates the protein across the OMM and hands them off to the presequence translocase of the inner membrane (TIM23) (Abe et al., 2000; Gomkale et al., 2021; Busch et al., 2023). IMM membrane proteins with a presequence are either laterally released into the lipid bilayer directly by the TIM23 complex or are imported into the matrix followed by export back into the IMM through Oxa1 (Bohnert et al., 2010; Stiller et al., 2016). Not all IMM membrane proteins carry a presequence; some instead contain several internal targeting elements that are again recognized by the TOM complex and translocated across the OMM (Diekert et al., 1999). This is then followed by transfer to the carrier translocase of the inner membrane (TIM22) which mediates their insertion into the IMM (Sirrenberg et al., 1996; Rehling et al., 2003).

For membrane proteins in the OMM, the two fundamentally different types of membrane proteins, the β-barrel and the α-helical proteins, require different machineries and mechanisms for their biogenesis. β-barrel proteins are conserved from the mitochondria's bacterial ancestor and so is part of their biogenesis machinery. Conserved from the bacterial β-barrel assembly machinery, the sorting and assembly machinery (SAM) complex inserts β-barrel proteins into the OMM, following translocation into the IMS via the TOM complex (Busch et al., 2023, Dukanovic & Rapaport, 2011, Höhr et al., 2015, Kutik et al., 2008, Takeda et al., 2021). On the other hand, α-helical membrane proteins typically bypass the TOM complex and employ distinct machineries for their biogenesis into the OMM.

More than 90% of the OMM proteome, roughly 100 integral membrane proteins, are α-helical membrane proteins (Rath et al., 2021). Recent studies have identified distinct protein machineries involved in α-helical membrane protein biogenesis in different organisms: the mitochondrial import (MIM) complex in fungi, the peripheral archaic translocase of the outer membrane 36 (pATOM36) in trypanosomes, and the mitochondrial carrier homolog 2 (MTCH2) in mammals (Becker et al., 2011; Doan et al., 2020; Vitali et al., 2018; Guna et al., 2022). The first to be identified and characterized was the MIM complex in fungi composed from the subunits Mim1 and Mim2. The MIM complex was found to be required for the biogenesis of both multi-pass and single-pass α-helical membrane proteins in the OMM. The MIM complex can facilitate the biogenesis of membrane proteins as a free complex or through transient interactions with the TOM and SAM complexes (Becker et al., 2008; Becker et al., 2011; Doan et al., 2020). While pATOM36 shows no sequence or structural homology to the MIM complex, it had been shown to be involved in the insertion and assembly of OMM proteins in trypanosomes (Bruggisser et al., 2017). Heterologous expression of Mim1/Mim2 and pATOM36 demonstrated that they can functionally replace each other in promoting α-helical insertion, with Mim1/Mim2 compensating for the absence of pATOM36 in trypanosomes and pATOM36 compensating for the loss of Mim1/Mim2 in yeast (Vitali et al., 2018), thus identifying the second OMM insertase.

α-helical membrane protein biogenesis in the mammalian OMM remained elusive as no prior studies were able to identify homologs of the MIM complex or pATOM36. This raised the possibility that mammalian cells had evolved a distinct and specialized OMM insertase. It was only recently that a study from our lab identified MTCH2 to be involved in the biogenesis of a mitochondrial OMM TA protein in human cells (Guna et al., 2022).

1.5 TA protein biogenesis at the OMM and MTCH2

Mitochondrial TA proteins play roles in a variety of vital cellular processes including protein translocation and maturation (Tom5, Tom6, Tom7, Tom22), mitochondrial fission (Fis1), and cellular apoptosis (Bcl2 family) (Mozdy et al., 2000; Wattenberg & Lithgow, 2001; Cory & Adams, 2002; Beilherz et al., 2003). Recently, MTCH2 was identified through a genetic screen searching for biogenesis factors of mitochondrial TA proteins in mammalian cells. Through a series of in cell and *in vitro* assays, MTCH2 was shown to physically associate with mitochondrial TA proteins and be essential for their biogenesis. The study also demonstrated that MTCH2 was both necessary and sufficient for the insertion of mitochondrial TA proteins into the lipid bilayer. Proteomic analysis of

MTCH2 depleted cells revealed that the depletion also impacted other protein classes, including SA proteins and multi-pass membrane proteins in the OMM. This established MTCH2 as a bona fide OMM insertase for α-helical membrane proteins in mammalian cells (Guna et al., 2022).

MTCH2 is a member of a solute carrier family, the SLC25 transporter family. Members of the SLC25 family are IMM resident proteins and typically transport solutes across the IMM. However, MTCH2 and the related proteins MTCH1 and SLC25A46 are divergent members localized to the OMM (Ruprecht & Kunji. 2020). In addition, MTCH2 further differs from the canonical members of the family as it has no known transporter activity and the AlphaFold predicted model only predicts 5 TMDs that create a hydrophilic vestibule exposed to the lipid bilayer (Guna et al., 2022).

The initial discovery of MTCH2 was in its pivotal role in apoptotic signaling through interactions with a Bcl2 family protein, truncated BID (tBID), in the OMM (Grinberg et al., 2005; Zaltsman et al., 2010; Raemy et al., 2016). Since, MTCH2 has been implicated in numerous cellular processes. First, as a modulator of mitochondrial dynamics, MTCH2 is a regulator of mitochondrial fusion and elongation (Bahat et al., 2018; Labbé et al., 2021). Second, as a regulator of lipid homeostasis and linked to obesity in multiple genome wide association studies (Bauer et al., 2009; Schmid et al., 2012; Bernhard et al., 2013; Landgraf et al., 2016; Kong et al., 2019). And third, involved in oxidative phosphorylation homeostasis as a repressor of oxidative phosphorylation (Maryanovich et al., 2015; Buzaglo-Azriel, et al., 2016). Additionally, several genetic variants of MTCH2 have been found to be linked to obesity, heart failure, and polycystic ovary syndrome (Takeuchi et al., 2011; Louwers et al., 2014; Kang et al., 2020; Fischer et al., 2023). The identification of MTCH2 as an OMM insertase complements these findings and provides a molecular explanation for the pleiotropic relationships.

The atomic structures and the precise molecular mechanism of any of the OMM insertases have not been elucidated. Provided its function as an insertase, understanding the mechanistic details of membrane protein insertion by MTCH2 will be key in understanding general principles of α-helical membrane protein biogenesis in the OMM as well as manipulation of proteostasis for therapeutic benefits.

1.6 Methods to study OMM membrane protein biogenesis in mammalian cells

Mitochondrial membrane protein biogenesis has been more extensively studied in other organisms like the budding yeast, *S. cerevisiae*, than in humans. Several factors contribute to this disparity. First,

the increased skills and resources required to study processes in human cells as opposed to in yeast. Second, the smaller yeast genome is easily manipulated compared to the human genome. This makes it more feasible to conduct high-throughput screens to identify novel gene functions in yeast. In contrast, the complexity of human cells and their genome makes such screens more challenging and resource intensive. A third key difference is the lack of robust experimental tools and techniques to study mitochondrial membrane protein biogenesis in human cells. Specifically, tools to study membrane protein biogenesis in the OMM in human cells have been lacking. Mitochondria are encased by two membranes, each with distinct protein biogenesis pathways. The double membrane structure of mitochondria makes it difficult to distinguish between general mitochondrial import and specific OMM integration. This distinction is difficult to achieve using traditional methods to study protein localization, such as microscopy, highlighting the need for novel techniques to specifically study protein biogenesis at the OMM. Development of tools to specifically query membrane protein integration into the OMM will be crucial for advancing our understanding of the biogenesis and function of this small but vital class of membrane proteins.

1.7 Overview of the thesis

The overarching aim of this thesis is the elucidation of the mechanistic details of membrane protein biogenesis at both the ER and OMM. A combination of biochemical, cell biological, structural, and genetic techniques were used to dissect and probe at the question. Chapter 2 focuses on membrane protein biogenesis at the ER and the molecular mechanism of the EMC insertase activity. Leveraging our improved structural characterization of the EMC, we employ biochemical analyses to probe the interaction between the EMC and its TA protein substrate, and map the path of a TA protein through the EMC. Additionally, we dissect the molecular basis for accurate membrane protein sorting at the ER and describe it in mechanistic detail. My work describes the identification of a selectivity filter in the EMC which limits misinsertion of mitochondrial TA proteins and prevents topological errors of multi-pass membrane proteins at the ER.

Chapter 3 describes a set of tools we developed to study the biogenesis of α-helical membrane proteins in the OMM. We highlight three methods to monitor α-helical protein insertion both in human cells and *in vitro*: a split fluorescent reporter system in cells; an *in vitro* import assay with functional, insertion competent mitochondria isolated from human cells; and the reconstitution of purified MTCH2 into proteoliposomes for studies in a minimal system. Building on this, Chapter 4 utilizes the tools described to characterize MTCH2's insertase activity at the molecular level. My

work probes for a selectivity mechanism in MTCH2 for mitochondrial TA proteins, and instead identifies a possibility that MTCH2 is under regulation. I further show that the metazoan and holozoan homologs of MTCH2 may also be under the same regulation as human MTCH2.

Finally, Chapter 5 summarizes the work in this thesis, highlighting how our findings have added to our understanding of membrane protein biogenesis, together with concluding remarks.

Chapter 2

A SELECTIVITY FILTER IN THE ER MEMBRANE PROTEIN COMPLEX LIMITS PROTEIN MISINSERTION AT THE ER

The following chapter is adapted from Pleiner, Hazu, and Pinton Tomaleri et al., 2023 and modified according to the Caltech Thesis format.

Pleiner, T.*, **Hazu, M.***, Tomaleri, G.P.*, Nguyen, V.N., Januszyk, K., & Voorhees, R.M. (2023). A selectivity filter in the ER membrane protein complex limits protein misinsertion at the ER. Journal of Cell Biology 222 (8), doi: 10.1083/jcb.202212007

2.1 Abstract

Tail-anchored (TA) proteins play essential roles in mammalian cells, and their accurate localization is critical for proteostasis. Biophysical similarities lead to mistargeting of mitochondrial TA proteins to the ER, where they are delivered to the insertase, the ER membrane protein complex (EMC). Leveraging an improved structural model of the human EMC, we used mutagenesis and site-specific crosslinking to map the path of a TA protein from its cytosolic capture by methionine-rich loops to its membrane insertion through a hydrophilic vestibule. Positively charged residues at the entrance to the vestibule function as a selectivity filter that uses charge-repulsion to reject mitochondrial TA proteins. Similarly, this selectivity filter retains the positively charged soluble domains of multipass substrates in the cytosol, thereby ensuring they adopt the correct topology and enforcing the "positive-inside" rule. Substrate discrimination by the EMC provides a biochemical explanation for one role of charge in TA protein sorting and protects compartment integrity by limiting protein misinsertion.

2.2 Introduction

A hallmark of eukaryotic cells is their organization into subcellular compartments that spatially separate otherwise incompatible biochemical reactions. The evolution of compartmentalization enabled the increasingly complex cellular processes required for emergence of multicellular life. To carry out distinct functions, each compartment must contain a unique and precisely defined set of proteins and metabolites.

Membrane proteins comprise ~20% of the human proteome (Krogh et al., 2001), and their localization is a primary determinant of organellar identity, underscoring the importance of their accurate sorting. Due to the presence of one or more hydrophobic transmembrane domains (TMDs), targeting and insertion of membrane proteins must be tightly regulated to prevent their aggregation in the aqueous cytosol. Canonical localization of many membrane proteins to mitochondria and the ER relies on cleavable targeting sequences that direct proteins to the correct organelle. Both the mitochondrial targeting sequence and the ER-specific signal sequence are proteolytically removed upon arrival at their respective compartment, and thus have evolved principally to ensure accurate sorting without the need to serve a functional role in the mature protein.

However, given the functional and topological diversity of the membrane proteome, many nascent proteins cannot utilize these stereotypical biogenesis pathways. In these cases, membrane proteins instead rely on recognition of a TMD and its surrounding residues for accurate sorting (Rapoport et al., 2017; Guna and Hegde, 2018). These sequences must therefore play dual roles, experiencing evolutionary pressure to both function in the mature protein (i.e. insertion, folding, and assembly) and ensure accurate localization.

One important family of membrane proteins that rely on their TMD and its flanking residues for recognition, targeting, and insertion are tail-anchored (TA) proteins (Kutay et al., 1993; Chio et al., 2017; Hegde and Keenan, 2011; Guna et al., 2022a). TA proteins are characterized by a single C-terminal TMD followed by a short soluble domain of up to 30-40 amino acids. Their globular N-termini are localized to the cytosol and are responsible for carrying out their diverse functions. Because of their topology, the TMD of a TA protein emerges from the exit tunnel of the ribosome only after translation termination, and they must be post-translationally targeted to the correct organelle. TA proteins are found on all cellular membranes and regulate essential processes such as neurotransmitter release via exocytosis (SNARE proteins), cholesterol synthesis at the ER (squalene

synthase [SQS]), and the onset of apoptosis at mitochondria (BCL-2, Bak). Given their biophysical diversity and the limited information for targeting, how TA proteins are accurately sorted between compartments has been a long-standing open question in the field.

TA protein localization is thought to be primarily dictated by two features: (i) properties of the TMD including its hydrophobicity and helical propensity, and (ii) properties of the C-terminal soluble domain that must be translocated across the bilayer during insertion (Costello et al., 2017; Fry et al., 2021; Kalbfleisch et al., 2007). TAs with highly hydrophobic TMDs are preferentially targeted to the ER membrane for insertion via the guided entry of tail-anchored protein (GET) pathway (Schuldiner et al., 2005; Schuldiner et al., 2008). Its central targeting factor in human cells, GET3 (Stefanovic and Hegde, 2007; Favaloro et al., 2008), binds TMDs using an ordered methionine-rich substrate binding groove and delivers its substrate TA proteins to the GET1/2 insertase for membrane integration (Mariappan et al., 2011). TAs with lower hydrophobicity TMDs, however, do not efficiently bind GET3 and thus cannot access the GET pathway (Guna et al., 2018). The largest classes of such low hydrophobicity TAs are those targeted to the ER, where they are inserted by the ER membrane protein complex (EMC) (Jonikas et al., 2009; Christianson et al., 2012; Guna et al., 2018), and those targeted to the outer mitochondrial membrane, where they are inserted by MTCH1 and 2 (Guna et al., 2022). Because of their biophysical similarity, there is thought to be some constitutive levels of mistargeting between these compartments, necessitating dedicated quality control machinery at the ER and mitochondria to extract mislocalized TA proteins (Chen et al., 2014; Okreglak and Walter, 2014; McKenna et al., 2020).

Because functional constraints limit the potential diversity of the TMD alone, a second sequence element, the short polar C-terminal domain, is known to contribute to TA protein sorting (Isenmann et al., 1998; Kuroda et al., 1998; Borgese et al., 2007). Though biophysically diverse, mitochondrial TA proteins are enriched for positive charges in their C-terminal tails, while the C-termini of ER targeted TA proteins are more likely to be net neutral or negatively charged. Manipulation of C-terminal charge is known to be sufficient to shift the localization of TA proteins between the ER and mitochondria (Horie et al., 2002; Rao et al., 2016; Costello et al., 2017). However, the biochemical basis for how changes in charge can alter TA protein sorting is fundamentally not clear. Considering recent advances in our mechanistic understanding of TA protein insertion into the ER (Pleiner et al., 2020; Bai et al., 2020; O'Donnell et al., 2020; Miller-Vedam et al., 2020), we sought to re-examine

the molecular basis for sorting specificity between mitochondrial and ER TA proteins at this cellular compartment.

2.3 Results

Selectivity at the ER membrane

Previous studies of the canonical co-translational insertion pathway suggest that sorting fidelity is the combined result of contributions from cytosolic targeting steps and selectivity at the membrane (Trueman et al., 2012; Akopian et al., 2013; Jomaa et al., 2022). In the case of TA proteins, the source of this specificity at either step has remained elusive. While specificity during cytosolic targeting must undoubtedly contribute to TA protein localization, we found that even when loaded onto the identical chaperone *in vitro*, some mitochondrial TA proteins cannot be efficiently inserted into the ER membrane (Figure 2.1A). This selectivity appeared to correlate with C-terminal charge, because when positively charged amino acids were introduced within the C-terminus of the canonical ER TA protein squalene synthase (SQS), its insertion efficiency was dramatically diminished. Based on these observations, we concluded that there must be a source of substrate discrimination directly at the ER membrane, with selectivity occurring at the insertion step.

The EMC is the major insertase for ER-destined TA proteins with lower hydrophobicity TMDs, which are similar to those of mitochondrial TA proteins. Consistent with this biophysical similarity, we and others have demonstrated that the EMC is responsible for misinsertion of mitochondrial TA proteins into the ER (Figures 2.1B-D; Guna et al., 2022b; McKenna et al., 2022). Using an established split GFP system to specifically query TA integration into the ER (Figure 2.1B; Inglis et al., 2020), we found that multiple mitochondrial TA proteins were misinserted in an EMC, but not GET1/2, dependent manner (Figures 2.1C-D). We therefore reasoned that one source of discrimination against TAs with positively charged C-termini at the ER, either mitochondrial or the SQS mutants, must originate from properties of the EMC.

Substrate TMDs physically associate with the EMC's hydrophilic vestibule

With the goal of determining the biochemical basis of EMC's substrate specificity, we sought to map the path of a TMD from the cytosol into the bilayer through the EMC. Structures of the yeast and mammalian EMC identified two intramembrane surfaces that could potentially catalyze TMD insertion: a hydrophilic vestibule that positions several conserved positively charged residues within

the cytosolic leaflet of the bilayer, and a hydrophobic crevice that contains a large lipid-filled wedge within the membrane (Pleiner et al., 2020; Bai et al., 2020; O'Donnell et al., 2020; Miller-Vedam et al., 2020). Site-specific crosslinking experiments previously identified EMC3 as the major substrate interaction partner within the purified EMC (Pleiner et al., 2020), consistent with EMC3's homology with other members of the Oxa1 superfamily of insertases (Anghel et al., 2017). However, the path of a substrate TMD has never been directly determined, and potential contributions to insertion from both intramembrane surfaces of the EMC have been proposed.

To map direct physical association of substrates with the EMC, we exploited several independent zero-length crosslinking approaches to chart substrate interaction at single-residue resolution. First, we introduced the site-specific crosslinker 4-Benzoylphenylalanine (BpA) into the TMD of a canonical EMC TA substrate and identified UV-dependent crosslinks to both EMC3 and EMC4 by immunoprecipitation (Figure S2.1A). Unlike EMC3, which is present on both sides of the complex, the cytosolic and intramembrane surfaces of EMC4 partially enclose only the hydrophilic vestibule, suggesting substrates must at least transiently localize with this side of the EMC. Second, we exploited the fact that endogenous EMC3 does not contain any naturally occurring cysteine residues to perform disulfide crosslinking between a TA protein and the EMC. Because disulfide-bond formation can only occur between residues within 3-5 Å of each other, productive crosslinking necessarily indicates a direct physical association. Zero-length disulfide formation between single cysteines introduced at defined positions in EMC3, and a unique cysteine at two different positions within a substrate TMD, identified a strong preference for substrate binding to the hydrophilic vestibule of detergent-solubilized EMC (Figures 2.2A-B and S2.1B). A similar preference was observed when comparing matched positions on either side of EMC3 at the base of the membrane. This preferential crosslinking was independent of cysteine position within the substrate TMD (Figure S2.1C) and was also observed upon incorporation of orientation-independent photo-crosslinkers in EMC3 (Figure S2.1D).

Finally, and most definitively, we developed a strategy to capture the transient interaction between a substrate TMD and the EMC by disulfide crosslinking in native, insertion competent, ER membranes (Figures 2.2C and S2.1E). Using this approach, we again observed a marked preference for interaction of TAs with the hydrophilic vestibule of EMC3 compared to the hydrophobic crevice. In native membranes and with purified EMC, substrates preferentially crosslinked to a cytosol-facing position

on EMC3 at the entrance to the lipid bilayer, suggesting a potential increase in dwell time at this location.

To further exclude that the opposite hydrophobic crevice is involved in TA protein insertion, we introduced multiple mutations to polar and hydrophobic residues in this region and found that they are all dispensable for TA protein biogenesis in human cells (Figures S2.1F-H). These data, in combination with sequence conservation, homology to Oxa1 superfamily insertases, and mutational analysis, definitively identify the hydrophilic vestibule as the insertase competent module of the EMC.

An improved model of the EMC defines intramembrane surfaces required for insertion

Having identified the hydrophilic vestibule as the major site of substrate binding to the EMC, we sought to better define its architecture and thereby identify potential sources of substrate specificity. The insertase core of the EMC (composed of EMC3 and 6) is partially enclosed by the dynamic subunits EMC4, 7 and 10. However, whether EMC7 and 10 contain TMDs, how these may be positioned, as well as the specific contributions of all three auxiliary subunits, was incompletely defined.

To characterize the biophysical properties of the hydrophilic vestibule we obtained an improved cryo-electron microscopy (cryo-EM) reconstruction of the human EMC that allowed us to unambiguously assign and position the three TMDs of EMC4 and the single TMDs of EMC7 and 10 (Figures 2.3A, S2.2 and S2.3A-C; Table 2.1). In support of this model, we biochemically confirmed that human EMC7 and 10 both contain single C-terminal TMDs that span the lipid bilayer (Figure S2.3D). Examination of the roles of these subunits suggested that, consistent with previous studies, EMC4 and 7, but not 10, are required for TA protein biogenesis (Figure S2.3E; Louie et al., 2012; Volkmar et al., 2019; Lakshminarayan et al., 2020). These auxiliary subunits do not play an architectural role in complex stability, as their depletion did not affect assembly of the core EMC subunits (EMC1, 2, 3, 5, 6, 8) (Figure S2.3F). However, we additionally found that complete loss of EMC4 impaired the assembly of EMC7 and 10 into the EMC. Because EMC4's C-terminal β-strand completes the membrane-proximal β-propeller of EMC1, it is possible that loss of EMC4 disrupts the lumenal binding sites of EMC7 and 10. We concluded that the hydrophilic vestibule formed by the TMDs and cytosolic loops of EMC3 and 6 is partially enclosed by the five dynamic TMDs of EMC4, 7 and 10.

Capture of substrate TAs in the cytosol by the EMC

Based on this improved model of the EMC, we determined that the cytosolic loops of EMC3 and 7 are positioned immediately below the hydrophilic vestibule, making them prime candidates for cytosolic capture of substrates. We had previously shown that the flexible loops of EMC3 contain conserved methionine residues, commonly found in the TMD binding domains of cytosolic chaperones, that were important for EMC function (Pleiner et al., 2020). We therefore hypothesized that the loops of EMC3 and 7 could be involved in physically interacting with substrate TMDs in the cytosol. We set out to test key facets of this working model, with the goal of understanding whether the molecular details of substrate capture could contribute to discrimination between ER and mitochondrial TA proteins.

Consistent with earlier data, we found that methionine residues within the cytosolic loop of EMC3 were essential for TA protein biogenesis in cells (Figures 2.3B and S2.4A-B). Similarly, we found that the flexible C-terminus of EMC7 was required for EMC function (Figures 2.3C and S2.4C-F). Deletion of twelve residues to disrupt a predicted amphipathic α-helix, but not deletion of a matched upstream α-helix, strongly impaired SQS biogenesis, nearly phenocopying EMC7 knockout. We further demonstrated that the hydrophobicity of conserved residues within both this amphipathic helix of EMC7 and the methionine-rich loops of EMC3 is important, because their mutation to leucine, but not alanine or glutamate, supported wild type levels of EMC function in cells (Figures 2.3C and S2.4A-F). However, for these loops to be directly involved in TA protein capture, they must be capable of physically interacting with substrate TMDs. Indeed, using zero-length disulfide crosslinking, we found that the cytosolic loops of EMC3 and 7 specifically interact with substrates in a TMD-dependent manner (Figures 2.3B, 2.3D and S2.4G-H).

We concluded that the primary role of these flexible loops is to position hydrophobic residues within the cytosol, which physically capture substrate TMDs for subsequent insertion into the membrane. To test whether TA capture in the cytosol could contribute to substrate selectivity by the EMC, we used site specific crosslinking to compare the interaction of the TMD of wild type and mutant SQS, containing a positively charged C-terminus, with the loops of EMC3. We observed only a modest decrease in cytosolic capture of the positively charged SQS mutant (Figure S2.4I), suggesting that capture by EMC3 and 7 did not substantially contribute to substrate discrimination based on C-terminal charge. We therefore turned to consideration of the intramembrane surfaces of the hydrophilic vestibule.

Substrates must passage through a positively charged hydrophilic vestibule for insertion

The improved atomic model of the EMC enabled detailed structure-function analysis of the biophysical requirements of the hydrophilic vestibule for TA protein insertion. The defining characteristic of the hydrophilic vestibule is a network of conserved polar and positively charged residues within the cytosolic leaflet of the lipid bilayer. Previous analysis suggests that charged and polar residues required for EMC function are positioned within the TMDs of the core insertase subunits EMC3 and 6 (Pleiner et al., 2020). Mutations to the positively charged residues in EMC3 strongly impaired insertion in cells, whereas mutations to EMC6 had only mild effects.

A more complete understanding of the localization of EMC4, 7 and 10 allowed us to systematically introduce mutations to all of the polar residues that face the EMC3/6 insertase core (Figure 2.3E). However, we found that mutations to polar, charged, and methionine residues within EMC4's TMDs had little to no effect on TA protein biogenesis (Figures 2.3E and S2.5A-C). Only mutations of residues that likely affect TMD packing (N140) or lipid headgroup interaction (K67) showed significant phenotypes. If EMC4 does not directly contribute to function, it may instead be playing a role in regulating access to the hydrophilic vestibule, as deletion of its cytosolic EMC2-binding site strongly impaired SQS biogenesis (Figures S2.5D-E). Of all the polar intramembrane residues tested within the hydrophilic vestibule, the highly conserved R31 and R180 of EMC3 are the most crucial for TA protein insertion, and their combined mutation displayed an additive effect on substrate biogenesis (Figures 2.3E and S2.5F-G).

Positively charged soluble domains impede insertion by the EMC

Both these mutational data and our crosslinking results together suggest that substrates must passage into the membrane directly along a positively charged surface of EMC3. Mislocalization of a mitochondrial TA protein into the ER requires both insertion of its TMD and translocation of its associated positively charged C-terminal domain. Thus, we reasoned that the positively charged hydrophilic vestibule is ideally positioned to discriminate mitochondrial and ER TA proteins through charge repulsion (Figure 2.4A).

To test the fundamental premise of this hypothesis, we first characterized the impact of charge on insertion by the EMC. In order to directly query the role of C-terminal charge, without confounding effects from comparing different substrates or TMDs, we generated a series of mutants of the

canonical ER TA protein, SQS, containing increasing amounts of positive charge within its soluble C-terminal domain (Figure 2.4B). Using the split GFP reporter system, we found that while all SQS mutants inserted into the ER in an EMC-dependent manner, insertion efficiency was inversely correlated with positive charge (Figures 2.4C-D). Even addition of a single positive charge to the C-terminus of SQS resulted in a dramatic decrease in integration into the ER. Validating that this effect is specifically occurring at the insertion step and cannot be explained by other effects in cells (e.g. substrate stability), we observed a similar trend between charge and insertion into ER microsomes *in vitro* (Figure 2.4E).

In addition to its role in TA protein insertion, the EMC co-translationally inserts the first N_{exo} TMD (N-terminus facing the ER lumen) of many GPCRs that do not contain signal sequences (Chitwood et al., 2018). Like the C-termini of ER TA proteins, these GPCRs contain N-termini that are typically short, unstructured, and net negatively charged (Figure 2.5A; Wallin and von Heijne, 1995). Using the EMC-dependent GPCR OPRK1, we found that introduction of positive charge is again inversely correlated with insertion propensity by the EMC (Figures 2.5B-C). We therefore propose that inefficient translocation of positively charged extracellular domains is an inherent property of the EMC shared by both its co- and post-translational insertase function.

The EMC selectivity filter enforces TA protein sorting fidelity and the positive inside rule

The EMC's strong bias against translocation of positively charged domains provides a biochemical explanation for discrimination of mitochondrial TA proteins at the ER. To determine if this selectivity is due at least in part to charge repulsion between the hydrophilic vestibule of the EMC and the soluble C-terminal domain of a substrate TA protein, we tested whether manipulation of the electrostatic potential of the EMC could alter substrate selectivity.

Due to the prominent location of R31 and R180 of EMC3 at the cytosolic entrance to the hydrophilic vestibule, these residues are ideally positioned to form a charge barrier that selectively prevents translocation across the lipid bilayer. If true, mutations that alter the electrostatic potential of these residues could alleviate repulsion between the EMC and positively charged soluble domains, allowing increased misinsertion of mitochondrial TA proteins. Mutation of both EMC3 R31 and R180 to alanine or glutamate did not affect EMC assembly, and as expected markedly impaired insertion of SQS in cells using our ratiometric fluorescent reporter system (Figures 2.6A-B and S2.5H). However, SQS variants containing increasingly positively charged C-termini showed

increased insertion by the glutamate, but not the alanine mutant EMC. A similar trend was observed for insertion of SQS variants *in vitro* into wild type, alanine, or glutamate mutant ER microsomes, validating that charge specifically affects insertion propensity (Figure 2.6C). Similarly, these EMC3 mutations differentially affected the insertion of the co-translational substrate OPRK1 and its positively charged N-terminal domain mutants in cells (Figure 2.6D).

Because these SQS variants serve only as a proxy for the effects of charge on insertion, we tested whether manipulation of the EMC selectivity filter could also affect mislocalization of bona fide mitochondrial TA proteins into the ER. Indeed, we found that multiple mitochondrial TA proteins, most notably RHOT1, showed increased ER insertion upon expression of the glutamate, but not the alanine mutant of EMC3 in cells and *in vitro* (Figures 2.7A-B). Fis1, MAOA and MAOB similarly showed increased ER insertion. Even with increased mistargeting of TA proteins to the ER, induced by depletion of the outer mitochondrial membrane insertase MTCH2 (Guna et al., 2022b), the selectivity filter at the EMC limited mitochondrial TA protein mislocalization to the ER (Figure S2.5I).

Based on this strong preference by the EMC against translocation of positively charged domains, we next tested whether charge repulsion could be used by the EMC to more broadly enforce the correct topology of multipass membrane proteins. Earlier work suggests the EMC assesses the topology-defining signal-anchor of nascent membrane proteins after ER targeting and hand-over from SRP (Chitwood et al., 2018). The N-terminal domains of type II (N_{cyt}) multipass proteins face the cytosol when inserted in the correct topology and are enriched for positive charge. We postulated that the positively charged selectivity filter of the EMC would therefore reject such TMDs. To test this directly, we analyzed the extent of N_{exo} misinsertion of the GFP11-tagged N_{cyt} model protein TRAM2 in the presence of the EMC3 selectivity filter mutations. Indeed, the negatively charged glutamate, but not alanine mutant, increased insertion of TRAM2 in the incorrect N_{exo} topology (Figures 2.7C and S2.5J). This misinserted population is subject to ER-associated degradation because it can be stabilized by the p97 inhibitor CD-5083. We therefore concluded that the EMC selectivity filter additionally limits misinsertion of multipass proteins in the incorrect topology and thus contributes to enforcing the ‘positive-inside’ rule (von Heijne, 1986).

2.4 Discussion

These results suggest that charge repulsion at the EMC provides a selectivity filter to control the subcellular localization of TA proteins (Figure 2.7D), enforcing their accurate sorting between the ER and mitochondrial outer membrane. The enrichment of positive charge in the C-termini of mitochondrial (and likely peroxisomal) TA proteins serves as a flag for discrimination at the ER by the EMC. Unlike their TMDs, which must mediate function and targeting, the C-terminal domains of most TA proteins are functionally dispensable and may have evolved primarily to facilitate sorting specificity. The combined evolution of mitochondrial TA protein's positively charged C-termini and the positively charged hydrophilic vestibule of the EMC thereby limits misinsertion of TA proteins at the ER membrane.

The molecular basis for TA protein discrimination was revealed by a systematic analysis of substrate insertion *in vitro* and in cells that defines the path through the hydrophilic vestibule of the EMC into the membrane. After delivery to the ER by a cytosolic chaperone, the first step in substrate insertion is handover and capture by the EMC. We found that substrate TMDs physically interact with the conserved, hydrophobic loops of EMC3 and EMC7 located immediately beneath the vestibule in the cytosol. Mutational analysis suggests that only the hydrophobicity of these loops, but not their specific amino acid sequence, is important for TA protein insertion. Indeed, comparison of EMC3 with its bacterial and archaeal homologs suggests that methionine-rich cytosolic loops are a conserved feature of Oxa1 superfamily insertases (Borowska et al., 2015), but the specific positioning of these hydrophobic residues is not strictly critical. We propose that these hydrophobic loops represent the first transient, flexible interaction site for substrate TMDs by the EMC.

We observed that substrates crosslink more efficiently to both these loops and the cytosol-exposed residues of the hydrophilic vestibule than to residues within the lipid bilayer. This difference was especially pronounced in native insertion-competent membranes, more likely to represent on-pathway intermediates that are not artefacts of detergent solubilization. These data would be consistent with a longer dwell time of substrates in this cytosolic intermediate followed by faster partitioning into the lipid bilayer. Similarly, a recent kinetic analysis of the bacterial insertase YidC suggests rapid substrate capture via its cytosolic loops and substantially slower translocation of the polar domain and membrane insertion (Laskowski et al., 2021). A plausible explanation for this observation might be that translocation of a polar domain across the hydrophobic lipid bilayer has a high energetic barrier and thus is a rate-limiting step to insertion.

This would be consistent with molecular dynamics simulations that suggest that TMD partitioning into the membrane is an energetically favorable process and membrane protein insertases are primarily required to decrease the energetic barrier for translocation of a soluble domain across the bilayer (Nicolaus et al., 2021; White and Wimley, 1999). Therefore, interaction of a substrate TMD with EMC's cytosolic hydrophobic loops could prevent aggregation, while its C-terminus probes the hydrophilic vestibule. For correctly targeted TA proteins, the EMC's hydrophilic vestibule serves as a funnel that catalyzes translocation of their C-termini into the ER lumen by providing a hydrophobicity gradient between the aqueous cytosol and the core of the bilayer. Positioning of similar hydrophilic grooves or vestibules within a locally thinned membrane is a common feature of evolutionary distinct protein translocases (Kumazaki et al., 2014; Voorhees et al., 2014; McDowell et al., 2020; Wu et al., 2020), and represents a striking example of convergent evolution. In the case of the EMC, the dynamic TMDs of EMC4, 7 and 10 provide a protected environment, devoid of any potential off-pathway interaction partners, for the nascent protein to sample the bilayer.

However, for mistargeted mitochondrial or peroxisomal TA proteins, the positive net charge of the hydrophilic vestibule would impose a kinetic barrier to translocation of their positively charged C-terminal domains. In these TA proteins, positive charges are frequently found clustered near their TMD, suggesting that simple net charge alone may not determine the extent of charge repulsion at the EMC. Repulsion likely delays translocation and thus increases the chance of TA protein dissociation from the hydrophobic loops. Using purified components, we previously showed that the cytosolic domain of the EMC does not contain an ordered high-affinity TMD binding site (Pleiner et al., 2021), as can be found in GET3 or SRP (Guna and Hegde, 2018). A composite transient TMD capture surface formed by flexible hydrophobic loops might allow for faster dissociation of TA protein clients and thus enable quicker accept/reject decisions. Rejected TA proteins in the cytosol could then be either recaptured for targeting to the correct organelle or triaged for degradation by quality control machinery. In this way, the EMC provides an additional layer of specificity to the accurate sorting of the ~600 TA proteins that must be expressed and localized in human cells.

The degree to which mitochondrial TA protein misinsertion into the ER is affected by the EMC selectivity filter is variable and likely influenced by multiple factors. For example, the inherent propensity for mistargeting to the ER differs amongst mitochondrial TA proteins (Guna et al., 2022b). Additionally, detailed sequence features of a TA protein's C-terminal domain (i.e. total charge, charge density/positioning, secondary structure propensity) or TMD itself (i.e. helical propensity, length,

hydrophobicity) might alter the effect of the EMC selectivity filter. The rules that determine the dependency of an individual TA protein on the selectivity filter represent an important question for future work.

The two positively charged residues in EMC3, which provide the charge barrier for entrance to the hydrophilic vestibule, are universally conserved in all Oxa1 superfamily insertases. As a result, its homologs, including GET1 and YidC, have also been suggested to inefficiently translocate positively charged soluble domains (Rao et al., 2016; Soman et al., 2014). Indeed, the effect of charge on insertion efficiency appears to be an inherent quality of the EMC and affects both its post- and co-translational substrates. Similar to EMC's TA protein substrates, GPCRs that lack an N-terminal signal sequence and are therefore potential EMC clients, typically contain neutral or negatively charged N-terminal extracellular domains (Figure 2.5A; Wallin and von Heijne, 1995). Using the same strategy for discrimination of mitochondrial TA proteins, the EMC also enforces the 'positive-inside' rule (von Heijne, 1986) for a subset of co-translational multipass substrates that meet its general client criteria (i.e. those without signal sequence containing a short and unstructured N-terminal domain). For N_{cyt} multipass clients, the EMC selectivity filter imposes correct topology by limiting translocation of their typically positively charged N-terminal cytosolic domains into the ER lumen using charge repulsion. The resulting longer dwell times at the EMC for N_{cyt} clients then likely triggers transfer to Sec61 for insertion in the correct topology.

Given that signal-sequence containing proteins are delivered to the ER membrane via the same route as multipass membrane proteins, it is likely that signal sequences also transiently sample EMC's hydrophilic vestibule. Their frequently positively charged N-terminal region (N-region) could mediate their rejection by the EMC selectivity filter and thus trigger handover to Sec61 for insertion in the correct N_{cyt} topology, required for signal sequence cleavage. In this model, the biophysical properties of the N-region would dictate the extent of charge repulsion at the EMC and therefore modulate signal sequence topogenesis. We thus propose that the EMC might contribute to the previously observed N_{exo} misinsertion of signal sequence-containing proteins that makes them substrates of corrective quality control pathways (McKenna et al., 2022). By extension, the selectivity filter in the EMC would play a further role in enforcing the correct topology of secreted proteins, along with TAs and multipass membrane proteins.

In summary, we have characterized the molecular logic for how the EMC contributes to selective membrane protein localization in human cells. Its function is analogous to the active role Sec61 plays

in substrate selection and rejection at the ER (Trueman et al., 2012). Whether MTCH1 and 2 also confer similar contributions to substrate selectivity at the mitochondrial outer membrane is an important question for future research. However, specificity at the membrane is only one layer of the multi-faceted approach used to regulate protein sorting. Cells employ a sieved strategy in which the overall fidelity of protein localization is the combined result of selectivity at each biogenesis step including chaperone binding in the cytosol, insertion at the membrane, and extraction of misinserted substrates (Rao et al., 2016). How specificity is imparted during the targeting and extraction steps is an area that warrants further study. Particularly in metazoans, where membrane protein mislocalization can lead to disease (Juszkiewicz and Hegde, 2018), these steps are tightly coupled to quality control machinery that ensures immediate recognition and degradation of failed intermediates. By limiting misinsertion of TA proteins and preventing topological errors in multipass membrane proteins, the EMC serves as a guardian for protein biogenesis at the ER.

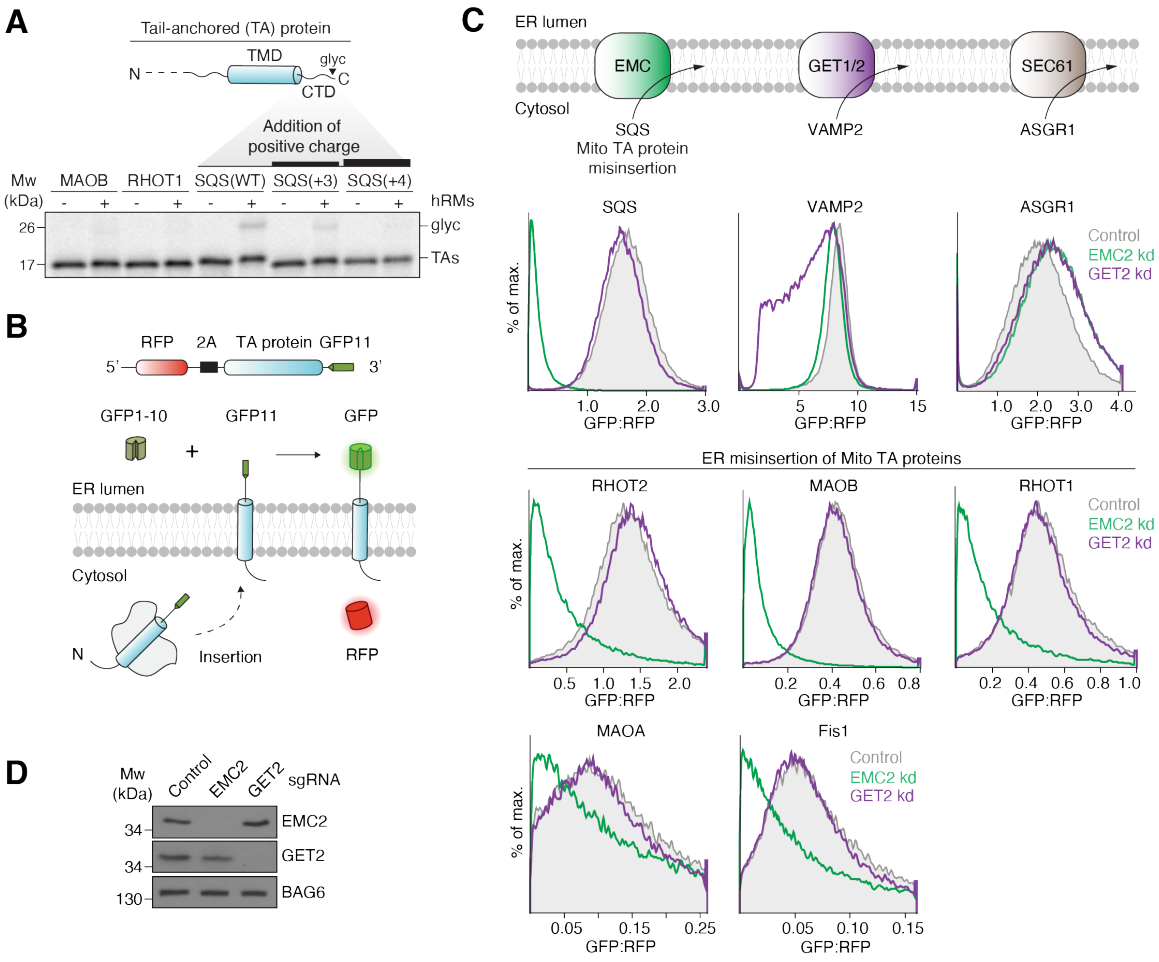

Figure 2.1. Selectivity at the ER membrane limits misinsertion of mitochondrial TA proteins by the EMC.

(**A**) (Top) Topology of a TA protein. (Bottom) ^{35}S-methionine-labeled TA protein with the indicated TMDs and C-terminal domains (CTDs), were expressed in the PURE system and purified as complexes with the cytosolic chaperone calmodulin. Glycosylation (glyc) of the CTD upon incubation with human ER microsomes (hRMs) indicates successful insertion. Samples were analyzed by SDS-PAGE followed by autoradiography. (**B**) Schematic of the split GFP reporter system used to selectively monitor TA protein insertion into the ER. TA proteins fused to GFP11 are expressed in K562 cells constitutively expressing GFP1-10 in the ER lumen, along with a translation normalization marker (RFP). Successful integration into the ER results in GFP complementation and fluorescence. (**C**) (Top) ER insertion pathways. (Bottom) ER insertion of the indicated ER (SQS, VAMP2, ASGR1) and mitochondrial (RHOT2, RHOT1, MAOA, MAOB, Fis1) TA proteins, using

the split GFP system as described in (B), was assessed in cells transduced with either a non-targeting (control), EMC2, or GET2 knockdown (kd) single guide RNA. GFP fluorescence relative to the normalization marker RFP was determined by flow cytometry and displayed as a histogram. (**D**) Cells from (C) were harvested and samples of total cell lysates were analyzed by SDS-PAGE and western blotting with antibodies against EMC2, GET2, and BAG6, a non-targeted control protein.

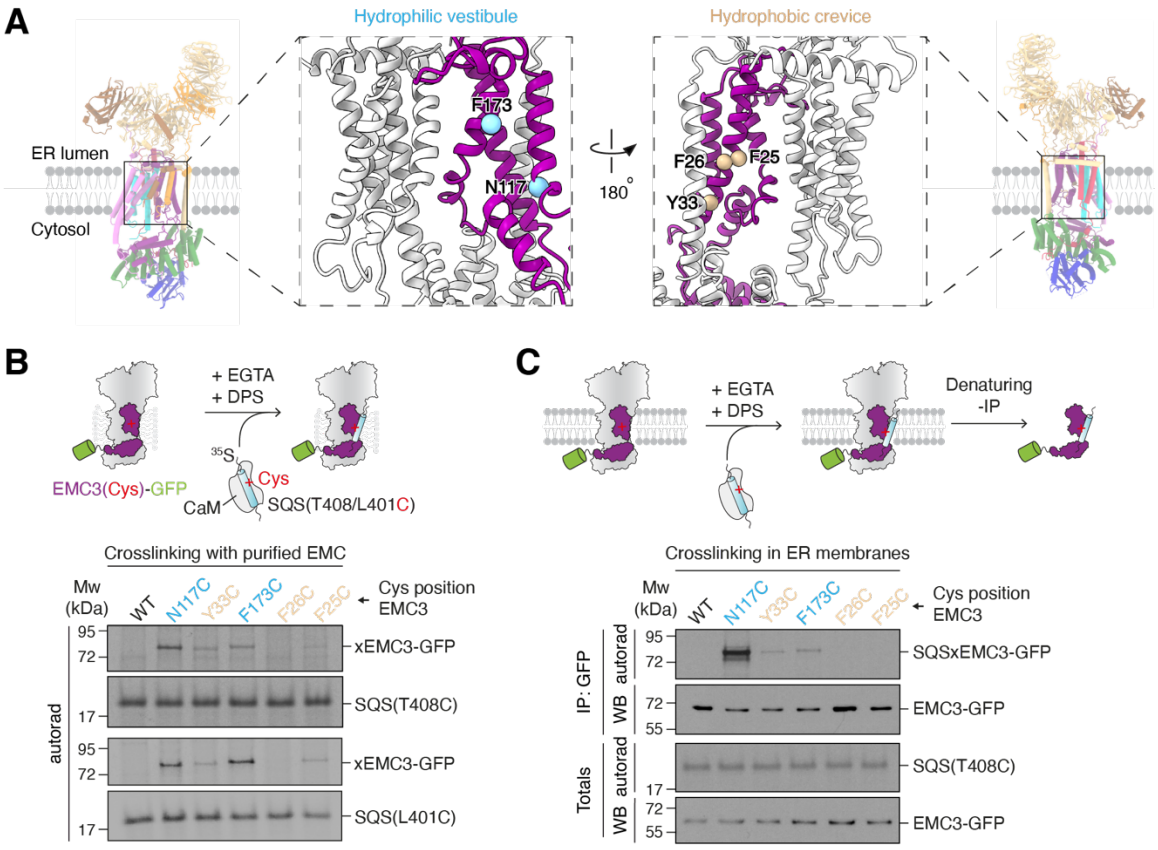

Figure 2.2. The EMC uses a hydrophilic vestibule for TA protein insertion.

(**A**) Views of the two intramembrane surfaces of the EMC. Residues in EMC3 (purple) lining either the hydrophilic vestibule or hydrophobic crevice were mutated to cysteines for disulfide crosslinking and are highlighted in blue or tan, respectively. EMC4, 7 and 10 are omitted in the inset for clarity. (**B**) Purified wildtype (WT) or EMC3 cysteine (Cys) mutant EMC was incubated with CaM-SQS containing a cysteine in the TMD at either position T408 (CaM-SQS[T408C]) or L401 (CaM-SQS[L401C]). After substrate release from CaM with EGTA, cysteines in close proximity were crosslinked with the zero-length disulfide crosslinker DPS. Quenched reactions were analyzed by SDS-PAGE and autoradiography. (**C**) Human ER-derived microsomes (hRMs) prepared from EMC3 WT or Cys mutant cell lines were mixed with CaM-SQS(T408C) for crosslinking as described in (B). Substrate crosslinks were enriched by denaturing purification of EMC3-GFP. Samples were analyzed by SDS-PAGE followed by autoradiography or western blotting.

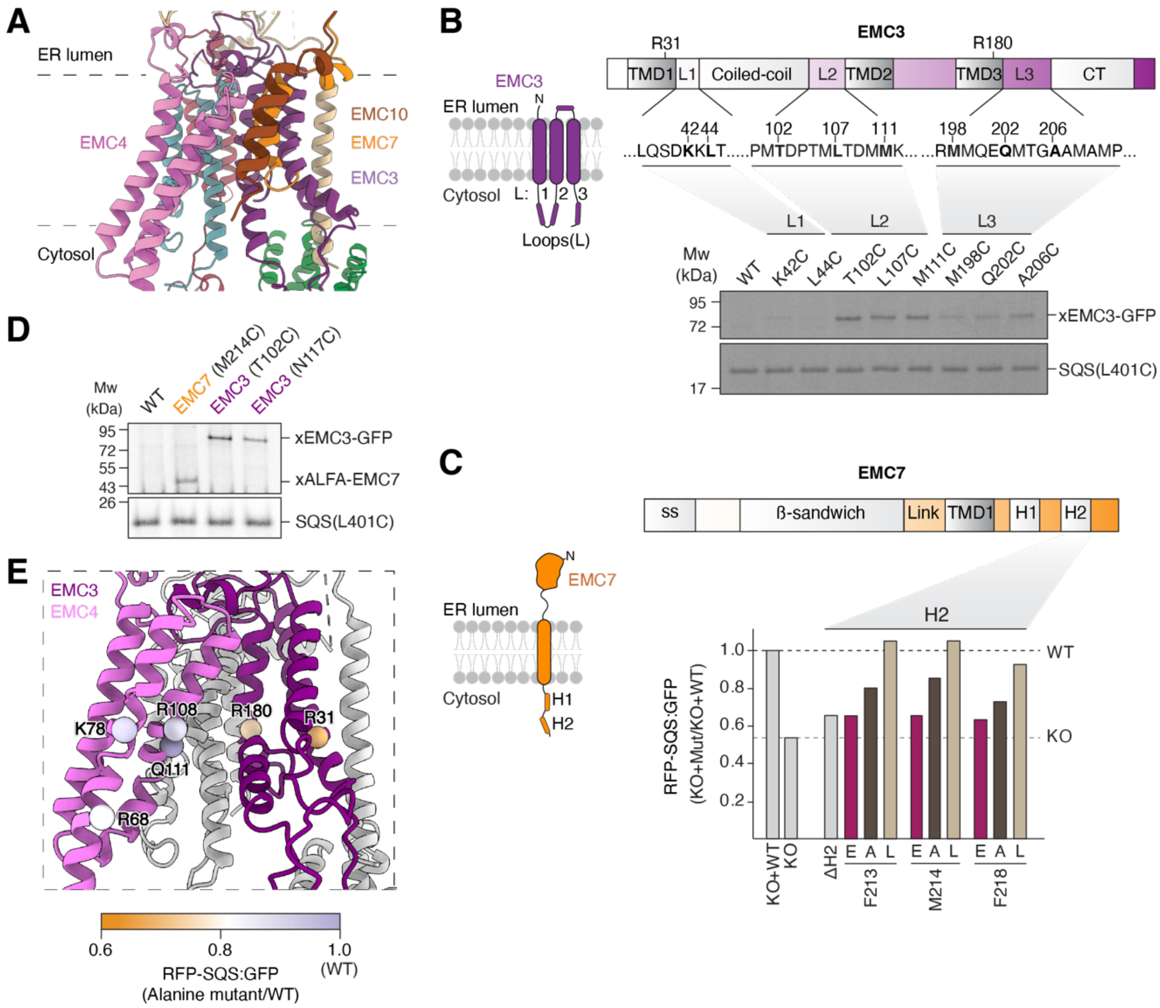

Figure 2.3. Characterization of the cytosolic and intramembrane residues required for insertion by the EMC.

(**A**) Displayed is an improved model of the human EMC determined using cryo-EM. View of the insertase core composed of EMC3/6, enclosed by the three TMDs of EMC4, and the single TMDs of EMC7 and 10. (**B**) (Top) Schematic of the topology and domain organization of EMC3, highlighting three flexible cytosolic loops (L1-3) located beneath the hydrophilic vestibule of the EMC. (Bottom) Purified wildtype (WT) or EMC3 Cys mutant EMC were incubated with purified CaM-SQS(L401C) complexes for disulfide crosslinking and analysis as in Figure 2.2B. (**C**) (Top) Schematic of the topology and domain organization of EMC7. ss = signal sequence; Link = linker; H1 = helix 1; H2 = helix 2. (Bottom) HEK293 EMC7 knockout (KO) cells were transduced with lentivirus to express WT EMC7, or the indicated mutants of EMC7 helix 2 (H2). The effects of each mutant on biogenesis

of SQS was determined using the ratiometric fluorescent reporter assay, normalized to WT and plotted as a bar chart. (**D**) Disulfide crosslinking, as described in Figure 2.2B, of SQS(L401C) with purified EMC complexes, containing cysteines either in H2 of EMC7 (M214S), loop 2 of EMC3 (T102C) or within the membrane (EMC3 N117C). (**E**) View of the hydrophilic vestibule with EMC7 and 10 omitted for clarity. Residues indicated with spheres are colored according to the effects of individual alanine mutations at these positions in EMC3 and 4 on expression of SQS in HEK293T cells. The effect of each mutant was determined by flow cytometry using the ratiometric fluorescent reporter assay as in (C), normalized to wildtype, and is displayed according to the indicated legend.

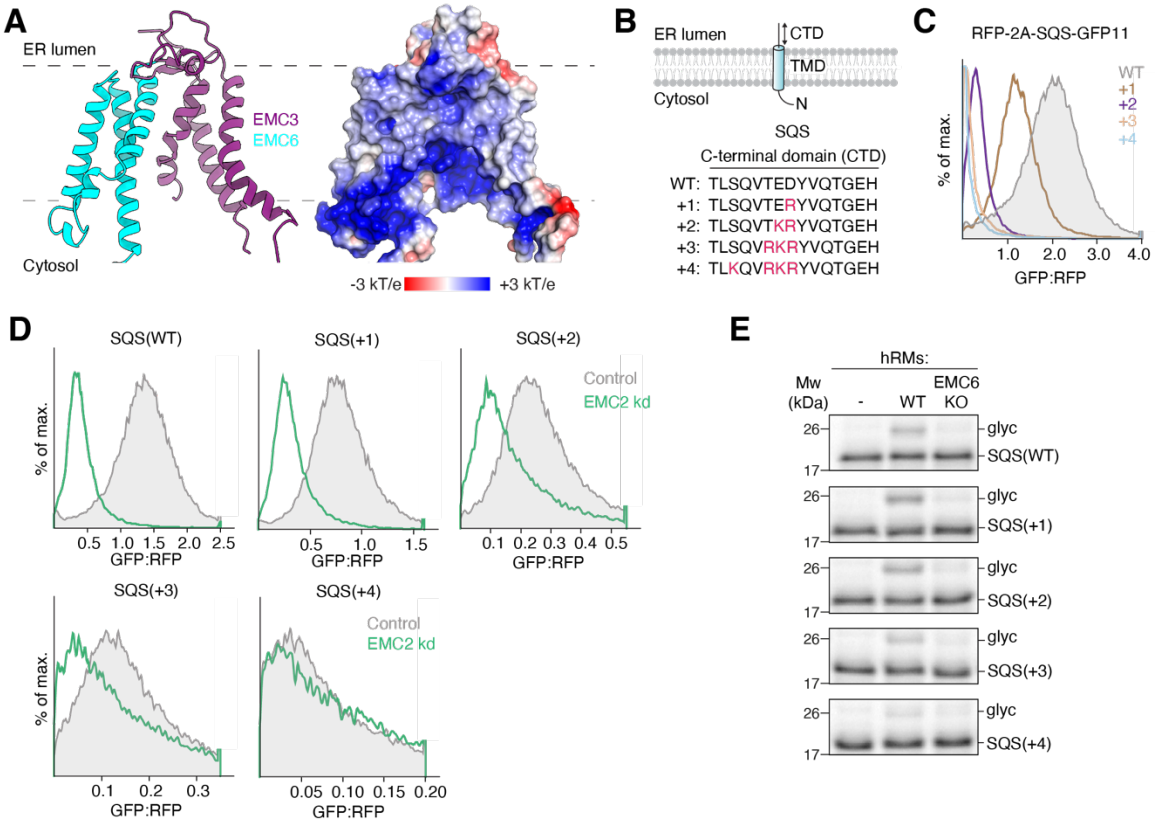

Figure 2.4. Positively charged C-terminal domains of TA proteins impair insertion by the EMC.

(**A**) (Left) Model of the TMDs of EMC3 and 6 that constitute the central insertase of the EMC. (Right) Surface representation of the electrostatic potential of the insertase core ranging from -3 to +3 kT/e. EMC4, 7, and 10 were omitted for clarity. (**B**) Schematic of the SQS C-terminal domain (CTD) charge series. The C-terminus of SQS was mutated to introduce positively charged residues at the indicated positions. (**C**) Integration of the indicated SQS mutants into the ER was determined using the split GFP reporter system described in Figure 2.1B. (**D**) Same assay as in (C), but with cells expressing either a non-targeting (control) or EMC2 knockdown (kd) single guide RNA. (**E**) The indicated ^{35}S-methionine labeled SQS charge mutants were expressed in rabbit reticulocyte lysate and incubated with human ER-derived microsomes (hRMs) prepared from HEK293 wildtype (WT) or EMC6 knockout (KO) cells. ER insertion is monitored by glycosylation (glyc) of an acceptor motif fused to the C-terminus of the TA protein substrates.

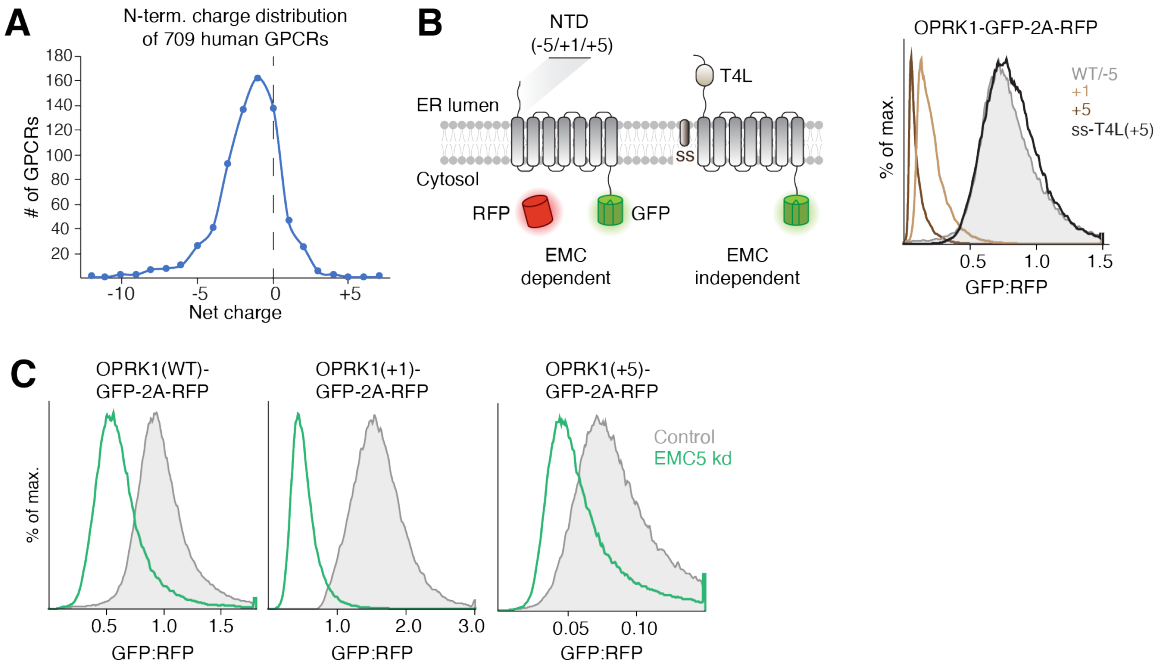

Figure 2.5. Positively charged N-terminal domains of GPCRs impair EMC insertion.

(**A**) Distribution of charge within the soluble N-terminal domain of the 709 human GPCR sequences annotated in the Uniprot database. Only those GPCRs lacking a signal sequence (i.e. signal anchored) were included, because these represent substrates that could potentially rely on the EMC for insertion of their first TMD in an N_{exo} topology (N-terminus facing the ER lumen) (Chitwood et al., 2018). (**B**) WT (total N-terminal charge of -5) or the indicated N-terminal domain (NTD) charge mutants of the GPCR OPRK1 GFP-fusions were expressed along with an RFP normalization marker in RPE1 cells. Cells were analyzed by flow cytometry and the GFP:RFP ratio is displayed as a histogram. Bypassing insertion by the EMC by fusion to a cleavable signal sequence (ss) enhances ER integration of the OPRK1(+5) charge mutant. (**C**) As in (B), but cells were treated with scrambled (control) or EMC5 knockdown (kd) siRNAs and analyzed by flow cytometry. Note that though the stability of the positively charged NTD variants is reduced, they remain EMC-dependent for their insertion.

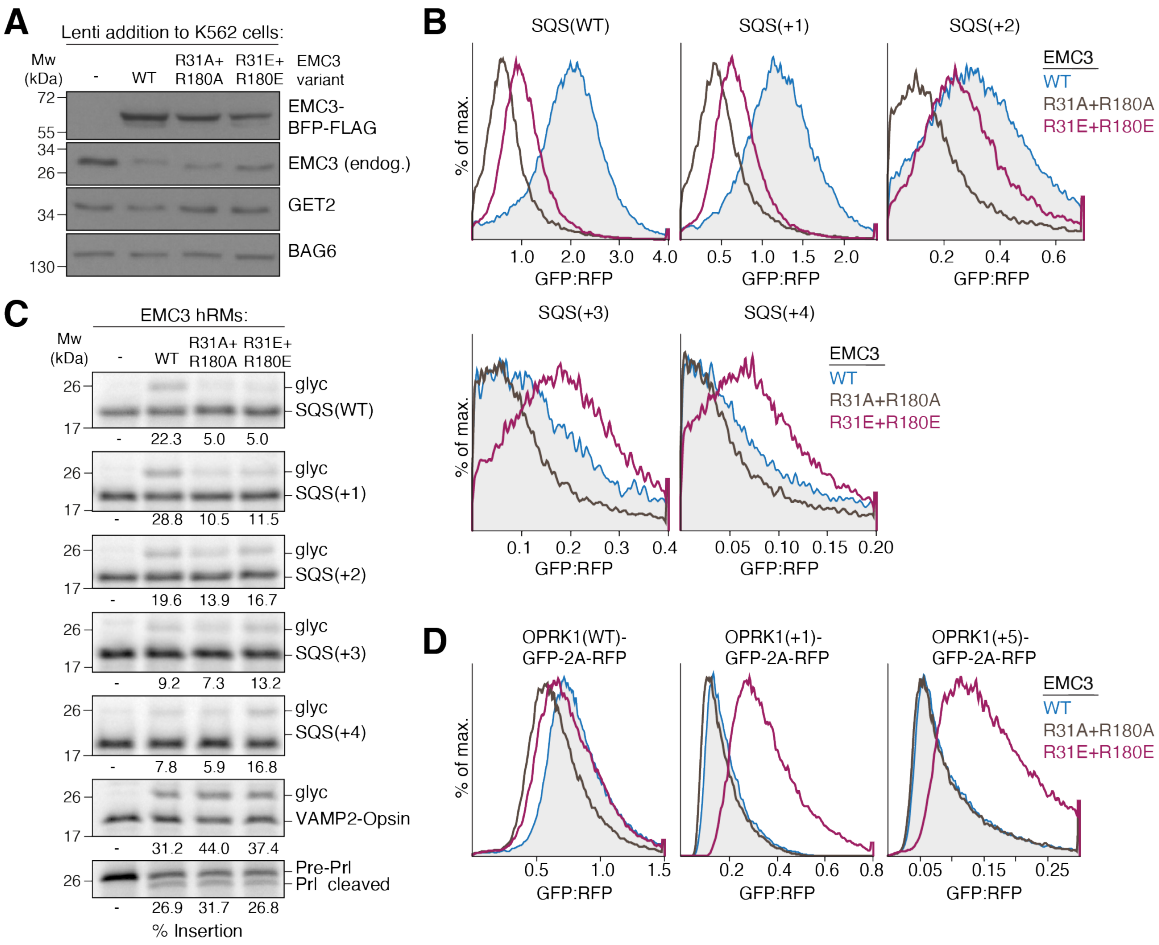

Figure 2.6. Charge reversal in the hydrophilic vestibule alleviates charge repulsion.

(**A**) K562 ER GFP1-10 cells were transduced with lentivirus to express either WT, R31A+R180A or R31E+R180E EMC3. Cells were harvested, solubilized and samples of the total lysates were analyzed by SDS-PAGE and Western blotting with the indicated antibodies. (**B**) ER insertion of the indicated SQS charge mutants was measured in cells expressing either wild type (WT), R31A+R180A, or R31E+R180E EMC3 using the split GFP reporter system described in Figure 2.1B. (**C**) The indicated SQS mutants were prepared as in Figure 2.4E and incubated with hRMs from WT, R31A+R180A or R31E+R180E EMC3 expressing cell lines. Successful ER insertion is monitored with a glycosylation (glyc) acceptor motif fused to the C-terminus of each substrate. The percent glycosylated is indicated below the gel. Expression of both EMC3 mutants does not impair the biogenesis of GET1/2-dependent VAMP2 or the secreted protein prolactin (Prl) that depends on the Sec61 complex (translocon). (**D**) WT (-5) or the indicated charge mutants of OPRK1 were fused to

GFP and expressed with RFP as a translation normalization marker in RPE1 cells. Cells additionally expressed either BFP-tagged EMC3 WT, R31A+R180A or R31E+R180E. Cells were analyzed by flow cytometry to derive the GFP:RFP ratio of BFP positive cells.

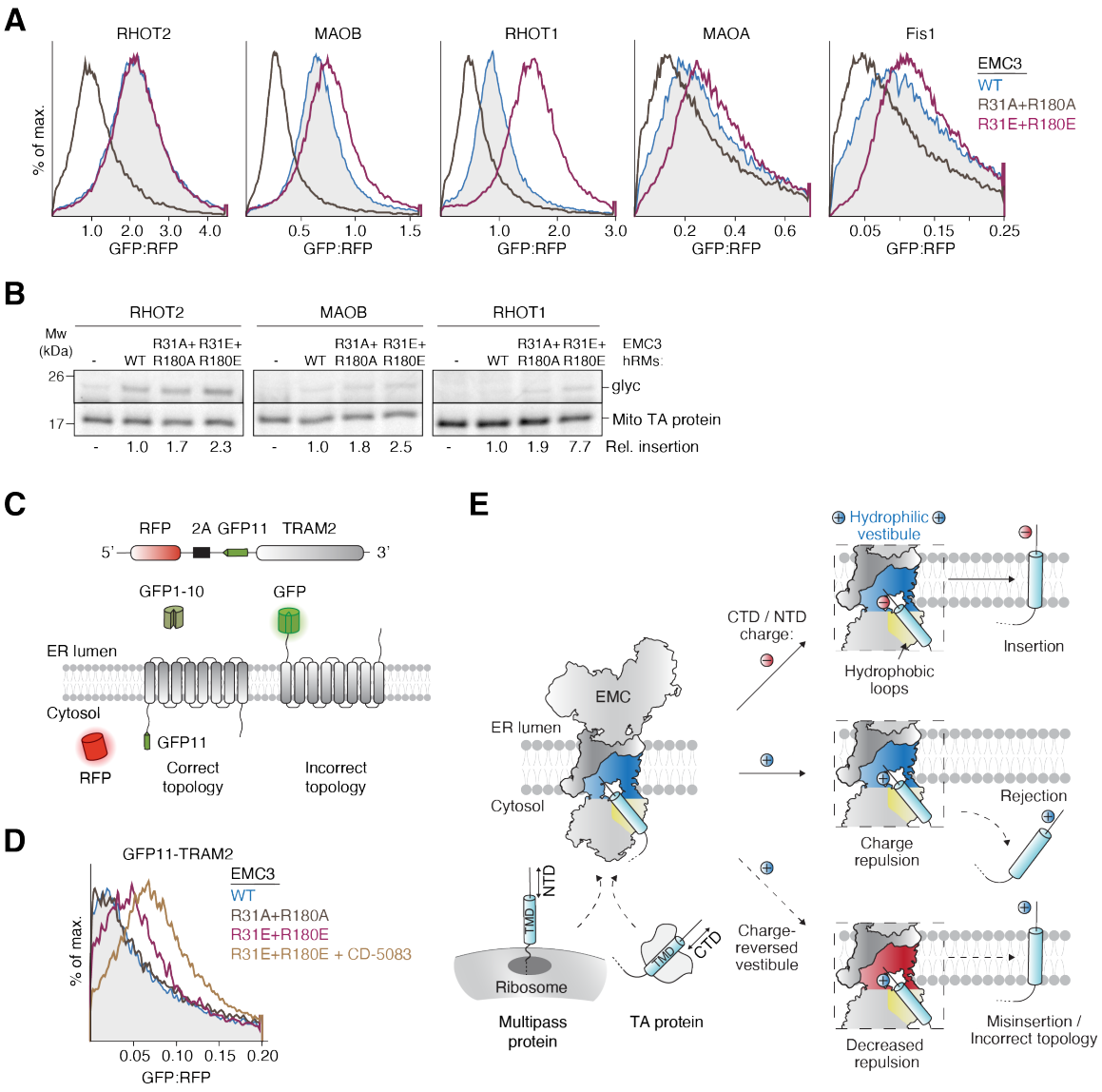

Figure 2.7. A selectivity filter in the EMC limits mitochondrial TA protein misinsertion at the ER.

(**A**) As in Figure 2.6B, but with the indicated mitochondrial TA proteins. Note the strong increase in ER mis-localization of RHOT1 in EMC3 R31E+R180E expressing cells. (**B**) As in Figure 2.6C but expressing the TMD and C-terminus of the indicated mitochondrial TA proteins in non-nucleased rabbit reticulocyte lysate. (**C**) Schematic of the split GFP reporter system used to selectively monitor TRAM2 insertion in the incorrect topology into the ER. GFP11-tagged TRAM2 is expressed in K562 cells constitutively expressing GFP1-10 in the ER lumen, along with a translation normalization

marker (RFP). Successful integration of TRAM2 in the correct topology will result in no fluorescence. Insertion in the incorrect topology results in GFP complementation and fluorescence. (**D**) ER insertion of GFP11-TRAM2 was measured in cells expressing either wild type (WT), R31A+R180A, or R31E+R180E EMC3 with or without the p97 inhibitor CD-5083 using the split GFP reporter system described above. (**E**) Model for how the EMC distinguishes clients by polar domain charge. A TA protein TMD or the first TMD of a multipass membrane protein is initially captured by flexible hydrophobic loops in the cytosol, allowing their C- or N-terminal domain (CTD/NTD) to probe the net positively charged hydrophilic vestibule. In the absence of positive charge, the polar domain is translocated rapidly, enabling TMD insertion. Insertion of TA proteins with positively charged C-termini or multipass TMDs with positively charged N-termini is slowed by charge repulsion, which facilitates TMD dissociation (rejection). Charge repulsion can be alleviated by introducing negative charge into the hydrophilic vestibule, resulting in increased misinsertion of mitochondrial TA proteins into the ER membrane, as well as increased insertion of multipass proteins in the incorrect topology.

2.5 Material and Methods

Plasmids and antibodies

Constructs for *in vitro* translations in rabbit reticulocyte lysate were based on the pSP64 vector (Promega, USA). Constructs for *in vitro* translation in the E. coli PURExpress system were generated from the T7 PURExpress plasmid (New England Biolabs, USA). pSpCas9(BB)-2A-Puro (PX459) and lentiCRISPR v2 were gifts from Feng Zhang (Addgene plasmids #48139 and #52961). pLG1-puro non-targeting sgRNA 3, used for cloning CRISPRi sgRNAs, was a gift from Jacob Corn (Addgene plasmid #109003). The second generation lenti-viral packaging plasmid psPAX2 (Addgene plasmid #12260) and envelope plasmid pMD2.G (Addgene #12259) were gifts from Didier Trono. The pHAGE2 lenti-viral transfer plasmid was a gift of Magnus A. Hoffmann and Pamela Bjorkman. For expression in K562 cells, a lenti-viral backbone containing a UCOE-EF-1α promoter and a 3′ WPRE element was used (Addgene #135448), which was a kind gift of Martin Kampmann and Jonathan Weissman. The expression plasmid for the $SENP^{EuB}$ protease (Addgene ID #149333) was a gift of Dirk Görlich. Plasmids for amber suppression in mammalian cells were kind gifts of Simon Elsässer. Note that the mCherry variant of RFP was used throughout this study, but the simpler nomenclature of RFP is used in the text and figures. Similarly, EGFP is used throughout this study, but referred to as GFP.

The following antibodies were used in this study: rabbit polyclonal anti-EMC2 (25443-1-AP, Proteintech, USA); mouse polyclonal anti-EMC3 (67205-1-Ig, Proteintech, USA); rabbit polyclonal anti-EMC4 (27708-1-AP, Proteintech, USA); rabbit polyclonal anti-EMC5 (A305-833, Bethyl Laboratories, USA); rabbit polyclonal anti-EMC7 (27550-1-AP, Proteintech, USA); rabbit monoclonal anti-EMC10 (ab180148, Abcam, UK); rabbit polyclonal anti-GET2 (#359 002, Synaptic Systems, Germany); mouse monoclonal anti-HA-HRP (H6533, Millipore-Sigma, USA); mouse monoclonal anti-FLAG M2-HRP (A8592, Millipore-Sigma, USA). The rabbit polyclonal antibodies against BAG6 and GFP were gifts from Ramanujan Hegde (Chakrabarti and Hegde, 2009; Mariappan et al., 2010). Secondary antibodies used for Western blotting were: Goat anti-mouse- and anti-rabbit-HRP (#172-1011 and #170-6515, Bio-Rad, USA). The chemiluminescent substrates used were SuperSignal West Pico PLUS and SuperSignal West Femto Maximum Sensitivity (34580 and 34096, Thermo Fisher Scientific, USA). The signal was detected on Blue Devil Autoradiography Film (#30-101, Genesee Scientific, USA).

The following sgRNAs were cloned into PX459 or lentiCRISPR v2 and used to generate knockout cell lines: EMC3 (AAGAAAGTGATGATAACGAT); EMC4 (TCATACACACCATCATAGTA); EMC6 (GCCGCCTCGCTGATGAACGG); EMC7 (TTCTCCGTCTACCAGCACTC); EMC10 (AGTGCCAACTTCCGGAAGCG). The following sgRNAs were cloned into pLG1 for CRISPRi knockdowns: non-targeting control (GGCTCGGTCCCGCGTCGTCG); EMC2 (GCCATCTTCCCAGAACCTAG); GET2 (ATGTTGGCCGCCGCTGCGA); MTCH2 (GACGGAGCCACCAAGCGACC).

The following siRNAs were used in this study: negative control no. 2 siRNA (#4390846) and EMC5 siRNA s41131 (both Silencer Select; Thermo Fisher Scientific, USA)

Expression and purification of biotinylated anti-GFP and anti-ALFA nanobody

Protease-cleavable biotinylated anti-GFP and anti-ALFA tag nanobodies (Götzke et al., 2019; Kirchhofer et al., 2010) that were used for EMC purifications throughout this study were expressed in *E. coli* and purified using Ni^{2+}-chelate affinity chromatography using protocols described in detail before (Pleiner et al., 2015; Pleiner et al., 2020; Stevens et al., 2023). The expression of His_{14}-Avi-$SUMO^{Eu1}$-anti GFP nanobody from plasmid pTP396 (Addgene #149336) was carried out with the following modification. Instead of biotinylating the nanobody *in vitro* with purified biotin ligase BirA, pTP396 was expressed in the *E. coli* strain AVB101 (Avidity, USA), which contains an IPTG-inducible plasmid for BirA co-expression. 50 µM biotin was added to the main culture 1 h before induction of nanobody and BirA expression.

The sequence of the $ALFA^{ST}$ nanobody was derived from the original study describing its generation (Götzke et al., 2019) and cloned into pTP396. Expression was carried out in E. coli Rosetta-gami 2 cells (Millipore-Sigma, USA) in a 1 L scale for 6 h at 18˚C after induction of protein expression with 0.2 mM IPTG. The resulting His_{14}-Avi-$SUMO^{Eu1}$-anti ALFA nanobody fusion protein was purified from cell lysate using Ni^{2+}-chelate affinity chromatography for *in vitro* biotinylation with purified biotin ligase BirA as described before (Pleiner et al., 2020).

Immobilized biotinylated nanobodies were cleaved off of streptavidin magnetic beads using an engineered SUMO protease ($SENP^{EuB}$) that recognizes the $SUMO^{Eu1}$ module (Vera Rodriguez et al., 2019). His_{14}-Tev-tagged $SENP^{EuB}$ protease (Addgene ID #149333) was expressed in *E. coli* NEB express I^q as described before (Pleiner et al., 2020). For sequential immunoprecipitations, a

commercial system with orthogonal cleavage sites based on the SUMOStar tag and SUMOStar protease (LifeSensors, USA) (Liu et al., 2008) was used.

Conjugation of ALFA nanobody to HRP for Western blotting

To use the ALFA nanobody in Western blotting, it was coupled to HRP-maleimide via a single engineered C-terminal cysteine residue as described for other nanobodies before (Pleiner et al., 2018).

Mammalian *in vitro* translation

In vitro translation reactions in rabbit reticulocyte lysate (RRL) were carried out with *in vitro* transcribed mRNA as described before (Sharma et al., 2010). PCR products generated from pSP64-derived plasmids or gene fragments (synthesized by Integrated DNA Technologies or Twist Biosciences, both USA) served as templates for run-off transcription and contained a 5' SP6 promoter followed by an open-reading frame and a 3' stop codon. A 10 µl transcription reaction contained 7.6 µl T1 mix (Sharma et al., 2010), 0.2 µl SP6 polymerase (New England Biolabs, USA), 0.2 µl RNAsin (Promega, USA), 100 ng PCR product, and was carried out for 1.5 h at 37˚C. Transcriptions were added directly to RRL. Unless indicated otherwise, RRL was treated with S7 micrococcal nuclease (Roche, Germany) in the presence of $CaCl_2$ to remove endogenous hemoglobin mRNA. Nascent proteins are labeled during translation reactions of 15-30 min at 32˚C in RRL by incorporation of radioactive ^{35}S-methionine (Perkin Elmer, USA). Nascent TA proteins were released from the ribosome with 1 mM puromycin and then incubated with 5% (v/v) of either canine pancreatic rough microsomes (cRMs) (Walter and Blobel, 1983) or human ER-derived microsomes (hRMs), prepared from engineered cell lines as described below, for another 20 min at 32˚C. Samples were analyzed by SDS-PAGE and autoradiography to detect the translated 35S-labeled TA protein.

Successful post-translational insertion into microsomes was monitored by glycosylation of a canonical NXS/T acceptor motif. This was appended either as part of a charged C-terminal opsin tag (MNGTEGPNFYVPFSNKTVD) or where no additional C-terminal domain charge was desired, an NGT motif was placed 22 amino acids downstream of the TMD after a neutral glycine-serine linker and followed by an additional C-terminal GS dipeptide.

Protease protection assay

To assess the membrane spanning topology of EMC7 and EMC10, they were tagged with an N-terminal 1xHA and a C-terminal 3xFLAG tag and translated in RRL in the presence of cRMs as described above. Protease-accessible regions of both proteins were digested by incubation with 0.5 mg/ml Proteinase K for 1 h at 4˚C in the presence or absence of 0.05% (v/v) Triton X-100 to solubilize cRM membranes. Proteinase K was inactivated by addition of 5 mM PMSF and quick transfer into boiling SDS buffer (100 mM Tris/HCl pH 8.4; 1% [w/v] SDS). Denatured digestion reactions were diluted tenfold with IP buffer (50 mM HEPES/KOH pH 7.5; 300 mM NaCl; 0.5% [v/v] Triton X-100) and incubated with anti-HA or anti-FLAG M2 resin (Millipore-Sigma, USA) for 1 h at 4˚C for immunoprecipitation of protected fragments.

Preparation of human ER-derived microsomes (hRMs)

To prepare hRMs from Expi293 suspension cell lines, cells were harvested and then washed twice in 50 ml 1x PBS. Cells were then resuspended in 4x pellet volume of sucrose buffer (10 mM HEPES/KOH pH 7.5.; 2 mM MgAc; 250 mM Sucrose, 1x Protease inhibitor cocktail [Roche, Germany]) and lysed with ˜50 strokes in a tight-fit dounce homogenizer. Complete cell lysis was verified by trypan blue staining. The lysate was then diluted twofold and spun for 30 min at 3,214 xg in a table-top centrifuge at 4˚C to remove nuclei and cell debris. This spin was repeated and the resulting supernatant was then centrifuged for 1 h at 75,000 g at 4˚C (TLA-100.3 rotor or Type60 Ti rotor; Beckman Coulter, USA). The supernatant was aspirated and the membrane pellet gently resuspended in microsome buffer (10 mM HEPES/KOH pH 7.5; 1 mM MgAc; 250 mM Sucrose, 0.5 mM DTT). Membranes prepared for disulfide crosslinking were resuspended in microsome buffer without DTT. The absorbance at 280 nm of the resuspended membranes was measured by boiling an aliquot in SDS buffer (100 mM Tris/HCl pH 8.4; 1% [w/v] SDS). The hRM preparation was then adjusted to an absorbance of 75 at 280 nm using microsome buffer. To remove endogenous mRNAs, the adjusted hRM preps were further treated with S7 micrococcal nuclease (Roche, Germany) at a concentration of 0.075 U/µl in the presence of 0.33 mM $CaCl_2$ for 6 min in a 25˚C water bath, then quickly removed to ice and quenched by Ca^{2+}-chelation with 0.66 mM EGTA. Nucleased hRMs were snap-frozen in liquid nitrogen in single-use aliquots and stored until further use at -80˚C.

In vitro translation of TA proteins in the PURExpress system

Plasmids containing a 5' T7 promoter, followed by an open-reading frame, stop codon and 3' T7 terminator were used as templates for the coupled *in vitro* transcription/translation PURExpress system (New England Biolabs, USA). The various SQS constructs used for cysteine crosslinking comprised an N-terminal 3xFLAG tag, the human Sec61β cytosolic linker (residues 2-59) with the natural cysteine at position 39 mutated to serine, as well as the five N-terminal flanking residues, TMD and complete C-terminus of human FDFT1/SQS (residues 378-end). Cysteine residues were introduced at the indicated positions using site-directed mutagenesis. TA protein translations were supplemented with radioactive ^{35}S-methionine and 10 µM purified Calmodulin (CaM) (Shao et al., 2017).

For use in photocrosslinking reactions, TA protein substrates were generated that contained the unnatural amino acid and photocrosslinker 4-Benzoylphenylalanine (BpA) (Bachem, Switzerland), which was incorporated into the TMD by amber stop codon suppression in the PURExpress system lacking all release factors (ΔRF123; New England Biolabs, USA). The release factors RF2 and RF3, but not RF1 (which recognizes the UAG [amber] stop codon) were added back to the reaction. BpA was added at 100 µM and incorporated at UAG codons using purified BpA aminoacyl-tRNA synthetase and suppressor tRNA, prepared as described before (Shao et al., 2017).

All PURE translation reactions were carried out for 2 h at 32˚C and then ribosome-associated nascent chains were released by addition of 1 mM puromycin (Thermo Fisher Scientific, USA) and further incubation for 10 min at 32˚C. To remove aggregated protein, the translation reactions were layered over a 20% (w/v) sucrose cushion prepared in physiological salt buffer (PSB) (50 mM HEPES/KOH pH 7.5; 130 mM KAc, 2 mM MgAc) that further contained 100 nM $CaCl_2$. After a 1 h spin at 55,000 rpm (TLS-55 rotor; Beckman-Coulter, USA) at 4˚C, soluble TA protein-CaM complexes were retrieved from the supernatant.

Photocrosslinking

Purified EMC complexes in detergent micelles for photocrosslinking were obtained via anti-GFP nanobody IP from stable human suspension cell lines that ectopically express GFP-EMC2. They were mixed with ^{35}S-Methionine labeled BpA-containing TA protein-CaM complexes generated in the PURExpress system as described above. TA proteins were released from CaM shortly before UV

radiation by addition of 1 mM EGTA to chelate calcium. Except for the -UV control sample, all reactions were irradiated at a distance of ~7-10 cm with a UVP B-100 series lamp (Analytik Jena, Germany) for 15 min on ice before quenching with SDS-PAGE sample buffer. Samples were adjusted to 1% (w/v) SDS and boiled. Denatured reactions were diluted tenfold with IP buffer (50 mM HEPES/KOH pH 7.5; 300 mM NaCl; 0.5% [v/v] Triton X-100) and incubated with Protein A sepharose beads (Thermo Fisher Scientific, USA) and EMC3 or EMC4 antibodies for immunoprecipitation. Samples were analyzed by SDS-PAGE and autoradiography.

Site specific incorporation of the photocrosslinking amino acid 3'-azibutyl-N-carbamoyl-lysine (AbK) into EMC3 in mammalian cells was performed by amber suppression using the *Methanosarcina mazei* pyrrolysyl-tRNA synthetase (PylRS)/$tRNA^{Pyl}_{CUA}$ (PylT) pair (Ai et al., 2011). Constructs for amber suppression in mammalian cells were created as follows using previously reported plasmids as a template (Elsässer et al., 2016). The first plasmid encodes 4 copies of PylT(U25C), as well as WT PylRS, which was further modified by mutating Y306A and Y384F to accommodate the bulky AbK (Yanagisawa et al., 2008; O'Donnell et al., 2020). The coding region of EMC3 was inserted with a C-terminal GFP-tag into a second plasmid which also encoded 4 additional copies of PylT(U25C). Selected amino acid positions in EMC3 were mutated to amber stop codons, for incorporation of AbK at these sites. To generate AbK-containing EMC, Expi293 cells (Thermo Fisher Scientific, USA) were transiently co-transfected with 4xPylT/PylRS(Y306A, Y384F) and 4xPylT/EMC3(Amber[TAG])-GFP plasmids at a ratio of 4:1 using PEI "MAX" (Polysciences, USA). The cells were grown in the presence of 0.5 mM AbK (Iris Biotech, Germany) and harvested 72 h after transfection. EMC complexes with successfully suppressed Amber stop codons contained full length AbK-modified EMC3 and could thus be purified via the C-terminal GFP-tag as described below. The purified EMC complexes were mixed with ^{35}S-Methionine labeled SQS(WT)-CaM complexes generated in the PURExpress system and irradiated with UV as described above. Samples were analyzed by SDS-PAGE and autoradiography.

Disulfide crosslinking

EMC complexes containing wild type or cysteine mutant EMC3 or EMC7 variants were purified from stable human suspension cell lines as described below and mixed with wild type or cysteine mutant SQS-CaM complexes generated in the PURExpress system as described above. The zero-length disulfide crosslinker 4,4'-Dipyridyldisulfide (DPS) (Millipore-Sigma, USA) was added to a final concentration of 250 µM to initiate the crosslinking of cysteines in close proximity after SQS

release from CaM with 1 mM EGTA. The reaction was incubated for 2 h on ice and analyzed by SDS-PAGE and autoradiography.

For disulfide crosslinking in membranes, hRMs were prepared from stable human suspension cell lines expressing wild type or cysteine mutant EMC3 variants as described above. hRMs were mixed with PURE translated SQS-CaM complexes in PSB and 500 µM DPS. After substrate release with 500 µM EGTA, reactions were incubated for 2 h on ice before quenching with 5 mM L-Cysteine (Millipore-Sigma, USA). The reactions were then adjusted to 1% (w/v) SDS and incubated at room temperature for 10 min to denature the EMC complex. The denatured reactions were diluted tenfold with IP buffer (50 mM HEPES/KOH pH 7.5; 300 mM NaCl; 0.5% [v/v] Triton X-100) and the EMC3-GFP subunit was specifically enriched via anti-GFP nanobody IP. After elution by boiling in sample buffer containing 0.5 M urea, the samples were analyzed by SDS-PAGE and autoradiography.

Cell culture and cell line generation

Adherent HEK293 cell lines were cultured in Dulbecco's Modified Eagle Medium (DMEM) supplemented with 10% fetal calf serum (FCS) and 2 mM L-Glutamine. For Flp-In T-Rex 293 cell lines containing integrated doxycycline-inducible reporters, tetracycline-free FCS was used and culture medium additionally supplemented with 15 µg/ml blasticidin S and 100 µg/ml hygromycin B. RPE1 cells were cultured in DMEM/F-12 (1:1) supplemented with 10% FCS and 2 mM L-Glutamine.

Flp-In 293 T-Rex cells were purchased from Thermo Fisher Scientific (USA). Stable Flp-In 293 T-Rex cell lines designated as GFP-2A-RFP-SQS/VAMP2 express the RFP-tagged transmembrane domain and flanking regions of human squalene synthase (SQS/FDFT1) or vesicle-associated membrane protein 2 (VAMP2). The generation of these cell lines was described previously (Guna et al., 2018; Pleiner et al., 2020). In these cell lines, GFP is expressed as a soluble cytosolic protein from the same mRNA as RFP-SQS/VAMP2 using a viral 2A sequence that induces peptide-bond skipping by the ribosome (de Felipe et al., 2006). Their RFP and GFP fluorescence intensity can be measured by flow cytometry to derive an RFP:GFP ratio. Changes in this ratio after perturbation, e.g. expression of a mutant EMC subunit, reflect differences in the post-translational stability of the TA protein reporter.

The stable, doxycycline-inducible GFP-EMC2 Flp-In 293 T-Rex cell line and its adaptation to suspension growth in FreeStyle 293 Expression Medium (Thermo Fisher Scientific, USA) was described before (Pleiner et al., 2020). Clonal knockouts of EMC4, 7 and 10 in this background were obtained by transfecting the adherent parental cell line with PX459 encoding the respective sgRNA using TransIT-293 transfection reagent (Mirus, USA). 48 h post transfection, 1 µg/ml puromycin was added for three consecutive days. Medium was subsequently exchanged to allow for two days of recovery before single cell clones were seeded into 96-well plates by limiting dilution. Knockout efficiency of the selected clones was verified by Western blotting and the resulting adherent knockout cell lines were either used directly for flow cytometry experiments or adapted to suspension growth for EMC purifications.

Expi293 cells (Thermo Fisher Scientific, USA) were maintained at a concentration of 0.5-2.0 million cells per ml in Expi293 Expression Medium (Thermo Fisher Scientific, USA). An EMC3 knockdown suspension cell line was generated by transient transfection of Expi293 cells with an EMC3 sgRNA cloned into lentiCRISPR v2 using PEI "MAX" (Polysciences, USA). Transfected cells were treated with 10 µg/ml puromycin for four consecutive days. Then the medium was exchanged to allow for 10 days of recovery. The polyclonal cell population demonstrated a sufficient level of consistent downregulation of endogenous EMC3 and was thus used directly to re-introduce wild type EMC3 or various mutants tagged with a C-terminal TagBFP or GFP via lenti-viral transduction as described below. Transduced cell lines were sorted using fluorescence of the fused TagBFP or GFP to obtain a homogenous population of cells with near full replacement of endogenous EMC3 with a tagged mutant copy of interest. Wild type EMC7 or various cysteine mutants with an N-terminal ALFA tag were introduced via lenti-viral transduction into the EMC3-GFP cell line.

A K562 CRISPRi cell line, stably expressing dCas9-BFP-KRAB Tet-ON (Jost et al., 2017), was transduced with lentivirus as described below to constitutively express β-strands 1-10 of superfolder GFP (residues 2-214) (Cabantous et al., 2005) in the ER lumen via fusion to an N-terminal signal sequence and a C-terminal KDEL sequence as described previously (Guna et al., 2022b).

CRISPRi knockdowns

K562 dCas9-BFP-KRAB Tet-ON, ER GFP1-10 cells were transduced via spinfection as described below with lentivirus containing a pLG1-puro backbone and a sgRNA targeting a gene of interest. Sequences of sgRNAs were derived from the hCRISPRi-v2 compact library (Horlbeck et al., 2016).

48 h after spinfection, 1 μg/ml puromycin was added for three consecutive days to select cells with a successfully integrated sgRNA expression cassette. After two days of recovery, cells were transduced with GFP11-tagged TA protein reporters expressed from a lentiviral backbone under control of a UCOE-EF1α promoter. Cells were analyzed 48 h after reporter spinfection by flow cytometry (8 days after sgRNA transduction).

Lenti-viral transduction

Lentivirus was generated by co-transfection of HEK293T cells with a desired transfer plasmid and two packaging plasmids (psPAX2 and pMD2.G) using the TransIT-293 transfection reagent (Mirus, USA). 48 h post transfection, culture supernatant was harvested, aliquoted, and flash frozen in liquid nitrogen.

For transduction of Expi293 or suspension-adapted Flp-In 293 T-Rex cells, 20 million cells were mixed with 2.5 ml freshly harvested lenti-viral supernatant (i.e. the complete supernatant from one 6-well of lenti-producing HEK293T cells 48 h after transfection) in 20 ml medium in a 125 ml vented Erlenmeyer flask (Celltreat, USA) (Stevens et al., 2023). Then the flask was transferred to a shaking incubator and transduced cells were grown for around 16 h. Cells were then pelleted, resuspended in 50 ml of fresh medium, and grown for 2-3 days before sorting of successfully transduced cells on a SH800S cell sorter (Sony Biotechnology, USA).

K562 cells were transduced by spinfection. Briefly, 250,000 cells were mixed with 50-200 μl of lentiviral supernatant and RPMI medium in the presence of 8 μg/ml polybrene in a total volume of 1 ml in a 24-well plate. 24-well plates were spun at 1,000 xg for 1.5 h at 30˚C. Cells were then resuspended and transferred to a 6-well plate. Lenti-viral reporter constructs used in K562 cells for flow cytometry analysis all contained an upstream UCOE-EF1α promoter, followed by RFP, a P2A site, and the full length human coding regions for all mitochondrial TA proteins fused to GFP11 via a five residue Gly-Ser linker. SQS mutants were expressed in the same cassette, but contained the cytosolic linker (residues 2-70) of human Sec61β at the N-terminus followed by the TMD, N-terminal flanking region and complete C-terminus of human FDFT1/SQS (residues 378-417 [end]). Charge mutations were introduced as shown in Figure 2.4B. EMC3 WT or its arginine mutants were expressed in K562 cells from a lentiviral transfer plasmids with an upstream EF1α promoter and fused to a C-terminal TagBFP-3xFLAG tag.

For lenti-viral transduction of adherent HEK293 or RPE1 cells, 50-200 µl lentiviral supernatant and 8 µg/ml polybrene (Millipore-Sigma, USA) were usually added directly to ~70% confluent cells in 2.5 ml culture medium in a 6-well. Lenti-viral reporter constructs of SQS and VAMP2 for use in HEK293 cells (Figures 2.3C,E, S2.3E, S2.4A,D-E, S2.5A-B,D) contained an upstream CMV promoter, followed by GFP, a 2A site, and RFP, which was directly fused to the TMD and flanking regions of human FDFT1/SQS or VAMP2 as described before (Guna et al., 2018; Pleiner et al., 2020). OPRK1 reporter constructs used in RPE1 cells, expressed full length human OPRK1 (WT/-5), OPRK1(E45K, D46R, E50K) (+1 variant) or OPRK1(E35K, D37R, E45K, D46R, E50K) (+5 variant) as N-terminal fusions to GFP, followed by a 2A site, and RFP from a CMV promoter.

Flow cytometry analysis of reporter cell lines

All adherent cells were trypsinized, washed, and resuspended in 1xPBS for flow cytometry analysis. K562 cells were analyzed directly. Analysis was either on an Attune NxT Flow Cytometer (Thermo Fisher Scientific, USA) or a MACSQuant VYB (Miltenyi Biotec, Germany). Flow cytometry data was analyzed using FlowJo v10.8 Software (BD Life Sciences, USA). Unstained cells transiently transfected with either GFP, RFP (or BFP if needed) were analyzed separately along every run as single-color controls for multicolor compensation using the FlowJo software package.

For experiments in K562 cells, lenti-viral fluorescent reporters were introduced via spinfection as described above usually 48 h before analysis. To probe the effect on EMC2 or GET2 knockdown on reporter insertion, cells were additionally transduced with sgRNA expressing lenti-viral vectors as described under ‘CRISPRi knockdowns’. To analyze the effect of EMC3 mutations on TA protein reporters, K562 cells were first spinfected with lentivirus expressing EMC3(WT/mut)-BFP. After 48 h, mitochondrial TA protein or SQS charge mutant reporter lentivirus was spinfected. Cells were analyzed by flow cytometry after another 48 h. For experiments with p97 inhibitor (CD-5083 [Selleckchem, USA]) the cells were treated with 1.25 µM inhibitor for the last 6 h before analysis. Adherent HEK293 or RPE1 cells were analyzed 48 h after transduction as described above.

Purification of engineered EMCs from stable suspension cell lines

Stable human suspension cell lines expressing tagged wild type or mutant copies of EMC subunits were generated and grown as described above. EMC complexes were purified using anti-GFP or anti-ALFA nanobody essentially as described before (Pleiner et al., 2020; Stevens et al., 2023). Cells were

harvested by centrifugation for 10 min at 3,000 xg and washed in 1xPBS. Cell pellets were resuspended with 6.8 ml solubilization buffer (50 mM HEPES/KOH pH 7.5; 200 mM NaCl; 2 mM MgAc; 1% [w/v] LMNG [Anatrace, USA], 1 mM DTT, 1x complete EDTA-free protease inhibitor cocktail [Roche, Germany]) per 1 g of cell pellet and incubated for 30 min at 4˚C. Lysates were cleared by centrifugation for 30 min at 4˚C at 18,000 rpm (SS-34 rotor; Beckman-Coulter, USA).

In parallel, Pierce magnetic Streptavidin beads (Thermo Fisher Scientific, USA) were equilibrated in wash buffer (solubilization buffer with 0.0025% [w/v] LMNG) and then incubated with biotinylated anti-GFP or anti-ALFA tag nanobody, purified as described above. After nanobody immobilization, free biotin binding sites were blocked by incubation with wash buffer containing 10 µM $dPEG_{24}$-biotin acid (Quanta Biodesign, USA) for 10 min on ice. Blocked, nanobody-decorated beads were then added to cell lysate for binding to detergent-solubilized ALFA- or GFP-tagged EMC complexes for 1 h at 4˚C with head-over-tail mixing. Magnetic beads were then collected and washed three times with wash buffer, before resuspension of the beads in wash buffer containing 250 nM $SENP^{EuB}$ protease in a volume amounting to one half of the original bead suspension volume. Protease elution was allowed to proceed for 20 min on ice. All EMC complexes purified for disulfide crosslinking were eluted in wash buffer without DTT.

EMC complexes containing fully replaced cysteine mutant EMC7 variants were purified via a two-step procedure using first the C-terminal GFP tag on EMC3 and then the N-terminal ALFA tag on EMC7. The GFP nanobody eluate, obtained by $SENP^{EuB}$ cleavage, was diluted twentyfold with wash buffer and incubated with beads containing immobilized ALFA nanobody. The ALFA nanobody was tagged with an orthogonal SUMOStar protease cleavage site and bound EMC was then eluted along with the ALFA nanobody in wash buffer containing 500 nM SUMOStar protease. The resulting eluate was aliquoted and flash frozen in liquid nitrogen. The concentrations of purified EMC complexes for disulfide crosslinking were normalized by measuring GFP fluorescence on a BioTek Synergy HTX plate reader (Agilent, USA). Normalization was verified by SDS-PAGE and Sypro Ruby staining (Thermo Fisher Scientific, USA). If necessary, normalizations were adjusted based on the quantification of Sypro Ruby stained EMC subunit bands in Fiji.

Purification of EMC for structure determination

A suspension-adapted GFP-EMC2 Flp-In 293 T-Rex cell line (Pleiner et al., 2020) was used to purify the EMC for structural analysis. Additionally, EMC7 carrying a C-terminal ALFA tag was introduced

into this cell line via lenti-viral transduction as described above. The lenti-viral transfer plasmid encoded EMC7-ALFA fused via a viral 2A sequence to BFP (EMC7-ALFA-2A-TagBFP). BFP fluorescence was used to sort a homogenous stable suspension cell line that ectopically expresses both GFP-EMC2 and EMC7-ALFA. EMC was purified as described above, but with the following minor modifications. Cells were solubilized with solubilization buffer containing 1% glyco-diosgenin (GDN) (Anatrace, USA). The wash buffer contained 0.05% [w/v] GDN. Finally, the EMC eluate was concentrated using an Amicon Ultra 0.5 ml 100K MWCO concentrator (Millipore-Sigma, USA) and further purified via size-exclusion chromatography using a Superose 6 Increase 3.2/300 column (Cytiva, USA) equilibrated in wash buffer (50 mM HEPES/KOH pH 7.5; 200 mM NaCl; 2 mM MgAc; 0.05% [w/v] GDN and 1 mM DTT). Fractions corresponding to the EMC were pooled and concentrated as above to 0.5 mg/ml. To reduce the conformational flexibility of EMC7 at the insertase side, we added stoichiometric amounts of purified ALFA nanobody (Götzke et al., 2019), which binds the C-terminal ALFA tag on EMC7.

Grid preparation and data collection

CryoEM grids were prepared by applying 3 µl of purified EMC at 0.5 mg/mL to glow discharged (60 seconds using a Pelco easiGlow, Emeritech K100X at a plasma current of 20 mA), Holey carbon grids (Quantifoil R1.2/1.3). The sample was blotted for 4-6 sec with filter paper at 8°C, 100% humidity at a -4-blot force prior to plunging into liquid ethane for vitrification using the FEI Vitrobot Mark v4 x2 (Thermo Fisher Scientific, USA). The data set was acquired on a Titan Krios electron microscope (Thermo Fisher Scientific, USA) operated at 300 keV equipped with a K3 direct electron detector and an energy filter (Gatan, USA) with a 20-eV slit width. A total of 11,822 micrographs were collected using 3-by-3 pattern beam image shift, acquiring movies for three non-overlapping areas per hole, using an automated acquisition pipeline in SerialEM (Mastronarde, 2005). Movies were recorded with 40 frames at a magnification of 105,000x in super resolution mode at a calibrated magnification of 0.416 Å/pixel using a dose of 60 e−/Å2 at a dose rate of 16.0 e−/pixel/s and a defocus range of −1.0 to −3.0µm.

Image processing

The data processing workflow is summarized in Figure S2.2 and was performed using cryoSPARC v.3.3–v.4.0 (Punjani et al., 2017). In short, 11,822 micrographs were motion corrected, dose weighted, and down sampled (two-fold to 0.832 Å/pixel) using the Patch Motion followed by patch-

based CTF estimation using Patch CTF. 10,206 movies were selected and manually curated using cut-offs for CTF fit (5.0 Å) and total motion (50 pix) for further processing. The particle picking was done using the automated Blob Picker function with particle diameter of 150 to 400 Å. After two rounds of 2D classification, 1,271,124 particles were used for two rounds of heterogeneous ab initio reconstruction (4 volumes), using Maximum/Initial resolution of 9 and 7Å respectively and an Initial/Final minibatch size of 400 and 1,200 particles respectively. Once we obtained an initial map with clear features of the EMC, we reclassified the 1.2 million particles using 3D heterogeneous classification using one well-defined class of the EMC and three decoy classes, using a batch size of 5,000 particles per class and initial low-pass filter of 50 Å. Prior to the final round of classification of 212,440 particles were re-extracted in a box size of 400 pix. The final round of classification yielded a population 193,900 particles that were further refined using non-uniform refinement to obtain a reconstruction at 3.5 Å resolution.

To explore the previously observed flexibility between the lumenal, membrane, and cytoplasmic domains, the particles were subjected to two rounds of 3D-variability analysis/clustering, selecting five modes and a filter resolution ranging from 4.0-8.0 Å. After carefully analyzing each reconstruction, a mode corresponding to a missing subunit of the EMC was identified. The subset of particles was then split into 20 clusters using 3D Variability Analysis Display for this mode. Particles belonging to the nine-subunit complex (156,706 particles) that contained high-resolution features were combined and refined using non-uniform refinement. This yielded a map with a resolution of 3.6 Å, in which we detected a stronger EM density for the TMDs of EMC4 and 7.

Particles belonging to the eight-subunit complex (37,194 particles) were combined and similarly to the nine-subunit complex, the particles were refined using non-uniform refinement. This yielded a map with a resolution of 3.9 Å. All three maps (consensus, 9- and 8-subunit) were post-processed by applying a sharpening B factor of -112 $Å^2$, -103 $Å^2$, and -76 $Å^2$, respectively. Finally, for the analysis of EMC10's TMD position a low-pass filter of 5.5 Å was applied to each map using volume tools in cryoSPARC.

All map resolutions were calculated at the final round of refinement using the gold standard FSC=0.143 criterion from the half maps. Statistic details of the EMC EM maps are reported in Table 2.1.

Model building and refinement

An initial model for the nine-subunit EMC was generated by docking the EMC structure in a lipid nanodisc (PDB: 6WW7) (Pleiner et al., 2020) into the cryo-EM density using UCSF Chimera (Pettersen et al., 2004) followed by an initial round of refinement using Phenix (Liebschner et al., 2019). Next, for the not well-ordered TMDs of EMC4 and 7 high-confidence subcomplexes EMC3 (residues 5-42 and 101-209), EMC4 (59- 155), EMC6 (12-end), and EMC7 (155-178) were generated using AlphaFold2-Multimer ColabFold (AlphaFold2_advanced.ipynb) (Mirdita et al., 2022) and then rigid body fitted into the densities. Finally, all models were combined and further manual refinement was conducted in COOT (Casañal et al., 2019; Emsley et al., 2010). Next, lipids, N-glycans and disulfide bond pairs were added where justified by both the EM density and its chemical environment. Finally, the final model was refined against the 9-subunit map using phenix.real_space_refine. Although we could successfully model a backbone through the contiguous density of the TMDs of EMC4 and 7, we could not unambiguously assign its registry and therefore these TDMs were assigned as poly-Ala/Gly in the final model. Statistic details of the EMC model are reported in Table 2.1. Figures were made using PyMol (Schrödinger LLC) and UCSF ChimeraX.

Online supplemental material

Figure S2.1 shows crosslinking and in cell reporter assay data in support of defining the hydrophilic vestibule as the insertase side of the EMC. Figure S2.2 shows an overview of the cryo-EM data processing pipeline. Figure S2.3 shows the updated atomic model of the EMC, as well as biochemical data characterizing the peripheral subunits EMC4, 7 and 10. Figure S2.4 shows in cell reporter assay and crosslinking data that demonstrate substrate capture by the cytosolic loops of EMC3 and 7. Figure S2.5 shows data demonstrating that intramembrane residues in EMC4 do not contribute significantly to TA protein insertion, as well as data highlighting the cooperative effect of mitochondrial insertase MTCH2 and the EMC selectivity filter in mitochondrial TA protein sorting. Table 2.1 lists cryo-EM data collection, refinement, and validation statistics.

Data availability

The data reported in this work are available in the published article and its online supplemental material. The atomic coordinates and cryo-EM maps have been deposited and openly available in the Protein Data Bank under accession code PDB 8S9S and in the Electron Microscopy Data Bank under

accession codes EMDB-40245 (nine-subunit map), EMDB-40246 (consensus map), and EMDB-40247 (eight-subunit map).

2.6 Supplementary Material

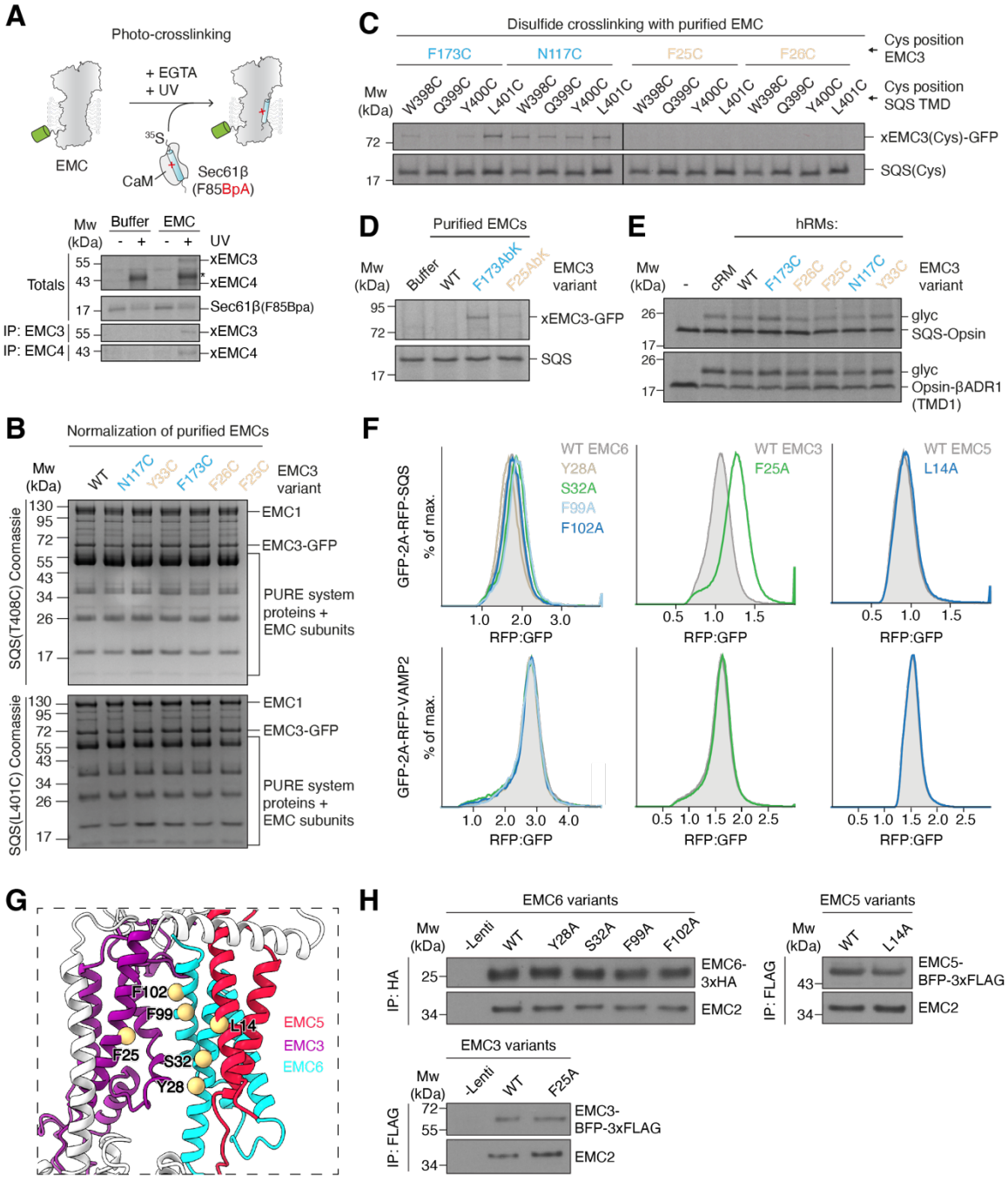

Figure S2.1. Defining the hydrophilic vestibule as the insertase-competent side.

(**A**) Schematic depiction of the site-specific photocrosslinking approach. The ^{35}S-methionine labeled TA protein substrate Sec61β, with a BpA photocrosslinker incorporated into its TMD, was produced

as a complex with calmodulin (CaM) in the PURE *in vitro* translation system. It was then incubated with EMC solubilized and purified in the detergent LMNG. Except for the -UV controls, all reactions were irradiated with UV light after substrate release from CaM with EGTA and then analyzed by SDS-PAGE and autoradiography. Crosslinks to EMC3 and EMC4 were identified by immunoprecipitation (IP) with anti-EMC3 and -EMC4 antibodies. The asterisk indicates the crosslinked TA protein dimer band. (**B**) Coomassie stained SDS-PAGE gel of the disulfide crosslinking experiments with purified EMC shown in Figure 2.2B before analysis via autoradiography. The gel shows that equal amounts of EMC were used in the different crosslinking reactions. (**C**) Disulfide crosslinking with purified EMC as in Figure 2.2B, but with cysteines positioned around a turn of the SQS TMD, showing that the observed crosslinking bias to residues on the hydrophilic vestibule (in blue) is independent of cysteine position. All crosslinking reactions were performed in parallel, and gels were exposed to the same film. (**D**) Purified EMC complexes containing the unnatural amino acid and photocrosslinker Abk incorporated into EMC3 at the indicated positions were mixed with SQS(WT)-CaM complexes prepared in the PURE system and irradiated with UV light after substrate release from CaM with EGTA. Samples were analyzed by SDS-PAGE and autoradiography. (**E**) Insertion activity of human ER-derived microsomes (hRMs) prepared from EMC3 WT or Cys mutant cell lines. Two well-characterized EMC substrates, SQS and TMD1 of the β-adrenergic receptor 1 (βADR1) (Chitwood et al., 2018; Guna et al., 2018), were translated in rabbit reticulocyte lysate in the presence of the indicated hRMs. Successful ER insertion results in the glycosylation (glyc) of the fused opsin tag. Canine pancreatic rough microsomes (cRMs) were used as a control. (**F**) HEK293 cells stably expressing RFP-SQS or -VAMP2 and cytosolic GFP as a normalization control were transduced with lentivirus to express the indicated mutants of EMC3, 5 and 6 in the hydrophobic crevice. The RFP:GFP ratio for each mutant was determined using flow cytometry and is plotted as a histogram. (**G**) Side-view of the membrane-spanning region of the EMC, focusing on the large cleft-like hydrophobic crevice. Residues on EMC3, 5 and 6 that were mutated in (F) line the cleft and are highlighted. (**H**) Incorporation of EMC subunit mutants into intact EMCs. A fraction of cells from (F) were harvested, solubilized, and subjected to anti-HA or anti-FLAG immunoprecipitation. Co-purification with the soluble subunit EMC2 indicates successful incorporation of WT and mutant EMC3, 5 and 6 variants, suggesting that all of the mutant subunits are assembled into the mature EMC.

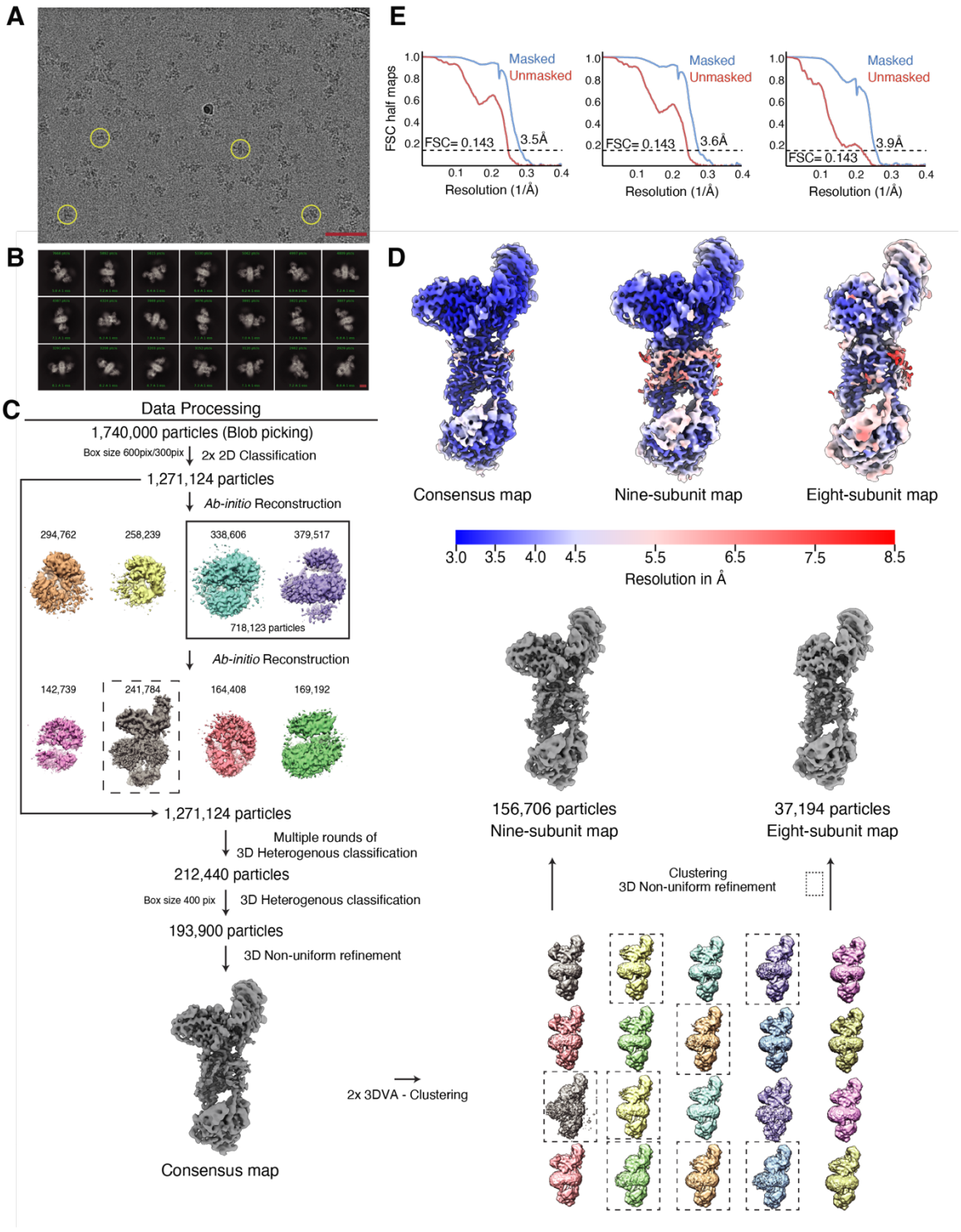

Figure S2.2. Classification and refinement procedure of an improved model of the human EMC.

(**A**) A representative micrograph with several particles highlighted with yellow circles. Scale bar = 75 nm. (**B**) Representative 2D class averages generated during data processing. Scale bar = 5 nm. The number of particles for each class and its resolution are indicated. (**C**) Flowchart highlighting the data processing pipeline used to obtain an improved structure of the EMC. The 3D Variability Analysis (3DVA) enabled the exploration of the heterogeneity of the sample and allowed to parse out a subset of particles that lack the subunit EMC10, which provided unique insights into the placement of EMC10's TMD. Particles with all nine subunits, or those missing EMC10 (dashed boxes) were combined separately. Particles with poorly-defined or low-resolution features were discarded (see Methods). (**D**) Final EM density maps colored by local resolution in Å. For clarity a dust filter was applied in ChimeraX. (**E**) Gold-standard Fourier Shell Correlation (FSC) curves for the consensus, 9- and 8-subunit complex maps generated by cryoSPARC V4.0.

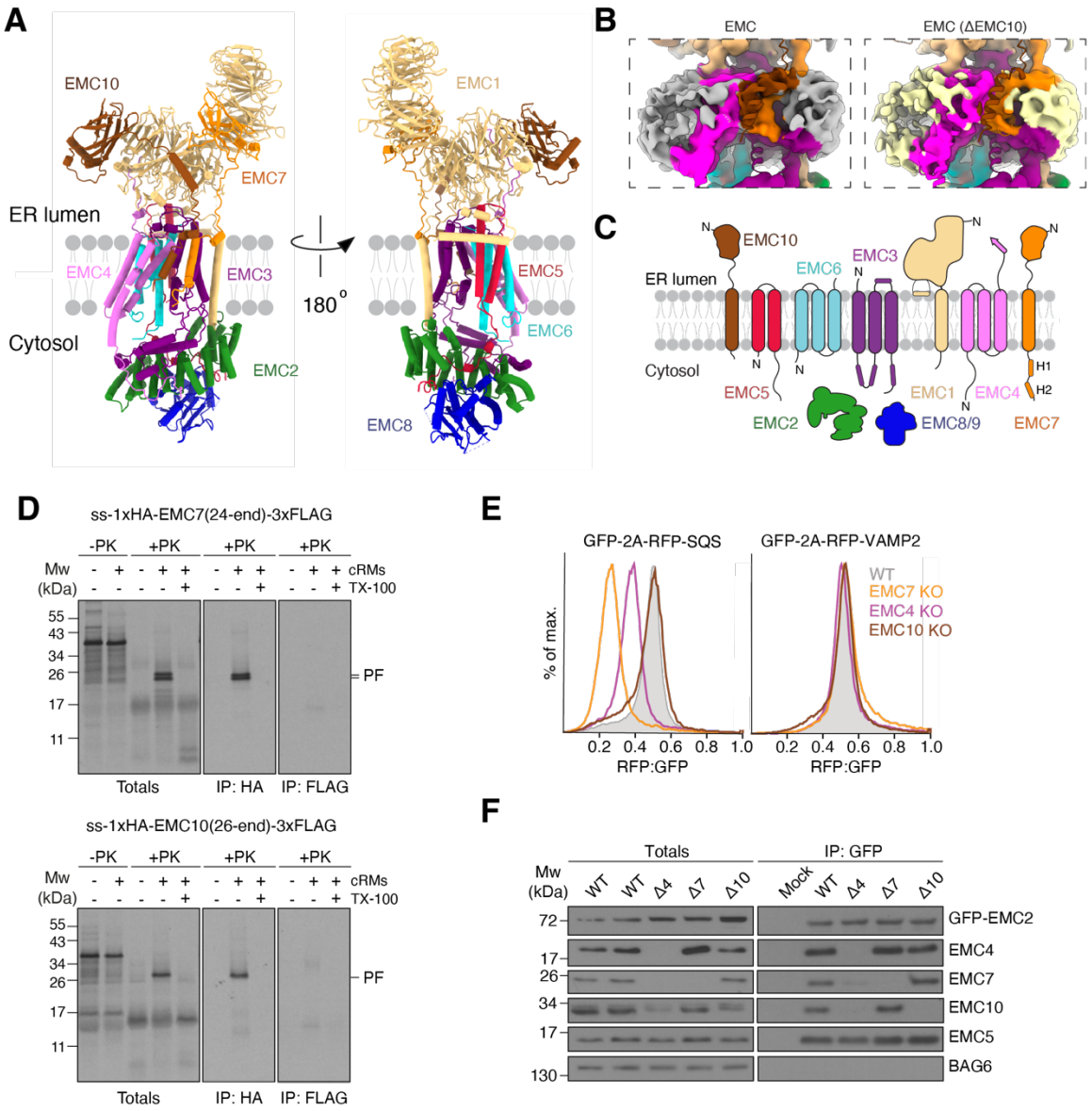

Figure S2.3. Architecture of the insertase-competent region of the EMC.

(**A**) Updated model of the EMC, with views of the hydrophilic vestibule (left) and hydrophobic crevice side (right). (**B**) Low-pass filtered maps (5.5 Å) generated using volume tools in cryoSPARC V4.0. (Left) 9-subunit EMC complex map colored by the EMC subunits with the atomic model displayed as a superimposed cartoon. The EM density for the detergent micelle is displayed in gray. (Right) 8-subunit EMC complex (ΔEMC10) map. Due to the inherently flexible nature of EMC10's TMD we could not unambiguously model its TMD; however, comparing +/Δ EMC10 maps gave insights into localization of its TMD because the ΔEMC10 map lacks additional density (colored in

brown) enclosing the hydrophilic vestibule of the EMC. (**C**) Updated schematic of the topology of all nine EMC subunits. EMC8 and 9 are mutually exclusive paralogs. (**D**) EMC7 and EMC10 span the membrane. ^{35}S-methionine labeled EMC7 (top) or EMC10 (bottom) carrying an N-terminal signal sequence (ss) and 1xHA tag, as well as a C-terminal 3xFLAG tag were in vitro translated in rabbit reticulocyte lysate supplemented with canine pancreatic rough microsomes (cRMs). Nascent chains were released from the ribosome with puromycin, and non-incorporated as well as cytosolically accessible proteins were digested with proteinase K (PK) in the presence or absence of Triton X-100 to solubilize the cRM membrane. The resulting protease protected fragments were subjected to denaturing anti-HA and anti-FLAG immunoprecipitations (IP). Note that only the N-terminal HA tags of EMC7 and EMC10 were protected (PF = protected fragment) from PK digestion, whereas the C-terminal 3xFLAG was PK-accessible, indicating a type I, single-spanning topology for both subunits. (**E**) EMC4 and EMC7, but not EMC10 are required for SQS biogenesis in human cells. WT or EMC4/7/10 KO HEK293 cells were transduced with lentivirus to express RFP-SQS or -VAMP2. The relative level of the RFP-fused TA protein to an internal GFP expression control was measured via flow cytometry and plotted as a histogram. (**F**) Purification of EMC complexes from HEK293 cells stably expressing GFP-EMC2 (WT), with or without additional knockout of EMC4, 7 or 10. Samples of total lysate and elution following an IP via GFP-EMC2 were analyzed by SDS-PAGE and western blotting with the indicated antibodies.

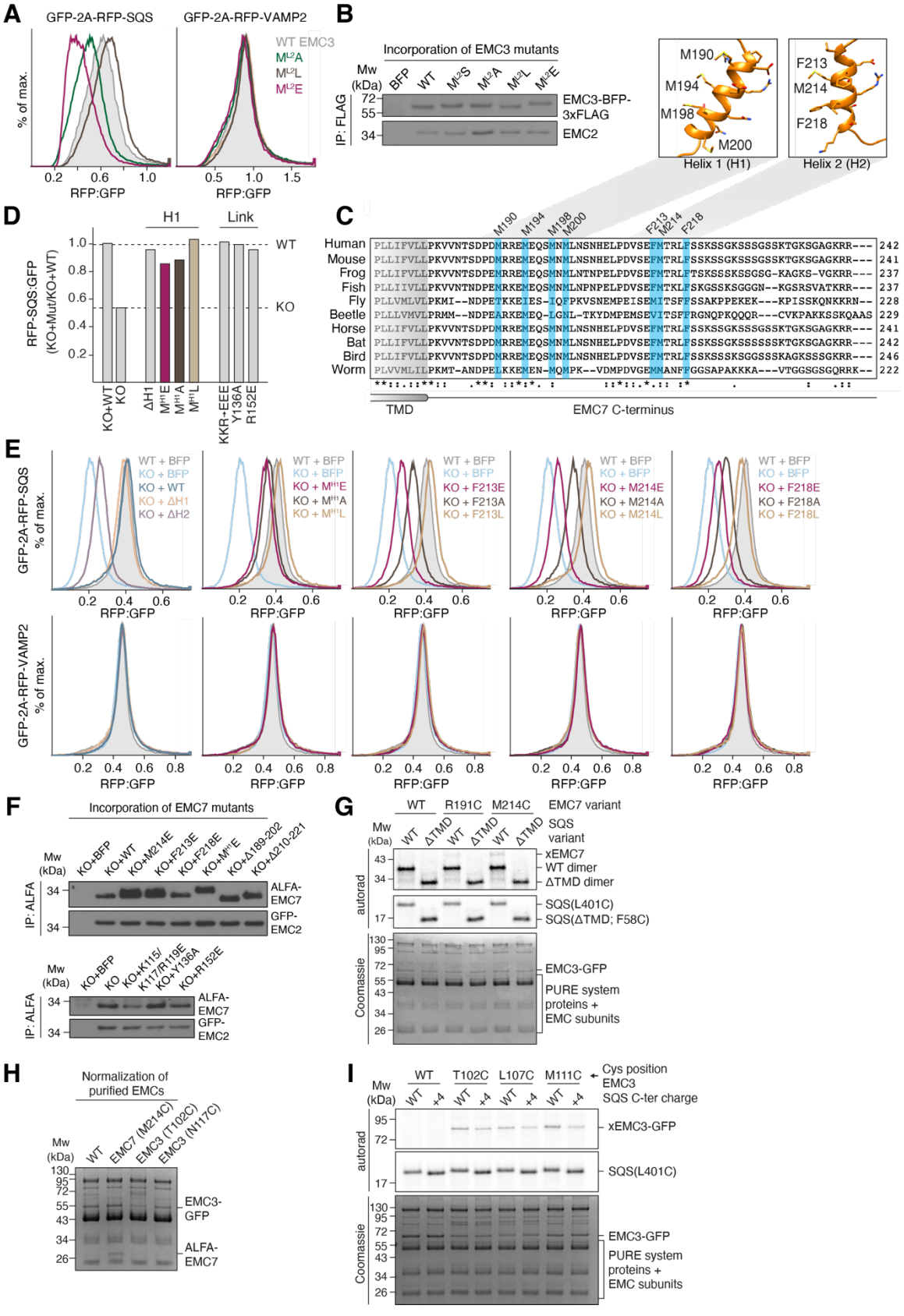
A
GFP-2A-RFP-SQS
GFP-2A-RFP-VAMP2
WT EMC3
M^L2A
M^L2L
M^L2E
% of max.
RFP:GFP
B
Incorporation of EMC3 mutants
Mw (kDa)
BFP
WT
M^L2S
M^L2A
M^L2L
M^L2E
IP: FLAG
EMC3-BFP-3xFLAG
EMC2
M190
M194
M198
M200
Helix 1 (H1)
F213
M214
F218
Helix 2 (H2)
C
M190
M194
M198
M200
F213
M214
F218
Human
Mouse
Frog
Fish
Fly
Beetle
Horse
Bat
Bird
Worm
TMD
EMC7 C-terminus
D
H1
Link
RFP-SQS:GFP (KO+Mut/KO+WT)
WT
KO
KO+WT
KO
ΔH1
M^H1E
M^H1A
M^H1L
KKR+EEE
Y136A
R152E
E
GFP-2A-RFP-SQS % of max.
GFP-2A-RFP-VAMP2 % of max.
WT + BFP
KO + BFP
KO + WT
KO + ΔH1
KO + ΔH2
KO + M^H1E
KO + M^H1A
KO + M^H1L
KO + F213E
KO + F213A
KO + F213L
KO + M214E
KO + M214A
KO + M214L
KO + F218E
KO + F218A
KO + F218L
RFP:GFP
F
Incorporation of EMC7 mutants
Mw (kDa)
KO+BFP
KO+WT
KO+M214E
KO+F213E
KO+F218E
KO+M^H1E
KO+Δ189-202
KO+Δ210-221
IP: ALFA
ALFA-EMC7
GFP-EMC2
KO+K115/K117/R119E
KO+Y136A
KO+R152E
G
WT
R191C
M214C
EMC7 variant
SQS variant
ΔTMD
xEMC7
WT dimer
ΔTMD dimer
SQS(L401C)
SQS(ΔTMD; F58C)
autorad
Coomassie
EMC3-GFP
PURE system proteins + EMC subunits
H
Normalization of purified EMCs
EMC7 (M214C)
EMC3 (T102C)
EMC3 (N117C)
EMC3-GFP
ALFA-EMC7
I
T102C
L107C
M111C
Cys position EMC3 SQS C-ter charge
+4
xEMC3-GFP
SQS(L401C)

Figure S2.4. Substrate capture by EMC3's hydrophobic loop 2 and EMC7's hydrophobic helix H2.

(**A**) HEK293 cells stably expressing RFP-SQS or -VAMP2 and cytosolic GFP as a normalization control were transduced with lentivirus to express the indicated EMC3 loop 2 mutants, along with BFP as a transduction marker. For each mutant, the RFP:GFP ratio of BFP-positive cells was derived via flow cytometry and is plotted as a histogram. ML2 refers to all four methionines in loop 2. (**B**) The indicated EMC3 loop 2 mutants were introduced into HEK293 cells via lentiviral transduction. Cells were harvested, solubilized and subjected to anti-FLAG immunoprecipitation (IP). Eluates were analyzed by SDS-PAGE and western blotting with the indicated antibodies. (**C**) Alignment of EMC7 C-terminus sequences from various eukaryotes using Clustal Omega (Sievers et al., 2011). Two conserved sequence stretches are predicted by secondary structure algorithms to form α-helices, termed H1 and H2. Residues mutated in (E) are highlighted in blue. AlphaFold 2 models of H1 and H2 are shown. H1 is methionine-rich and H2 is predicted to form an amphipathic α-helix. (**D**) As in Figure 2.3C, but with the indicated mutants of H1 or the lumenal linker (link) between the EMC7's β-sandwich and TMD. MH1 refers to all four methionines in helix 1. KKR→EEE denotes the combined mutation of K115E, K117E, and R119E. (**E**) Wild type (WT) or EMC7 KO HEK293 cells were transduced with lentivirus to express either BFP alone or BFP plus EMC7(WT) or the indicated mutants. 48 h after rescue construct transduction, cells were transduced with lentivirus expressing either RFP-SQS or -VAMP2, as well as a cytosolic GFP normalization control. The RFP:GFP ratio was determined by flow cytometry and is plotted as a histogram. Note that deletion of H2 strongly impaired SQS insertion in cells. Mutation of hydrophobic residues F213, M214 and F218 on H2 to either alanine or glutamate, but not leucine, similarly impaired SQS, but not VAMP2 biogenesis. (**F**) A BFP control, wild type EMC7 (WT), or the indicated mutants of EMC7 were introduced into EMC7 KO HEK293 cells via lentiviral transduction. Cells were harvested, solubilized and subjected to anti-ALFA immunoprecipitation. Eluates were analyzed by SDS-PAGE and western blotting with antibodies against EMC2 and 7. (**G**) Purified EMC complexes containing either WT EMC7 or EMC7 with cysteines in H1 (R191C) or H2 (M214C) were incubated with purified CaM-SQS complexes with or without a TMD. The cysteine was placed either in the TMD (L401C) or the soluble linker (F58C), for the WT and ΔTMD SQS constructs, respectively. Disulfide crosslinking was carried out as in Figure 2.2B. (**H**) Coomassie stained SDS-PAGE gel of the disulfide crosslinking experiment shown in Figure 2.3D before analysis via autoradiography. The gel shows that equal amounts of EMC were used in the different crosslinking reactions. (**I**) Purified wildtype (WT) or EMC3 Cys mutant

EMC were incubated with purified CaM-SQS(L401C) complexes with wildtype (WT) or positively charged (+4) CTD. Disulfide crosslinking and analysis were carried out as above.

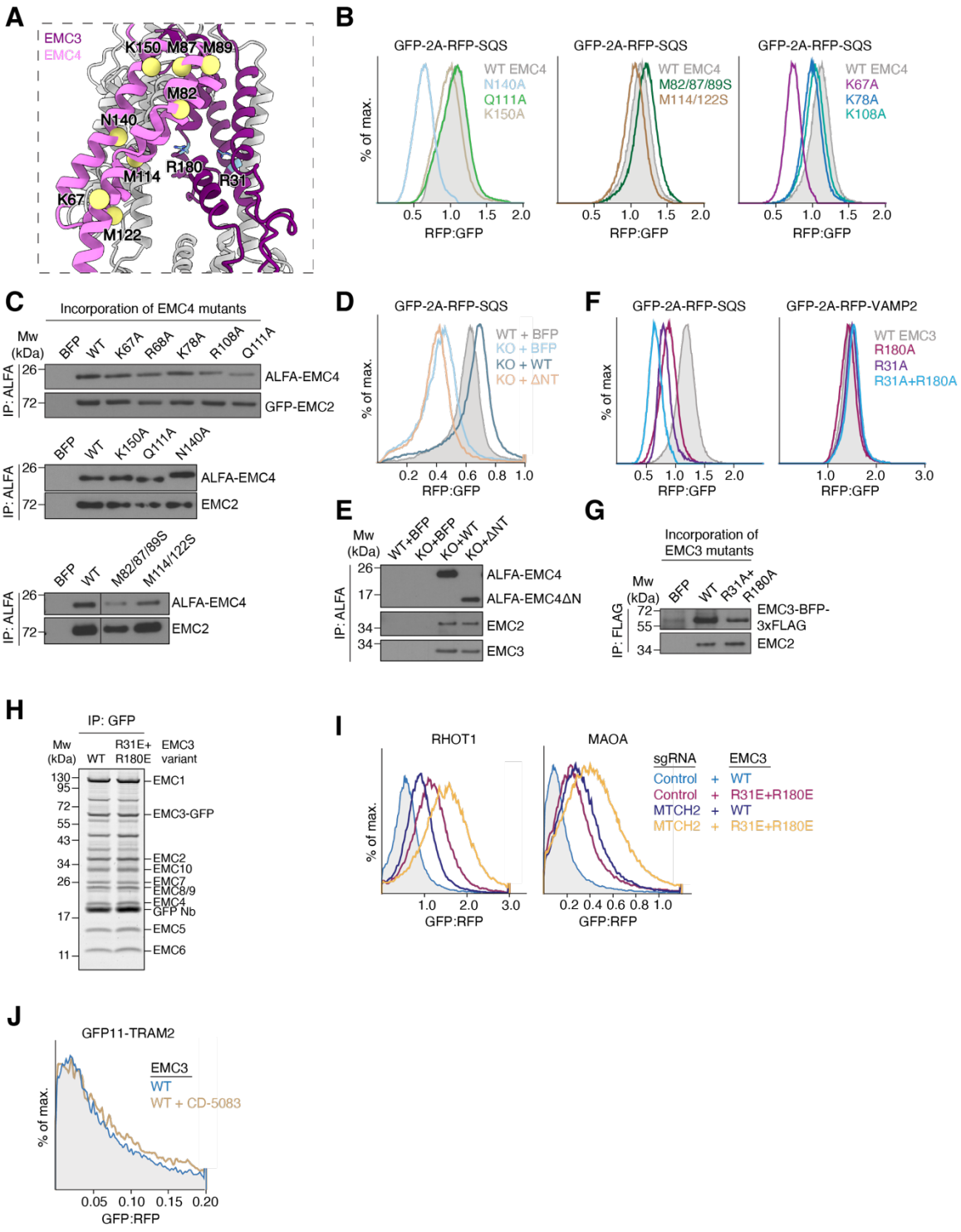

Figure S2.5. Biophysical properties of the hydrophilic vestibule.

(**A**) View of the insertase-competent side of the EMC. EMC7 and 10 were omitted for clarity. Residues of EMC4 mutated in (B) are highlighted. R31 and R180 of EMC3 are shown as blue sticks for reference. (**B**) HEK293 cells stably expressing RFP-SQS and cytosolic GFP as a normalization control were transduced with the indicated mutants of EMC4, along with BFP as a transduction marker. The RFP:GFP ratio of BFP-positive cells for each mutant was derived via flow cytometry and is plotted as a histogram. (**C**) The indicated EMC4 mutants from Figure 2.3D and (B) were introduced into HEK293 cells via lentiviral transduction. Cells were harvested, solubilized, and subjected to anti-ALFA immunoprecipitation (IP). Eluates were analyzed by SDS-PAGE and Western blotting with antibodies against EMC2 and 4. (**D**) The N-terminus of EMC4 is required for TA protein biogenesis in cells. HEK293 WT or EMC4 KO cells were transduced with lentivirus to express either BFP alone or BFP plus EMC4(WT) or a ΔNT mutant (residues 57-end). 48 h after rescue construct transduction, cells were transduced with lentivirus expressing RFP-SQS, as well as a cytosolic GFP normalization control. The RFP:GFP ratio of BFP-positive cells was derived via flow cytometry and is plotted as a histogram. (**E**) A portion of the cells from (D) was harvested, solubilized and subjected to purification of EMC4 variants via their N-terminal ALFA tag using the ALFA nanobody. The eluate was analyzed by SDS-PAGE and Western blotting with HRP-coupled ALFA nanobody or the indicated antibodies. (**F**) HEK293 cells stably expressing RFP-SQS or -VAMP2 and cytosolic GFP as a normalization control were transduced with lentivirus to express the indicated mutants of EMC3, as well as BFP. The RFP:GFP ratio of BFP-positive cells for each mutant was derived via flow cytometry and is plotted as a histogram. (**G**) A portion of the cells from (F) was harvested, solubilized, and subjected to purification of EMC3 variants via their C-terminal 3xFLAG tag. Incorporation of the single mutants was described before (Pleiner et al., 2020). (**H**) Expi293 suspension cells stably expressing EMC3-GFP WT or R31E+R180E were solubilized and subjected to anti-GFP nanobody purification. The eluate was normalized by GFP fluorescence and analyzed by SDS-PAGE followed by Sypro Ruby staining. Note that both EMC3 WT and R31E+R180E mutant incorporate into EMCs with similar efficiency as they co-purify with all other EMC subunits. (**I**) Same assay as in Figure 2.7A but in cells transduced with either a non-targeting (control) or MTCH2 knockdown single guide RNA (sgRNA). (**J**) Same assay as in Figure 2.7D measuring the ER insertion of GFP11-TRAM2, but showing only WT EMC3 -/+ p97 inhibitor CD-5083.

Table S2.1. Cryo-EM data collection, refinement, and validation statistics.

	Consensus (EMDB-40246)	Nine-subunit (EMDB-40245) (PDB 8S9S)	Eight-subunit (EMDB-40247)
Data collection and processing			
Microscope	FEI Titan Krios		
Voltage (kV)	300		
Camera	Gatan K3		
Magnification	105,000		
Defocus range (μm)	-1.0 to -3.0		
Pixel size (Å/pix)	0.416		
Electron exposure (e–/Å^2)	60		
Number of frames per movie	40		
Dose Rate (e-/pix/s)	16.0		
Automation software	SerialEM		
Number of micrographs	11,822		
Initial particle images (no.)	1,271,124		
Final particle images (no.)	193,900	156,706	37,194
Local resolution range	3.0 – 7.0	3.0 – 7.0	3.5 – 8.0
Map resolution range (Å, FSC=0.143)	3.5	3.6	3.9
Refinement			
Software (phenix.real_space_refine)	PHENIX 1.20.1-4487		
Initial model used (PDB code)		6WW7 + Alpha Fold	
Correlation coefficient (CC_{mask})		0.83	
Map sharpening *B* factor (Å^2)	-112	-103	-76
Model composition			
Non-hydrogen atoms		18,012	
Protein residues		2262	
Ligands		7 NAG & 6 PCW	
B factors (Å^2)			
Protein		106	
Ligand		102	
R.M.S deviations			
Bond lengths (Å) (# > 4σ)		0.003	
Bond angles (°) (# > 4σ)		0.612	
Validation			
MolProbity score		1.92	
Clashscore		12.13	
Poor rotamers (%)		0.27	
Cß deviations (%)		0.00	
CaBLAM outliers (%)		1.60	
Ramachandran plot			
Favored (%)		95.29	
Allowed (%)		4.71	
Disallowed (%)		0.00	

2.7 Acknowledgements

We thank Songye Chen and Oliver Clarke for technical assistance, all members of the Voorhees lab for thoughtful discussion, and Alina Guna for critical reading of the manuscript. We thank Pamela Bjorkman for access to her lab's cell sorter, as well as the Caltech Flow Cytometry facility, and the Caltech Cryo-EM facility. Cryo-electron microscopy was performed in the Beckman Institute Center for TEM at Caltech, and data was processed using the Caltech High Performance Cluster, supported by a grant from the Gordon and Betty Moore Foundation.

This work was supported by: the Heritage Medical Research Institute (R.M. Voorhees), the NIH's National Institute Of General Medical Sciences DP2GM137412 (R.M. Voorhees), the Deutsche Forschungsgemeinschaft (T. Pleiner), and the Tianqiao and Chrissy Chen Institute (T. Pleiner, M. Hazu).

Author contribution: T. Pleiner, M. Hazu, G.P. Tomaleri, and R.M. Voorhees conceived the study. T. Pleiner, M. Hazu, and G.P. Tomaleri performed most of the experiments and analysis with assistance from V.N. Nguyen and K. Januszyk. T. Pleiner, M. Hazu, and R.M. Voorhees wrote the manuscript with input from all authors.

Declaration of interests: R.M. Voorhees and G.P. Tomaleri are consultants for Gates Biosciences, and R.M. Voorhees is an equity holder. The authors have no additional competing financial interests.

C h a p t e r 3

MONITORING ALPHA-HELICAL MEMBRANE PROTEIN INSERTION INTO THE OUTER MITOCHONDRIAL MEMBRANE IN MAMMALIAN CELLS

The following chapter is adapted from Hazu et al., 2024 and modified according to the Caltech Thesis format.

Hazu, M., Guna, A., Stevens, T.A., Voorhees, R.M., (2024) "Monitoring alpha-helical membrane protein insertion into the outer mitochondrial membrane in mammalian cells" Methods in Enzymology, 707, 63-99; doi: 10.1016/bs.mie.2024.07.054

3.1 Abstract

Mitochondrial function is dependent on the correct localization and insertion of membrane proteins into the outer mitochondrial membrane (OM). In mammals, the OM contains ~150 proteins, the majority of which contain α-helical transmembrane domains. This family of α-helical proteins has significantly expanded in metazoans and has evolved to mediate critical signaling and regulatory processes including mitochondrial fusion and fission, mitophagy, apoptosis, and aspects of the innate immune response. Recently, the conserved OM protein MTCH2 has been identified as an insertase for α-helical proteins in human mitochondria. However, our understanding of the targeting, insertion, folding and quality control of α-helical OM proteins remains incomplete. Here we highlight three methods to monitor α-helical protein insertion both in human cells and *in vitro*. First, we describe a versatile split fluorescent reporter system that can be used to monitor the insertion of α-helical proteins into the OM in human cells. Second, we delineate a streamlined approach to isolating functional, insertion competent mitochondria from human cells that are compatible with *in vitro* import assays. Finally, we explain in detail how to reconstitute the insertion of α-helical proteins in a minimal system, by creating functional proteoliposomes containing purified MTCH2. Together these tools represent an integrated platform to enable the detailed mechanistic analysis of biogenesis of the diverse and physiologically essential α-helical OM proteome.

3.2 Introduction

Mitochondria have evolved to play central roles in metabolism, cellular stress, homeostasis, and signalling (Friedman and Nunnari, 2014, Nunnari and Suomalainen, 2012). In order to support these functions, the double-membrane bound mitochondria depend on an extremely diverse class of proteins, which are distributed among four sub-compartments: the outer membrane (OM), intermembrane space (IMS), inner membrane (IM), and the matrix (Morgenstern et al., 2017, Pagliarini et al., 2008). The vast majority of mitochondrial proteins are encoded in the cell nucleus, with the exception of a small number of highly hydrophobic subunits of the electron transport chain (Anderson et al., 1981). Nuclear encoded mitochondrial proteins are therefore translated on cytosolic ribosomes and must be subsequently targeted and imported into the correct compartment (Becker et al., 2019, Busch et al., 2023, Neupert and Herrmann, 2007, Pfanner et al., 2019, Richter-Dennerlein et al., 2015).

This biogenesis process is particularly important for the proteins in the OM, which are responsible for all communication between the mitochondria and the rest of the eukaryotic cell. The OM contains two major classes of membrane proteins, β-barrel and α-helical, which rely on distinct biogenesis machinery for integration into the bilayer. β-barrel proteins, which would have been present in the mitochondria's bacterial predecessor (Gray et al., 1999, Timmis et al., 2004), rely on a two-step process: translocation into the IMS via the translocase of the OM (TOM) and subsequent insertion into the OM by the sorting and assembly machinery (SAM) complex (Busch et al., 2023, Dukanovic and Rapaport, 2011, Höhr et al., 2015, Kutik et al., 2008, Takeda et al., 2021). By contrast, how α-helical proteins, which would not have been found in the ancestral endosymbiont, are inserted into the OM remains incompletely understood, particularly in mammals.

α-helical proteins are biophysically defined by the presence of one or more transmembrane domains that must be embedded within the bilayer. Foundational work performed in yeast has delineated the fundamental principles of α-helical protein integration into mitochondria (Becker et al., 2011, Doan et al., 2020, Krüger et al., 2017, Vitali et al., 2020). Additionally, functional analogues of α-helical membrane protein insertion machinery have been identified in trypanosomes (Vitali et al., 2018). However, in metazoans the increasingly multi-functional role of mitochondria led to the expansion of the α-helical OM proteome (Gabaldón and Huynen, 2004, Gabaldón and Huynen, 2007). In metazoans, this family of proteins regulate key aspects of apoptosis, innate immunity, and mitochondrial dynamics (Ravagnan et al., 2002, Saotome et al., 2008, Seth et al., 2005, Yoon et al.,

2003). Because of their essential roles, the mammalian cell has evolved specialized machinery responsible for the biogenesis and maintenance α-helical OM proteins.

Recently, MTCH2 was shown to be a central player in the insertion of a suite of α-helical OM proteins in mammalian cells (Guna et al., 2022). MTCH2 was identified through a genetic screen focused on identifying factors required for biogenesis of mitochondrial tail-anchored (TA) proteins. TA proteins are a functionally important subset of OM proteins, defined by the presence of a single C-terminal transmembrane domain. Using a series of *in vivo* and *in vitro* assays, MTCH2 was rigorously established as a bona fide protein insertase as it is (i) necessary for the biogenesis of TA proteins in cells, (ii) required for insertion into isolated mitochondria *in vitro*, (iii) physically associates with TAs, and (iv) is sufficient for insertion in a purified reconstituted system. Proteomic analysis of MTCH2 depleted cells showed that other classes of proteins were also affected, including signal-anchored proteins (defined by an N-terminal transmembrane domain and flanking regions serving as sorting signals and anchors to the membrane) and multipass proteins. The discovery of MTCH2 highlights the many aspects of the biogenesis and quality control of the OM proteome that remain incompletely understood.

In this chapter, we describe three methods to study both OM protein biogenesis and more specifically, the function of MTCH2. First, we outline strategies for monitoring insertion of OM proteins in cells using a split fluorescent reporter system suitable for imaging, genome-wide genetic screens, and flow cytometry-based reporter assays. We specifically focus on the construction and validation of cell lines, as well as subsequent design of a broad range of reporters. Second, we describe a protocol for monitoring OM protein insertion *in vitro* using purified mitochondria from human cells. Finally, we describe our method for generating a purified reconstituted system for OM protein insertion using minimal components, including how to integrate the OM insertase MTCH2 into functional proteoliposomes.

3.3 Experimental procedures

3.3.1 Tools to visualize outer membrane protein biogenesis in cells

Experimental Design and General Considerations

Studying α-helical OM proteins in mammalian cells, particularly using a fluorescent readout, requires a series of considerations. First, a subset of α-helical proteins are known to integrate into the

endoplasmic reticulum (ER) and/or peroxisomes, because roughly 15% of the mitochondrial proteome is dual localized (Dinur-Mills et al., 2008, Yogev and Pines, 2011). Overexpression of mitochondrial OM proteins can further exacerbate this problem, leading to non-physiological mislocalization to other organelles and/or aggregation and thereby persistence in the cytosol (Guna et al., 2022). Because of these issues, a simple GFP fusion cannot be used to specifically study the population of an OM protein that is correctly localized to the mitochondria. Further, fusion of a globular fluorescent tag to many α-helical proteins can perturb their targeting and localization in cells.

Therefore, to specifically query the population of α-helical proteins correctly inserted into the mitochondrial OM, we exploited a split fluorescent reporter system adapted from work from Le Vasseur et al., 2021. Here, the first ten β-strands of GFP (GFP1-10) are constitutively expressed in the IMS of the mitochondria and the final complementary β-strand (GFP11) is fused to the substrate of interest. The GFP11 is a smaller tag that does not interfere with the insertion of many α-helical proteins. Successful integration of the protein into the OM in the correct topology will result in reconstitution of GFP in the IMS and therefore fluorescence (shown as a schematic in Figure 3.1A). This strategy allows monitoring of α-helical insertion by microscopy or flow cytometry, enabling imaging, genetic, and cell biological experiments.

Cell line generation

Central to this strategy is the specific expression of GFP1-10 at high fidelity in the IMS in the cell line of interest. This is achieved by fusion of a canonical mitochondrial targeting sequence to the N-terminus of the first ten strands of GFP. Some general considerations when designing this cell line are as follows.

1. Targeting sequence: Though multiple targeting sequences can be used, we have tested those from MICU1 (residues 1-60) (Le Vasseur et al., 2021) and LACTB (residues 1-68) (Hung et al., 2014), which both result in efficient and specific targeting to the IMS.
2. Expression level: When generating the constitutive GFP1-10 cell line, it is critical to titrate the level of GFP1-10 to minimize cellular toxicity, which we've found can result when GFP1-10 levels are too high. Conversely, it is important that enough GFP1-10 accumulates to ensure efficient fluorescence upon integration of the GFP11 containing substrate. We recommend the generation of a monoclonal, homogenous cell line which can be expanded for downstream

experiments. This allows changes to resulting GFP fluorescence levels to be ascribed to reporter expression, rather than variability in GFP1-10 levels.

3. Cell type: We have had success generating compartment specific GFP1-10 cell lines in many backgrounds including K562s, HEK293Ts, U2OS, and RPE1s. Cellular background should therefore be selected depending on the intended downstream application and phenotype to be studied. For example, adherent cells may be more appropriate for imaging applications while many suspension cell lines can easily be expanded to the large number of cells required for genome-wide screening or other flow cytometry-based applications.
4. Fluorescent system: Although we will specifically describe use of the GFP1-10 system, both mCherry and mNeonGreen have been successfully used for other split-fluorescence applications (Feng et al., 2019, Tamura et al., 2021). Each fluorescent protein may have particular advantages depending on the intended downstream application, such as decreased background fluorescence and differential stability (Feng et al., 2017). Such considerations may be important when visualizing more subtle phenotypes. However, the toxicity of expressing an alternative fluorescent protein in the IMS must be empirically determined.
5. Cellular compartment: Finally, while OM protein integration is most easily monitored by fluorescence in the IMS, we have found that GFP1-10 expression is compatible with diverse compartments including the ER lumen (Inglis, Page, Guna, & Voorhees, 2020), mitochondrial matrix, peroxisome, and nucleus. An analogous strategy can therefore be flexibly leveraged for experiments in diverse cellular compartments.

Substrate reporter design

Once a suitable cell line has been generated, assaying mitochondrial protein insertion relies on the successful fusion of the 11th complementary β-strand of GFP (GFP11) to the protein of interest. When designing constructs, the following considerations should be made.

1. Topology: The GFP11 must be fused to a region of the substrate that is exposed to the IMS upon insertion into the OM. In general, we have used either the N or C-terminus, and testing of both termini can also be used to empirically determine protein topology. It may also be possible to include GFP11 in an internal soluble loop, provided sufficient flexibility can prevent steric inhibition of complementation, see point below.
2. Fusion considerations: We have empirically found that sufficient flexibility is required for efficient binding and complementation between GFP1-10 and GFP11. If the GFP11 sequence is

appended too close to a transmembrane domain (and therefore will be localized immediately adjacent to the bilayer), or if the soluble domain of the substrate contains rigid structural elements, this may impede complementation. At the same time, addition of a very long linker can alter mitochondrial targeting, translocation, and/or insertion. Therefore, in most cases we have utilized a 10 amino acid flexible linker between the transmembrane domain and GFP11, which generally allows complementation without impacting protein biogenesis. When the endogenous sequence flanking the transmembrane domain is less than 10 amino acids, a glycine and serine linker is added to extend the GFP11 a minimum of 10 amino acids away from the membrane.

3. Normalization: For many flow cytometry-based assays, including genetic screens, it may be useful to include an expression normalization marker in the reporter design. When testing cellular perturbations, such as knockdown or knockout of putative biogenesis factors, this permits discrimination of generalized effects on mRNA transcription and protein translation, from changes in targeting, integration, and stability of the mitochondrial substrate. In many cases we have relied on expression of both our GFP11-fused substrate and a second fluorescent protein (e.g. mCherry), separated by the viral 2A skipping sequence from a single open reading frame (Figure 3.1A). The ratio of GFP to mCherry fluorescence provides a normalized read out of the post-translational stability of the reporter substrate, which depends on targeting and integration into the mitochondrial OM (Pleiner et al., 2023, Yanagitani et al., 2017). For imaging-based applications however, expression of the substrate alone may be sufficient.

Generating a cell line expressing GFP1-10 in the IMS

Cell line generation involves two steps: stable expression of GFP1-10 preceded by either the MICU1 or LACTB1 targeting sequence, followed by confirmation of GFP1-10 integration by transient introduction of a GFP11 containing construct in the IMS. Depending on the cell type of interest, constitutive expression of GFP1-10 can be achieved through several strategies, including stable integration using a recombination-based strategy, such as the Flp-In system, or lentiviral transduction. Lentivirus is our method of choice for most applications because it allows easy titration by varying the multiplicity of infection (MOI), and results in rapid and stable expression in a variety of cell types. Because GFP1-10 itself cannot be directly visualized, to estimate the lentiviral titer of the GFP1-10, one can in parallel generate lentivirus and transduce with constructs expressing intact GFP.

Experimentally, we have found that generating monoclonal lines from an MOI that results in 60% - 80% GFP positive cells has the best outcomes.

Next, the GFP1-10 transduced cells must be identified by transient transfection of a substrate that positions GFP11 in the IMS, such that the resulting GFP fluorescence can be used for FACS. For this second step, the majority of cell lines are compatible with standard lipid-based transfection methods. However, many suspension cells like K562s require nucleofection for transient reporter expression, which we describe here. We recommend using this strategy to generate a monoclonal, homogenous cell line which can be expanded for downstream experiments.

Materials and Equipment

General

- K562 cells (human lymphoblast cells ATCC, USA; cat. no. CCL-243)
- HyClone Roswell Park Memorial Institute (RPMI)-1640 medium with HEPES, L-glutamine (Cytiva, USA; cat. no. SH30255.01)
- HyClone fetal bovine serum (FBS) (Cytiva, USA; cat. no. SH30071.03)
- Penicillin-Streptomycin (100x) (Millipore-Sigma, USA; cat. no. P4333-20 mL)
- Gibco Dulbecco's phosphate-buffered saline (DPBS), no calcium, no magnesium (Thermo Fisher Scientific, USA; cat. no. 14190136)
- Tissue culture incubator (Thermo Fisher Scientific, USA; model Heracell 240i CO_2 incubator)
- Automated Cell Counter (Thermo Fisher Scientific, USA; model Countess II)
- Cell counting slides (Bulldog-bio, USA; cat. no. DHC-N01)
- Water bath (Julabo, USA; model PURA 22) - set at 37 °C
- 24-Well Cell Culture Plate (Genesee Scientific, USA; cat. no. 25-107)
- 24-Well Cell Culture Plate (Genesee Scientific, USA; cat. no. 25-107)
- 15 mL centrifuge tube, sterile (Fisher Scientific, USA; cat. no. 05-539-12)
- 1.7 mL microcentrifuge tubes (VWR, USA; cat. no. 87003-294) - autoclaved

Lentiviral spinfection

- Benchtop Centrifuge (Eppendorf, USA; model Centrifuge 5810R with A-4-81 rotor)
- MTP/Flex buckets (adaptors for plates) (Eppendorf, USA; cat. no. 022638866)
- Polybrene Transfection Reagent (10 mg/mL) (Millipore-Sigma, USA; cat. no. TR-1003-G)

- Lentivirus (EF1α_MICU1(1-60)-GFP1-10 and/or EF1α_LACTB(1-68)-GFP1-10)
- Lentivirus (EF1α_MICU1(1-60)-GFP and/or EF1α_LACTB(1-68)-GFP)

Nucleofection

- Amaxa Nucleofector 96-well Shuttle System (Lonza, USA)
- 4D-Nucleofector Core Unit (Lonza, USA; cat. no. AAF-1003B)
- 4D-Nucleofector 96-well Unit (Lonza, USA; cat. no. AAF-1003S)
- SF Cell Line 96-well Nucleofector Kit (Lonza, USA; cat. no. V4SC-2096)
- Plasmid (Ef1α_mCherry-P2A-MICU1(1-60)-GFP11)

Cell sorting

- Cell Sorter (Sony Biotechnology, USA; model SH800S)
- FlowTubes with strainer cap (VWR, USA; cat. no. 76449-658)

Step-by-Step Methods

Maintain freshly thawed K562 cells in RPMI-1640 medium supplemented with 10% FBS, 100 U/mL Penicillin, and 100 µg/mL Streptomycin. Healthy cells have a doubling time of roughly 24 h and are therefore split 1:4 every 48 h to maintain them between 0.25 and 1.00 × 10^6 cells/mL. Cells are grown in a humidified incubator at 37 °C and 5% CO_2.

Day 1: Start lentivirus titration of MICU1(1–60)-GFP1-10 and/or LACTB(1−68)-GFP1–10 and MICU1(1−60)-GFP and/or LACTB(1−68)-GFP.

Enhanced BSL2 biosafety level precautions must be taken when working with lentivirus.

Here we outline an example spinfection protocol using four different lentiviral titers for both GFP1-10 and GFP (as a proxy for GFP1-10 titer). Titration is intended to identify how much virus results in the ideal level of GFP1-10 in the transduced population, using the full GFP as a proxy. The titration volumes can be adjusted as needed.

1. Pre-warm centrifuge capable of spinning tissue culture plates (6-well and 24-well) to 30°C - 32°C.

2. Resuspend stock K562 cells by gentle pipetting and determine cell count.

3. For a lentiviral spinfection in 24-well plates: 0.25×10^6 cells, 8 µg Polybrene, lentivirus, and RPMI medium are mixed in a total 1 mL of volume.

4. Make a 9x master mix for lentiviral spinfection for a titration of 2x four lentiviral titers (both the intact GFP as a proxy for lentiviral titer, and GFP1-10 in parallel).

    - Add 7.2 µL 10 mg/mL Polybrene (final 8 µg/mL) to a 15 mL tube.
    - Add 2.25×10^6 cells to the polybrene (2.25 mL cells at 1×10^6 cells/mL).
    - Add RPMI medium to the cells bringing total volume to 5.4 mL (9×600 µL).
    - Mix by inverting the tube ~3 - 5 times.

5. Aliquot 600 µL of master mix per well into eight wells in a 24-well cell culture plate.

6. Thaw frozen lentivirus aliquots rapidly in a 37°C water bath.

7. Add different volumes of each lentivirus (GFP1-10 and GFP) to each well, for a total volume of 1 mL in the well.

    - 100 µL lentivirus + 300 µL RPMI medium
    - 200 µL lentivirus + 200 µL RPMI medium
    - 300 µL lentivirus + 100 µL RPMI medium
    - 400 µL lentivirus

8. Mix the wells by gentle pipetting with a P1000.

9. Place the 24-well cell culture plate into centrifuge taking care to use a second plate to balance.

10. Centrifuge the plates at 1000 ×g for 2 h at 30°C.

11. Once the spin is complete, resuspend each well by gently pipetting with a P1000.

12. Place the cells in a humidified 37°C, 5% CO_2 incubator.

13. 48 h post-spinfection, check the transduction efficiency of the full GFP construct. Select the titer with a 60% - 80% GFP positive population. Keep the corresponding condition from the resulting GFP1-10 spinfection.

Day 2-4: Pre-nucleofection

Roughly 48 h are required for the integration and expression of a construct following lentiviral infection. Therefore, transient expression of a GFP11 construct *via* nucleofection should occur at least 48 h after transduction with GFP1-10. Select a construct which has been previously validated to result in GFP fluorescence upon integration into the OM or localization to the IMS. Realistically, only one sample is needed for each cell line once a population that is 60% - 80% positive is identified.

14. Subculture spinfected K562 cells at a density of 0.5×10^6 cells/mL for 1-2 days before nucleofection. Higher cell densities may cause decreased nucleofection efficiency.

Day 5: Nucleofection (SF Cell Line 96-well Nucleofector Kit)

15. Start up the Nucleofector 96-well Shuttle Software (Device and Software). Verify device connection and upload experimental parameter file.

16. Select the appropriate 96-well nucleofector program for K562 cells: **FF-120**

17. Pre-warm a 24-well cell culture plate with 800 µL RPMI medium per well (one well per nucleofection sample) and place in the incubator.

18. Prepare 1 µg plasmid DNA in a 1.5 mL tube. Use concentrated DNA to minimize volume.

19. Prepare Nucleofector Solution master mix. Add 3.6 µL Supplement 1 to 16.4 µL SF Cell Line Nucleofector Solution per sample.

20. Resuspend and count cells to determine cell density.

21. Centrifuge 2×10^5 cells per nucleofection, at 300 × g for 5 min at room temperature. Remove the supernatant.

22. Gently resuspend the cell pellet in 20 µL Nucleofector Solution.

23. Transfer the cells into the 1.5 mL tube containing DNA and mix gently.

24. Transfer the resuspended cells with DNA into the 96-well Nucleocuvette plate.

25. Gently tap the 96-well Nucleocuvette plate to make sure the sample covers the bottom of the well.

26. Place the 96-well Nucleocuvette plate, with the lid closed, into the retainer of the 96-well Shuttle Device. Confirm the orientation of the plate. Well A1 must be in the upper left position.

27. Start the nucleofection process by pressing the “Upload and start” button.

28. After the run is complete, open the retainer in the Shuttle Device and carefully remove the 96-well Nucleocuvette plate from the retainer.

29. Transfer 100 µL of pre-warmed RPMI medium from the 24-well plate and mix the cells by gently pipetting up and down a few times. Transfer the total volume (120 µL) into the 24-well cell culture plate. This step should be done as quickly as possible, as the Nucleofection Solution is toxic.

30. Incubate the cells in a humidified incubator at 37°C and 5% CO_2.

31. After 24 h, reporter expression should be clearly visible on a fluorescent microscope. If the transiently transfected reporter includes an expression marker such as mCherry, this should also be easily visualized in the cytosol.

Day 8: FACS sorting of cells expression the IMS GFP1-10

Nucleofection creates pores in the plasma membrane and is therefore often inherently toxic. Thus, cells will require at least 24 h of recovery post-nucleofection before further manipulation. Typically, we aim to sort individual cells 48–72 h post-nucleofection, which provides sufficient recovery time but limits dilution of the transiently transfected plasmid.

32. Prepare 96-well cell culture plates with 200 µL of RPMI-1640 medium supplemented with 20% FBS, 100 U/mL Penicillin, and 100 µg/mL Streptomycin.

33. Harvest 1×10^6 cells of non-nucleofected and nucleofected K562 cells, at 300 × g for 5 min.

34. Resuspend in 1 mL of DPBS supplemented with 20% FBS. Strain the resuspended cells through a strainer cap into a FACS tube.

35. Analyze non-nucleofected K562 cells first (we use a SONY SH800S, but other equivalent sorters can also be used). Adjust laser settings and gates for live and single cells. Finally, adjust laser settings and gates for background fluorescence of mCherry (if using) and GFP (resulting from complementation of GFP1-10 with IMS localized GFP11).

36. Analyze nucleofected K562 cells. 60% - 80% of cells should show GFP fluorescence, based off of the titer you chose to move forward with.

37. Sort single cells that express any GFP fluorescence (and mCherry if using) into the prepared 96-well plates. GFP fluorescence intensity variation is an indicator of the number of plasmid copies that got in during nucleofection rather than number of copies of GFP1-10 in the cell. Sort 1000 cells into a single corner well on each plate sorted to ensure successful sorting and monitor cell growth.

38. After the sort, check the 1000 cells well on each plate and confirm cells were sorted into the plate. Place plate into a humidified 37°C, 5% CO_2 incubator.

39. Allow the single cell clones to grow undisturbed for 2-3 weeks in a 96-well plate. As cells become confluent, expand into larger wells (48-well, 24-well, *etc.*). Pick 2-3 clones with the following properties.

    - Viability: Cell viability is ideally greater than 90%, similar to the wildtype K562 cells. Clones with low viability will not recover well and eventually die.
    - Growth: Cells should be doubling roughly every 24 h. Clones with longer doubling times are discarded.
    - Cell shape: Cell shape and size should be homogenous. There will always be some large and some small cells but these should not exceed 5% of the population.
    - GFP1-10: 100% of the cells should be expressing the GFP1-10 in the IMS. Confirm by expressing GFP11 in the IMS.

Notes

- The 1000 cells FACS sorted well also aids in finding the correct focal plane for visualizing sorted cells on the light microscope when screening for monoclonal colonies.

Split fluorescence reporter assay in human cells

To study OM biogenesis, a substrate fused to GFP11 must be introduced into the expanded GFP1-10 cell line that has been generated. As previously discussed, this can be achieved through several strategies, depending on the cell type of interest. Here, we outline a protocol for lentiviral transduction of an OM substrate fused to GFP11 along with a translation normalization marker, mCherry, into K562 cells. Prior to introduction of a reporter, GFP1-10 cells can be manipulated using either genetic perturbations (i.e. knockdown or knockout) or drug treatments before analysis by flow cytometry or FACS.

Materials and Equipment

General

- K562 cells (stably expressing GFP1-10 in the IMS) (generated in **above**)
- HyClone RPMI-1640 medium with HEPES, L-glutamine (Cytiva, USA; cat. no. SH30255.01)
- HyClone fetal bovine serum (FBS) (Cytiva, USA; cat. no. SH30071.03)
- Penicillin-Streptomycin (100x Pen) (Millipore-Sigma, USA; cat. no. P4333-20ML)
- Tissue culture incubator (Thermo Fisher Scientific, USA; model Heracell 240i CO_2 incubator)
- Automated Cell Counter (Thermo Fisher Scientific, USA; model Countess II)
- Cell counting slides (Bulldog-bio, USA; cat. no. DHC-N01)
- Water bath (Julabo, USA; model PURA 22) – set at 37°C
- 24-Well Cell Culture Plate (Genesee Scientific, USA; cat. no. 25-107)
- 96-Well Cell Culture Plate (Genesee Scientific, USA; cat. no. 25-109)
- 15 mL centrifuge tube, sterile (Fisher Scientific, USA; cat. no. 05-539-12)
- 1.7 mL microcentrifuge tubes (VWR, USA; cat. no. 87003-294) - autoclaved

Lentiviral spinfection

- Benchtop Centrifuge (Eppendorf, USA; model Centrifuge 5810 R with A-4-81 rotor)
- MTP/Flex buckets (adaptors for plates) (Eppendorf, USA; cat. no. 022638866)
- Polybrene Transfection Reagent (10 mg/mL) (Millipore-Sigma, USA; cat. no. TR-1003-G)
- Lentivirus (mCherry-P2A-reporter protein-GFP11)

Flow cytometer

- Flow Cytometer (Thermo Fisher Scientific, USA; model Attune NxT Flow Cytometer)
- Flow cytometry data analysis tool (FlowJo, USA; software FlowJo)

Step-by-Step Methods

Maintain freshly thawed K562 cells expressing GFP1-10 in the IMS in RPMI-1640 medium supplemented with 10% FBS, 100 U/mL Penicillin, and 100 µg/mL Streptomycin. GFP1-10 expressing cells should be maintained as normal, typically displaying a doubling time of roughly 24 h and should be split 1:4 every 48 h to maintain a density between 0.25 and 1.00 × 10^6 cells/mL. Cells are grown in a humidified incubator at 37°C and 5% CO_2.

Day 1: Spinfection

Enhanced BSL2 biosafety level precautions must be taken when working with lentivirus.

This is an example protocol for testing 5 reporter constructs.

1. Place tissue culture plate adaptor buckets into the centrifuge and pre-warm to 30 °C - 32 °C.

2. Resuspend by gentle pipetting and count the density of the K562 cells.

3. For a lentiviral spinfection in 24-well plates: 0.25 × 10^6 cells, 8 µg Polybrene, lentivirus, and RPMI medium are mixed in a total 1 mL volume.

4. Make a 6x master mix for lentiviral spinfection.

    - Add 4.8 µL 10 mg/mL Polybrene (final 8 µg/mL) to a 15 mL tube.
    - Add 1.5 × 10^6 cells to the polybrene (1.5 mL cells at 1 × 10^6 cells/mL).
    - Add RPMI medium to the cells bringing total volume to 5.4 mL (6 × 900 µL).
    - Mix by inverting the tube ~3-5 times.

17. Aliquot 900 µL of the master mix per well into 5 wells in a 24-well cell culture plate.

18. Thaw frozen lentivirus aliquots rapidly in a water bath.

19. Add appropriate volumes of lentivirus for each reporter to each well, for a total volume of 1 mL. The amount of lentivirus required will depend on the desired MOI, the lentiviral titer, and the goals of the experiment. Typically, we find that ranges between 25 and 200 µL is appropriate for many experiments, but this amount must be empirically determined for each lentiviral prep.

20. Mix the wells by gently pipetting with a P1000.

21. Place the 24-well cell culture plate onto the plate adaptor bucket and place inside the centrifuge. Make a balance plate with water and place in the centrifuge.

22. Spin the plates at 1000 ×g for 2 h at 30°C.

23. Once the spin is complete, resuspend each well by gently pipetting with a P1000.

24. Place the cells in a humidified 37°C, 5% CO_2 incubator overnight.

25. Maintain the cells at a density of 0.5×10^6 cells/mL until analysis.

Day 4: Analysis by flow cytometry (72 h post-spinfection)

14. Transfer 1 mL of parental GFP1-10 expressing cells with no reporter into a 1.5 mL tube.

15. Transfer cells transduced with reporters from the 24-well plate into 1.5 mL tubes.

16. Analyze fluorescence directly on a cell analyzer.

    - K562 cells can be analyzed directly in RPMI medium on a flow cytometry machine. If preferred, the cells can be washed in DPBS and resuspended in DPBS prior to running through the machine.

17. Use non-transduced cells to adjust lasers and gates for live cells, single cells, and background fluorescence.

    - Gating: Final gate should include all mCherry positive cells, which indicates successful reporter expression.

18. Aim to collect 10,000-30,000 events in the final gate for downstream analysis.

19. Use a flow cytometry software package that allows for ratiometric analysis, such as FlowJo, to compare the GFP levels (indicative of reporter insertion into the OM) relative to mCherry levels (indicative of reporter expression). As described above, gate events for live cells, single cells, and the final reporter fluorescence gate. Visualize the final gate of cells expressing the reporter as a histogram, with the ratio of GFP to mCherry fluorescence. Depletion of a putative biogenesis factor, including MTCH2, would be expected to decrease the GFP:mCherry ratio. Conversely, depletion of potential quality control factors may stabilize the reporter and increase the GFP:mCherry fluorescence.

    - In FlowJo this is possible by deriving your own parameter. This can be found under the "Tools" tab and selecting "Derive parameter". Here, you can create a new parameter "GFP:mCherry" and type out the formula using the "Insert reference" for the laser channels.

Notes

- The amount of reporter virus added is dependent on its quality. For many reporters, 100 µL of virus per 24-well is a recommended starting point, which typically results in over 90% mCherry positive cells. If lentivirus titer is poor, increased volumes can be added, or lentivirus can be concentrated as previously reported (Kohno et al., 2002, Lee and Lee, 2018).

- 24-48 h are required for the integration and expression of a lentivirally transduced construct. If the goal of this assay is to determine changes to OM biogenesis or quality control following drug treatment or factor depletion, we recommend analyzing at a 72-hour time point.

- If performing a genetic perturbation, reporter expression is recommended after the genetic perturbation. In instances where experimental conditions do not allow for a 48-72 h waiting period, reporters can be expressed from strong inducible promoters (e.g. EF1α) for shorter time periods.

- Multicolor compensation is necessary when using some combination of fluorescent proteins. Compensation can be achieved using single color controls (i.e. mCherry, GFP alone) directly on the flow cytometer or computationally during data analysis using standard techniques.

3.3.2 *In vitro* insertion assay

Experimental Design and General Considerations

One critical caveat to monitoring OM protein biogenesis in cells is that the observed phenotype is a combination of protein expression, targeting, insertion, and protein stability. Therefore, the fluorescent reporter experiments described in **Section 3.3.1** cannot directly pinpoint which step in the biogenesis process is affected by a particular perturbation. In contrast, *in vitro* experiments can be designed to mechanistically dissect a single biogenesis step (e.g. insertion) by utilizing isolated mitochondrial and cell free translation systems.

Here we will describe a strategy for *in vitro* insertion into isolated human mitochondria relying on three central components. (1) A cell-free system to generate protein that allows incorporation of a radioactive label such as ^{35}S-methionine. (2) A source of mitochondria that can be manipulated either genetically in cells or biochemically post isolation. Mitochondria can be isolated from diverse cell types including yeast and human cells (Mokranjac and Neupert, 2007, Murschall et al., 2021, Weckbecker and Herrmann, 2013). (3) Finally, an assay that reports on proper protein integration into the OM.

Here we describe use of a mammalian translational extract purified from rabbit reticulocyte lysate, human mitochondria purified from human cells, and monitor insertion using a protease protection assay followed by affinity purification of the protected fragment using an affinity tag. The samples are finally analyzed by SDS-PAGE and proteins are visualized by autoradiography.

Some general considerations when designing an *in vitro* import assay are below.

1. Mitochondrial isolation: In some cases, it is possible to use semi-permeabilized cells as a source of mitochondria for *in vitro* insertion experiments. However, the mitochondrial OM is particularly sensitive to detergents, including digitonin that is commonly used for semi-permeabilization. The resulting loss of integrity of the OM is therefore not compatible with assaying protein insertion by protease protection (Guna et al., 2022). Consequently, here we describe a procedure for isolating intact mitochondria from human cells. For most applications, particularly when assaying protein insertion, a mitochondrial enriched membrane fraction is sufficient. Depending on the substrate, the presence of contaminating ER, which can misinsert some mitochondrial OM proteins, may be problematic and can diminish or obscure

phenotypes. However, we have found that further purification (e.g. using a Percoll density gradient purification) results in a marked decrease in mitochondrial import efficiency.

2. Cell type: Mitochondria can be isolated from a wide variety of cell types. Here, we describe a procedure utilizing K562 cells, a suspension cell line that is highly tractable to genetic manipulation (i.e. knockdowns, knockouts, or overexpression of desired protein targets). Generally, isolation of sufficient amounts of mitochondria for *in vitro* insertion assays is limited by the starting cell number, which may motivate the selection of particular cell types (i.e. suspension vs adherent).

3. *In vitro* translation system: We describe an *in vitro* import assay that relies on the translation of substrates in a rabbit reticulocyte system which allows for the integration of ^{35}S-methionine into the target substrates (Sharma, Mariappan, Appathurai, & Hegde, 2010). However, numerous commercially available systems can be used including the Rabbit Reticulocyte Lysate System (Promega, USA), TnT Quick Coupled Transcription/Translation System (Promega, USA), and 1-Step IVT System (Thermo Fisher Scientific, USA). Translation extract can also be derived from human cell lysates. It is important to ensure translation systems are compatible with mitochondrial source (i.e. mammalian with mammalian vs yeast with yeast, etc.).

Important considerations for designing OM protein constructs for *in vitro* import assays.

1. DNA template: Most *in vitro* translation systems rely on an *in vitro* transcription reaction to generate an mRNA template. DNA templates should therefore contain a 5′ SP6 or T7 promoter, a Kozak sequence, an open reading frame encoding your protein, and a 3′ stop codon. For mammalian cell free translation systems, incorporation of a 5′-methyl-guanosine cap typically increases mRNA yield and can be achieved as previously described (Sharma et al., 2010).

2. Autoradiography: Assaying protein import by protease protection followed by autoradiography relies on the detection of a ^{35}S-methionine containing protected fragment. Therefore, at least one methionine residue must be within either the transmembrane domain or the IMS-localized fragment of the protein. Ideal signal strength will result from the protection of at least two methionine residues. If a methionine residue is not present in the endogenous sequence, it can be added at a position that does not perturb the behavior of the protein. We

have found additional methionines are typically tolerated adjacent to the affinity tag, as described below.

3. Affinity tags: In many cases, an additional affinity purification step following protease digestion can be useful to purify and enrich the protected fragment. This both confirms the identity and topology of the protected fragment and results in improved visualization by autoradiography. To do this, a short peptide tag is appended to the protein of interest on the terminus predicted to be localized to the IMS. When selecting a tag, it is important to be cognizant of the targeting sequence of the given substrate, and ensure the position, size, and charge of the chosen tag does not affect targeting or insertion. In general, we have found 6xHis tags to be well tolerated for many α-helical OM proteins. To empirically assess topology, or differentiate between insertion and translocation, distinct affinity tags can be fused to both the N and C-termini.

4. Use of standardized cytosolic domains: For many α-helical membrane proteins, the cytosolic domain is dispensable for both targeting and insertion into the OM. When comparing across multiple substrates it can therefore be useful to rely on a standardized cytosolic domain fused to a transmembrane domain and its flanking regions. This strategy can be particularly useful for studying OM proteins with large soluble domains that may not be efficiently expressed *in vitro*. For many OM proteins, the small, inert domain from the villin headpiece has been well-tolerated (Guna et al., 2022).

Isolation of mitochondria

Here, we describe the isolation of a highly enriched mitochondrial fraction by differential centrifugation from human cells. This is based on existing protocols from Richter-Dennerlein et al., 2014, and has been adapted for K562 suspension cells. Despite co-purifying with some ER membrane, we find that this preparation results in highly active mitochondria suitable for most import assays. Further purification, such as centrifugation over a Percoll density gradient, results in significantly less active mitochondria. When using K562 cells, we expect a yield of roughly 500-1000 µg enriched mitochondria from 500×10^6 cells. Each *in vitro* insertion reaction typically requires 15 ug of mitochondria, allowing preparations to be scaled accordingly. In order to maintain consistency between mitochondrial preps and the integrity of the membranes, we recommend not starting with less than 80×10^6 cells. For optimal activity, we recommend mitochondria to be used

immediately, and at most within 2-3 h of their isolation, during which they are stored exclusively on ice.

Materials and Equipment

- K562 cells (human lymphoblast cells ATCC, USA; cat. no. CCL-243)
- Floor centrifuge (Thermo Fisher Scientific, USA; model Sorvall RC 6 + with Fiberlite F14-6 x 250 y Fixed-Angle Rotor)
- Benchtop Centrifuge (Eppendorf, USA; model Centrifuge 5810 R, S-4-104 rotor, 4 × 750 mL round buckets, 50 mL and 15 mL tube adaptors)
- High-Speed Benchtop Centrifuge (Eppendorf, USA; model Centrifuge 5430 R with FA-45-48-11 rotor)
- Plate reader (BioTek, USA; model Synergy HT Microplate Reader)
- 50 mL centrifuge tube, sterile (Fisher Scientific, USA; cat. no. 05-539-8)
- 15 mL centrifuge tube, sterile (Fisher Scientific, USA; cat. no. 05-539-12)
- 5 mL microcentrifuge tube, sterile (Eppendorf, Germany; cat. no. 0030119487)
- 1.7 mL microcentrifuge tubes (VWR, USA; cat. no. 87003-294)
- 1 mL Glass Dounce homogenizer with tight pestle (DWK, USA; cat. no. 357538)
- 96-Well Cell Culture Plate (Genesee Scientific, USA; cat. no. 25-109)
- Pierce Bradford Protein Assay Kit (Thermo Fisher Scientific, USA; cat. no. 23200)
- Bovine Serum Albumin (BSA) (Millipore-Sigma, USA; cat. no. A2153-50G)
- Phenylmethanesulfonyl fluoride (PMSF) (Millipore-Sigma, USA; cat. no. 78830-5G)
- 2x Isolation Buffer (10 mM HEPES/KOH pH 7.5, 420 mM mannitol, 140 mM sucrose, 2 mM EDTA). Can be made in large batches and stored in 50 mL aliquots at -20°C.

Step-by-Step Methods

Here, we describe how to purify mitochondria from 400×10^6 K562 cells, which should result in roughly a 1 g cell pellet. Scale all buffers and volumes depending on starting cell pellet size. The activity of the mitochondria in import assays is dependent on their integrity, so great care must be taken to ensure all steps are performed at 4°C. Set all centrifuges to 4°C, and pre-chill all buffers, tubes, and tips. We recommend working in a cold room following step 7.

Preparations of fresh buffers

1. 20 mL of Homogenization Buffer: Weigh out 3 mg PMSF and 40 mg BSA. Dissolve in 10 mL cold water. Vortex for 30–60 s to dissolve (note: PMSF will not fully dissolve). Add 10 mL of 2x Isolation Buffer, and vortex to mix. Keep on ice.

2. 10 mL of Isolation Buffer: Dilute the 2x Isolation Buffer 1:1 with cold Millipore water. Keep on ice.

Cell Lysis

1. Pre-chill a 1 mL glass Dounce homogenizer with a tight pestle on ice in the cold room.

2. Harvest cells in a F14-6 x 250 y rotor at 300 xg for 5 min at 4°C. With culture volumes less than 100 mL of cells, split the cells into 50 mL tubes and pellet in benchtop centrifuge, with the same spin conditions.

3. Gently decant cell media and resuspend the cell pellet in 10 mL cold Homogenization Buffer. Transfer the resuspended cells to a 15 mL tube that has been weighed in advance.

4. Pellet the cells at 500 ×g for 5 min at 4°C in benchtop centrifuge.

5. Aspirate the supernatant. Weigh and subtract the empty tube weight to determine cell pellet weight.

6. Resuspend the cell pellet in 4 mL of cold Homogenization Buffer per gram. If the cell pellet weighs less than 0.5 g, resuspend in 2 mL.

7. Incubate the resuspended cells on ice for 10 min.

8. Transfer to the pre-chilled 1 mL glass Dounce homogenizer. Dounce slowly for 25 passes. Pause every 5 passes and pipette to resuspend the cells.

    - Number of passes should be determined empirically as it can vary between Dounce homogenizers and cell types. Refer to **Notes below**.

Differential centrifugation

9. Transfer the lysed cells into a 15 mL tube, labeled tube A. Centrifuge at 1300 ×g for 5 min at 4°C to pellet nuclei and unlysed cells.

   A schematic of the expected results is shown in Figure 3.2B. At the bottom you expect to see an opaque pellet of unlysed cells. In the middle is a translucent gel like layer of nuclei. On top is the supernatant containing mitochondria, ER, and cytoplasm.

10. Transfer the supernatant to a clean, pre-chilled 15 mL tube, labeled tube B. Avoid transferring the nuclei layer.

11. Add 1 mL Homogenization Buffer to tube A (which contains the remaining unlysed cells) and resuspend the pellet by pipetting with a P1000. The resuspension will become cloudy again.

12. Centrifuge both tubes A and B at 1300 ×g for 5 min at 4°C, to recover as much supernatant as possible.

    In tube A, the supernatant should be more transparent, and it is easier to distinguish the junction between the supernatant and nuclei layer. In tube B, there will be a small pellet of nuclei that was not completely sedimented in the first spin.

13. Transfer the supernatant from both tube A and B into a single clean, pre-chilled 5 mL tube (or 15 mL tube if you have more than 4 mL).

14. Centrifuge the pooled supernatant once more at 1300 ×g for 5 min at 4°C. There should only be a small pellet of nuclei and cell debris.

15. Transfer the supernatant and distribute into multiple pre-chilled 1.5 mL tubes.

16. Centrifuge the 1.5 mL tubes at 11,000 ×g for 10 min at 4°C in a benchtop centrifuge. There should be two layers in the pellet, a firm brown layer at the bottom and a soft white layer on top. The mitochondria are now in the pellet.

17. Aspirate the supernatant in all tubes, with caution to not remove any of the loose pellet, including both the white and brown layers. Combine all pellets by resuspending in a total of 1 mL Isolation Buffer and transfer to a single 1.5 mL tube.

18. Centrifuge at 11,000 ×g for 10 min at 4°C.

19. Aspirate the supernatant including as much of the white layer as possible.

20. Resuspend the firm brown mitochondria pellet in 1 mL Isolation Buffer.

21. Centrifuge once more at 11,000 ×g for 10 min at 4°C.

22. Gently aspirate the supernatant.

23. Add 10 µL Isolation Buffer to the mitochondrial pellet. If the mitochondria pellet is less than 30 µL, add 5 µL.

24. Resuspend by repeatedly pipetting with a P20 attached to a P10 tip. Dislodge the pellet with the tip of the pipette tip. Once dislodged, pipette up and down ~100 times to ensure uniform resuspension. Avoid introducing bubbles.

25. To measure the concentration of the resulting isolated mitochondria, mix 1 µL of resuspended mitochondria with 49 µL Isolation Buffer (1:50 dilution) in a new 1.5 mL tube and vortex.

26. Measure the protein concentration of the 1:50 dilution using the Pierce Bradford Protein Assay kit and a microplate reader (following the microplate procedure to minimize sample required).

Notes

- Trace salts carried over from cell media and/or PBS will impact the lysis efficiency and consistency of the nuclei pellet. The best lysis efficiency is achieved when the cells are washed once in Homogenization Buffer before their final resuspension.

- Avoid overlysing the cells, as it can result in mechanical damage to the mitochondrial OM. We typically assess lysis by visualization using a standard light microscope and aim for 80-90% lysis, estimated by the number of intact unlysed cells.

- The efficiency of a particular Dounce homogenizer must be empirically tested. Choose one that is most efficient for cell lysis. Both too tight (resulting in a clear supernatant in **step 9** with a large cell pellet) or too little lysis (a cloudy supernatant with no unlysed cells at the bottom) will affect mitochondrial integrity and subsequent activity.

- Mitochondria are extremely sensitive to heat. All steps should be performed at 4°C to avoid mitochondrial aggregation and subsequent difficulty in resuspension by pipetting.

In vitro import assay

Here, we describe how to assay the insertion of α-helical membrane proteins into isolated mitochondria by protease protection. The protein of interest is translated in rabbit reticulocyte lysate in the presence of ^{35}S-methionine to allow for tracking by autoradiography following SDS-PAGE. We use an in-house transcription (T1) and translation (cT2) mix as previously described (Sharma et al., 2010). The DNA template is generated from an SP64 promoter containing plasmid or gene fragment coding for a His-tagged α-helical protein. Standard primers are used to PCR amplify a template for use in the transcription reaction. Following translation in the presence of ^{35}S-methionine, the resulting reaction is mixed with isolated mitochondria to allow for import. The resulting reaction is then subjected to protease treatment, such that insertion into the lipid bilayer will result in a protease protected fragment. Finally, the protected fragment is affinity purified and analyzed by SDS-PAGE and autoradiography. The strength of the signal is proportional to integration efficiency into the lipid bilayer, as well as the number of expected protected methionine residues. We describe these steps in detail below.

Materials and Equipment

General

- Water baths (Fisher Scientific, USA; model Isotemp GPD 10) – set to 32°C and 37°C
- Heat block (Techne, USA; model Dri-Block DB 3A) – set at 95°C
- High-Speed Benchtop Centrifuge (Eppendorf, USA; model Centrifuge 5430 R with FA-45-48-11 rotor)
- 0.2 mL PCR tube (VWR, USA; cat. no. 137-231C(EX))
- 1.7 mL microcentrifuge tubes (VWR, USA; cat. no. 87003-294)
- 5x Sample Buffer (250 mM Tris/HCl pH 6.8, 5% SDS, 50% glycerol, 500 mM DTT, 40 mg Bromophenol Blue powder)

In vitro transcription and translation

- DNA template with SP6 promoter (plasmid or gene fragment)

- Q5 High-Fidelity 2X Master Mix (NEB, USA; cat. no. M0492S)
- PCR primers
- QIAquick PCR Purification Kit (Qiagen, USA; cat. no. 28104)
- T1 transcription mix (homemade; Sharma et al., 2010)
- SP6 RNA Polymerase (NEB, USA; cat. no. M0207S)
- Recombinant RNasin Ribonuclease Inhibitor (Promega, USA; cat. no. N2515)
- cT2 translation mix (homemade; Sharma et al., 2010)
- Methionine, L-[35S]-EasyTag, 5 mCi (Revvity, USA; cat. no. NEG709A005MC)
- 10 mg/mL Puromycin (Gibco, USA; cat. no. A1113803)

Import reaction

- Isolated mitochondria (from **above**)
- Isolation buffer (5 mM HEPES/KOH pH 7.5, 210 mM mannitol, 70 mM sucrose, 1 mM EDTA)
- Import Buffer (20 mM HEPES/KOH pH 7.5, 250 mM sucrose, 5 mM magnesium acetate, 20 mM potassium acetate, 2.5 mM ATP, 15 mM succinate)

Proteinase K digestion

- 10 mg/mL Proteinase K in 20 mM Tris/HCl pH 7.5
- Phenylmethanesulfonyl fluoride (PMSF) (Millipore-Sigma, USA; cat. no. 78830-5G)
- Dimethyl sulfoxide (DMSO) (Millipore-Sigma, USA; cat. no. D8418-50ML)
- SDS Buffer (1.67% SDS, 0.1 M Tris/HCl pH 8.0)

Immunoprecipitation of His-tag

- Ni-NTA Agarose (Qiagen, USA; cat. no. 30210)
- His-Wash Buffer (50 mM HEPES/KOH pH 7.5, 500 mM NaCl, 10 mM imidazole, 1% Triton X-100)
- 100 mM EDTA pH 7.0

SDS-PAGE analysis

- SDS-PAGE Electrophoresis apparatus (Bio-Rad, USA)
- Coomassie Stain (1 g/L Coomassie Brilliant Blue (R250), 40% methanol, 10% acetic acid)

- Destain (40% methanol, 10% acetic acid)
- Gel Dryer (Fisher Scientific, USA; model Hoefer GD 2000 Slab Gel Dryer System)
- Typhoon biomolecular imager (Cytiva, USA; model FLA 9500) with Phosphor stage

Step-by-Step Methods

The following reactions are temperature sensitive. Work on ice, unless otherwise specified.

***In vitro* transcription and translation**

1. PCR amplify the DNA template for *in vitro* transcription using forward and reverse primers in a 50 µL reaction volume. Use the Q5 High-Fidelity 2x Master Mix, or preferred PCR reagents.

2. Purify the PCR product using QIAquick PCR Purification Kit. Elute the final DNA in 30 µL water. Typically, concentrations of 100 ng/µL are obtained.

3. Dilute PCR product to 50 ng/µL.

4. It is recommended to confirm the expected size and purity of the PCR fragment on an agarose gel.

5. Prepare 10 µL transcription reactions on ice for each DNA template. Add 7.6 µL T1 mix, 0.2 µL SP6 polymerase, 0.2 µL RNasin, and 2.0 µL 50 ng/µL PCR product (final 100 ng). Mix by gentle pipetting with a P10.

6. Incubate the transcription reactions in a 37°C water bath for 1.5 hours. Return transcription reactions back onto ice.

7. Prepare 10 µL translation reactions on ice. Per sample, add 5 µL cT2 mix, 0.5 µL ^{35}S-methionine, 0.5 µL transcription product (RNA), and 4 µL water. Mix by gentle pipetting with a P10, while not introducing bubbles.

8. Incubate the translation reactions in a 32°C water bath for 30 minutes. Return translation reactions to ice.

9. For proteins expected to insert post-translationally, release nascent chains from the ribosome by adding 0.5 µL of 10 mg/mL puromycin (~18.37 mM; final ~1 mM). Incubate at 32°C for 10 min and return to ice.

Mitochondria import reaction

10. Dilute the isolated mitochondria to 5 mg/mL with Isolation Buffer.

11. For each import reaction, aliquot 3 µL isolated mitochondria (final 15 µg) into 1.5 mL pre-chilled tubes on ice. For control reactions without mitochondria, add 3 µL Isolation Buffer.

12. Add 47 µL Import Buffer (total 50 µL volume) to each tube. Mix by gently pipetting, with care not to introduce bubbles.

13. Add 4 µL of the translation reaction to each corresponding tube. Mix by pipetting.

14. Incubate the import reactions in a 32°C water bath for 30 minutes. Return import reactions back onto ice.

15. **Optional:** Take a sample of the Totals: 10 µL reaction + 10 µL 5x Sample Buffer. Load 10 µL on an SDS-PAGE gel.

Proteinase K (PK) digestion

16. Transfer 39 µL of import reaction into a new 1.5 mL pre-chilled tube on ice.

17. Add 1 µL of 10 mg/mL Proteinase K (PK) in 20 mM Tris pH 7.5 (final 0.25 mg/mL) to each reaction and mix by pipetting.

    - When working with multiple samples, add PK to all reactions first and then mix all samples.

18. Incubate on ice for 1 h.

19. Prior to the end of the hour, prepare one 1.5 mL tube per sample with 60 µL 1.67% SDS in 0.1 M Tris pH 8.0. Place in a heat block set to 95°C to boil.

20. Prepare a fresh solution of 250 mM PMSF in DMSO at room temperature. (DMSO freezes on ice.)

21. Add 0.8 µL 250 mM PMSF in DMSO (final 5 mM PMSF) to quench the PK digestion in each tube. Pipette to mix immediately and return tube back onto ice.

    - When working with multiple samples, add PMSF and mix immediately. Then repeat with the next sample. Working slowly will result in the DMSO freezing too quickly. We recommend having a second pipette with a larger volume ready for the mixing step.

22. Incubate on ice for 3 minutes.

23. Transfer the entire reaction (~40 µL) to the boiling 60 µL 1.67% SDS / 0.1 M Tris pH 8.0 and immediately mix by pipetting.

24. Boil samples at 95°C for 3 min. Remove the samples from the heat block, spin down the condensation on the lids, and leave the tubes on ice to cool down.

25. **Optional:** Take a sample of the PK digests: 10 µL reaction + 10 µL 5x Sample Buffer. Load 10 µL on an SDS-PAGE gel.

Affinity purification of the His-tagged protease protected fragment

26. Equilibrate Ni-NTA agarose beads in His-Wash Buffer. Transfer the total volume of Ni-NTA beads (20 µL of 50% slurry per sample) into a 1.5 mL tube on ice. Wash three times in 1 mL His-Wash Buffer, spinning down beads briefly prior to removing supernatant.

27. Resuspend the beads in cold His-Wash Buffer equal to initial bead volume to make a 50% slurry.

28. To each quenched sample from **step 24**, add 1 mL cold His-Wash Buffer.

29. Add 20 µL equilibrated Ni-NTA agarose beads (50% slurry) to each sample.

30. Incubate for 1 h at 4°C rotating head-over-tail.

31. Pellet the beads to the bottom of the tube using a fast spin, aspirate the supernatant, and wash the beads by resuspending with 1 mL His-Wash Buffer.

32. Wash twice more in His-Wash Buffer.

33. Resuspend the beads in 25 µL 2x Sample Buffer with 50 mM EDTA.

SDS-PAGE Analysis and Exposure

34. Boil all samples at 95°C for 10 min.

35. Analyze the samples by SDS-PAGE, loading 10 µL per sample.

36. Stain the gel with Coomassie and destain.

37. Dry the gel at 80°C for 30 min in a gel dryer.

38. Expose the dried gels to a phosphor screen.

39. Image on a Typhoon with the Phosphor stage. Adjust exposure relative to expected signal, typically overnight is sufficient for exposure of totals, but longer exposures are required for affinity purified fragments.

Notes

- T1 and cT2 should be rapidly thawed and immediately placed on ice. Avoid repeated freezing and thawing of the T1 and cT2 as it significantly reduces the efficiency of translation. We allow for up to five freeze/thaw cycles.

- Coordinate the *in vitro* transcription and translation such that freshly isolated mitochondria can be directly used in the import reaction.

3.3.3 Reconstitution of a-helical membrane protein insertion using MTCH2 proteoliposomes

Experimental Design and Considerations

While the previous two methods can be utilized to demonstrate a factor is necessary for insertion, neither can directly show a putative insertase alone is sufficient for insertion. The gold standard for demonstrating sufficiency is reconstitution of the putative insertase into a protoeliposome system that can be used for *in vitro* insertion assays (Görlich and Rapoport, 1993, Guna et al., 2018). Recently, using this reconstitution strategy MTCH2 was shown to be sufficient for the insertion of α-helical membrane proteins (Guna et al., 2022). Here, we describe an adapted protocol for the reconstitution

of MTCH2 into functional proteoliposomes for use in *in vitro* insertion reactions as described in **Section 3.3.2** above.

The goal of a reconstitution is to generate proteoliposomes containing only a purified, functional protein of interest (Figure 3.3). To do this, purification of the putative insertase in detergent is required. For example, MTCH2 is purified from human cells using a nanobody-based strategy (Stevens et al., 2024), by a procedure which is described in detail in Guna et al., 2022. Next, purified, detergent solubilized MTCH2 is mixed with detergent solubilized lipids. Finally, the detergent is then slowly removed through dialysis or more commonly, chemical adsorption. In parallel, empty liposomes without MTCH2 are generated using the same conditions to be used as negative controls for subsequent insertion assays.

Successful reconstitution requires two features: (1) integration of MTCH2 into the lipid vesicle in the correct orientation and (2) complete removal of detergent to ensure the vesicle is sealed and thus can be used in subsequent insertion and protease protection experiments.

There are numerous parameters that can be modified in order to ensure successful reconstitution, which are described in detail below.

1. Detergents: For membrane protein insertases like MTCH2, the most common detergent for protein purification and subsequent reconstitution is Deoxy-BigCHAP (DBC), a non-ionic detergent in the bile acid salt family. DBC can be efficiently removed from a protein-detergent micelle and adsorbed by Bio-Beads, and thus is well-suited for reconstitution.

2. Protein purification: It is critical to express and purify the target membrane protein in its native state without compromising function. For MTCH2, we have obtained successful reconstitutions from protein expressed and purified from human cells, which ensures access to native biogenesis/folding machinery and post-translational modifications.

3. Lipids: The lipid composition of the reconstituted proteoliposomes is an important variable that must be empirically determined for your target protein. Optimal membrane protein activity may be obtained by mimicking the appropriate native composition of the bilayer (Fresenius & Wohlever, 2021). For MTCH2, we use a mixture of phosphatidylcholine (PC), phosphatidylethanolamine (PE), and phosphoethanolamine-N-lissamine rhodamine B (Rh-PE,

to facilitate visualization of the liposomes), which we deemed reasonable for an OM protein. However, other lipids such as cholesterol and cardiolipin can also be included if appropriate.

4. Protein orientation: Because reconstitution occurs via a detergent-purified intermediate, membrane proteins can reconstitute in both orientations. For example, we observed MTCH2 was ~1/2 in the 'correct' orientation, with its N-terminus localized to the cytosol, and ~1/2 in the 'incorrect' orientation, with its N-terminus localized to the vesicle lumen (Guna et al., 2022). By addition of appropriate affinity tags, orientation can be empirically determined using protease protection experiments.

5. Freeze/thaw cycles: The integrity of the resulting proteoliposomes can be affected by freezing, allowing inappropriate leakage of protease into the lumen. This can be avoided by always using fresh proteoliposomes, or in some cases through addition of cholesterol during reconstitution.

Materials and Equipment

- Purified MTCH2 in 50 mM HEPES/KOH pH 7.5, 200 mM NaCl, 2 mM magnesium acetate, 1 mM DTT, 1x protease inhibitor cocktail, 0.25% DBC (as described in Guna et al., 2022)
- Egg Phosphatidylcholine (PC) (Avanti Polar Lipids, USA; cat. no. 840051)
- Egg Phosphatidylethanolamine (PE) (Avanti Polar Lipids, USA; cat. no. 840021)
- 1,2-dioleoyl-sn-glycero-3-phosphoethanolamine-N-lissamine rhodamine B (Rh-PE) (Avanti Polar Lipids, USA; cat. no. 810150). This allows for the visualization of lipids throughout the reconstitution process.
- Vacuum concentrator (Labconco, USA; model CentriVap Complete Vacuum Concentrator)
- NanoDrop Spectrophotometer (Thermo Fisher Scientific, USA; model ND-1000)
- Thermomixer (Eppendorf, USA; model ThermoMixer F1.5)
- Ultracentrifuge (Beckman Coulter, USA; model Optima MAX-XP Ultracentrifuge)
- TLA-100.3 Fixed Angle Rotor (Beckman Coulter, USA; cat. no. 349490)
- 1.5 mL Microfuge Tube Polypropylene (Beckman Coulter, USA; cat. no. 357448)
- 1.7 mL microcentrifuge tubes (VWR, USA; cat. no. 87003-294)
- 50 mL centrifuge tube, sterile (Fisher Scientific, USA; cat. no. 05-539-8)
- Gel-loading pipette tips (Stellar Scientific, USA; cat. no. GL200-960)
- Bio-Beads SM-2 (Bio-Rad, USA; cat. no. 1523920)

- Methanol (VWR, USA; cat. no. BDH1135-4LG)
- Deoxy-BigCHAP (DBC) (Millipore-Sigma, USA; cat. no. 256455-1GM-M)
- 10% DBC in water
- 1M dithiothreitol (DTT)
- Lipid Rehydration Buffer (50 mM HEPES/KOH pH 7.5, 15% glycerol)
- SDS Buffer (1% SDS, 0.1 M Tris/HCl pH 8.0)
- Buffer A (HEPES/KOH pH 7.5, NaCl, DBC) (concentration of each component is calculated in the protocol)
- Reconstitution Buffer (50 mM HEPES/KOH pH 7.5, 250 mM sucrose, 100 mM potassium acetate, 1 mM DTT)

Step-by-Step Methods

Preparing DBC solubilized lipid stock

1. In a fume hood, mix chloroform dissolved lipids PC:PE:Rh-PE in the following mass-based ratio 8:1.9:0.1, for a total mass of 5-20 mg. It is recommended to pipette quickly due to the rapid evaporation of chloroform at ambient temperatures.

2. Add DTT to a final concentration of 10 mM to the lipid mix after determining initial volume.

3. Evaporate chloroform in a vacuum concentrator overnight.

4. Add 1 mL of Lipid Rehydration Buffer per 20 mg of lipids.

5. To resuspend lipids, shake in a thermomixer at 1,200 rpm at room temperature, with intermittent vortexing. This process takes several hours and is complete when a homogenous mixture is seen in the tube.

6. Pipette 2 µL of 1 mg/mL Rh-PE (2 µg) into a 1.5 mL tube and leave open in a fume hood to evaporate chloroform. Dissolve evaporated Rh-PE in 100 µL 1% SDS, 0.1 M Tris pH 8.0. This sample is used to determine the concentration of your lipid stock.

7. To measure the concentration of the lipid mix, mix 2 µL of resuspended lipids with 18 µL 1% SDS, 0.1 M Tris pH 8.0.

8. Measure the absorbance at 573 nm of both samples using a nanodrop spectrophotometer. The estimated concentration (in mg/mL) of the resuspended lipid mix is calculated as follows: 20 × (Solubilized lipid mix 573 nm absorbance) ÷ (Solubilized Rh-PE 573 nm absorbance).

9. Prepare a 10 mg/mL lipid mix in Lipid Rehydration Buffer with final concentration of 2% DBC.

Activate Bio-Beads

10. Transfer 10 mL of dry Bio-Beads into a 50 mL tube. Fill the tube with methanol to resuspend the dry Bio-Beads. Let the Bio-Beads settle to the bottom of the tube and decant the liquid. Repeat this step 1 time.

11. Wash the Bio-Beads in water, by filling the tube with water, letting the beads settle, and decanting the water. Repeat at least 6 times for a thorough wash.

12. Bio-Beads can be stored at 4°C in a 50% slurry in water.

Reconstitution of MTCH2 into proteoliposomes

13. For a 60 µL reconstitution add reconstitution components into a 1.5 mL tube, in the following order: Buffer A (calculated such that the final overall concentration in the reconstitution mixture is 25 mM HEPES/KOH pH 7.5, 100 mM NaCl, and 0.8% DBC), 12 µL of 10 mg/mL lipid mix, and purified MTCH2. Mix by pipetting. At the same time, generate an empty liposome control using a matched buffer in place of MTCH2.

14. Transfer 120 µL of activated Bio-Beads (50% slurry) into a new 1.5 mL tube. Remove all water with a gel-loading pipette tip.

15. Add the reconstitution mix to the Bio-Beads. Shake in a thermocycler at 1,100 rpm placed in the cold room for 18 h.

16. Let the Bio-Beads settle to the bottom of the tube. Using a gel-loading pipette tip, transfer the reconstitution mix into a 1.5 mL polypropylene microfuge tube for use in an ultracentrifuge. Avoid transferring any Bio-Beads.

17. Dilute the reconstitution mix to 0.5 mL with cold water.

18. Centrifuge the reconstitution mix for 30 min at 70,000 rpm (max. acceleration and deceleration) in a TLA-100.3 rotor at 4°C.

19. Supernatant must be aspirated immediately after centrifugation stops, with caution to avoid disturbing the very loose pellet.

20. Resuspend the pellet in 12 µL of Reconstitution Buffer. Dislodge and break up the pellet, and transfer to a new 1.5 mL tube. Resuspend the pellet completely by pipetting at least 100 times with a P10 tip.

21. The proteoliposomes and empty liposome control are now ready to be used for *in vitro* experiments. We typically use 0.5 µL of the proteoliposome in a 10 µL import reaction as outlined in Guna et al., 2022.

Assessing successful reconstitution

To determine the success of the reconstitution we recommend the following experiments:

- Resuspended proteoliposomes can be assessed for protein incorporation using western blotting.
- Protease protection can be used to assess orientation with appropriate affinity tags or antibodies as described for MTCH2 (Guna et al., 2022).
- Empty liposomes prepared in parallel should be tested directly in protease protection assays to assess background leakiness and thereby efficiency of detergent removal.

Notes

- We purchase lipids in chloroform, as they are easier to handle compared to the hygroscopic powdered form.
- DTT is included to prevent oxidation of the lipids.
- DBC may vary significantly from lot to lot. Final DBC concentrations in the reconstitution mixture ranging from 0.25% to 1.0% may be tested to determine the optimal concentration for a particular lot based on insertion activity.

- It is necessary to empirically optimize the time and amount of Bio-Beads during the detergent removal step.

3.4 Summary and Conclusion

The mitochondrial OM is a central platform for signaling in eukaryotic cells. OM proteins relay critical communication between mitochondria and the cytosol, regulating cell fate through their control of stress pathways, apoptosis, and the innate immune system. The biogenesis of OM proteins therefore represents an important area for future discovery, with broad biological and biomedical implications. The ability to study OM targeting and insertion both in human cells and *in vitro* will be important in exploring the biogenesis and function of this small but essential class of human membrane proteins.

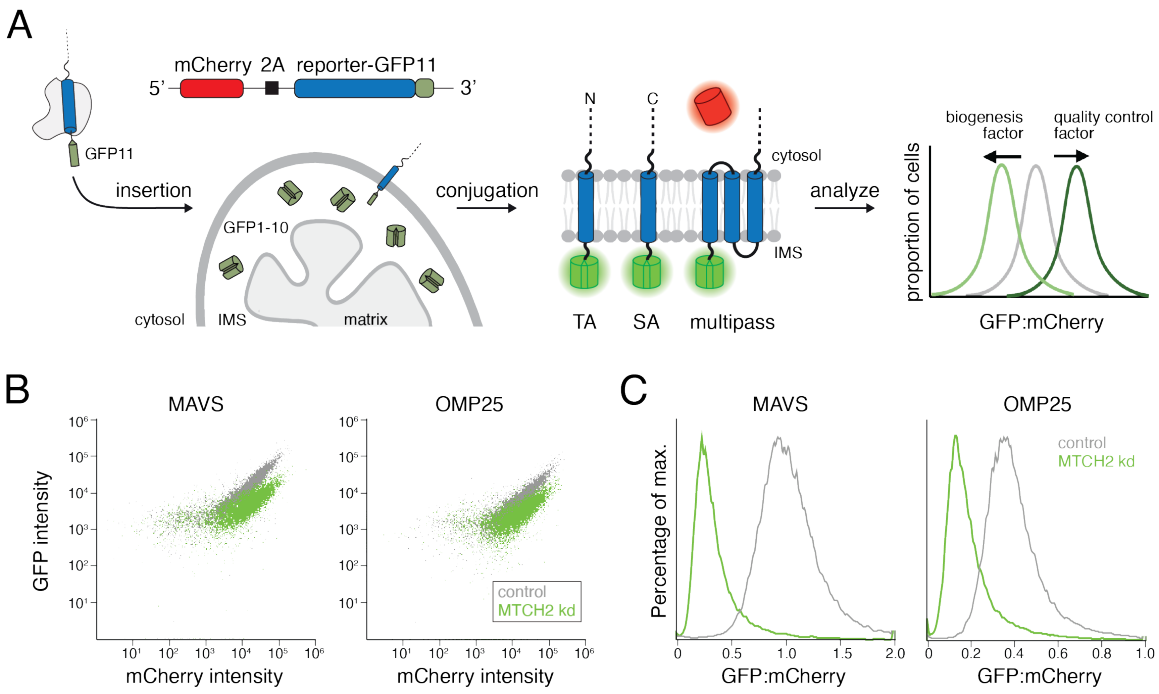

Figure 3.1. Split GFP reporter assay to selectively monitor insertion into the outer mitochondrial membrane (OM).

(**A**) Schematic of the split GFP reporter assay. The reporter construct expresses a translation normalization marker (mCherry) and a GFP11-tagged substrate in a cell constitutively expressing GFP1-10 in the intermembrane space (IMS). Successful insertion of the reporter substrate into the OM results in complementation of GFP11 with GFP1-10 and thereby GFP fluorescence. (**B**) Representative data using this reporter system to study MTCH2 function. Human K562 cells expressing a nontargeting (control) or MTCH2 knockdown single guide RNA (sgRNA) were transduced with reporters for the mitochondrial TA proteins, MAVS-GFP11 and OMP25-GFP11, as described in (A). Cells were analyzed by flow cytometry to determine mCherry vs GFP intensity. (**C**) GFP fluorescence relative to the normalization marker mCherry for the cells in (B) is displayed as a histogram.

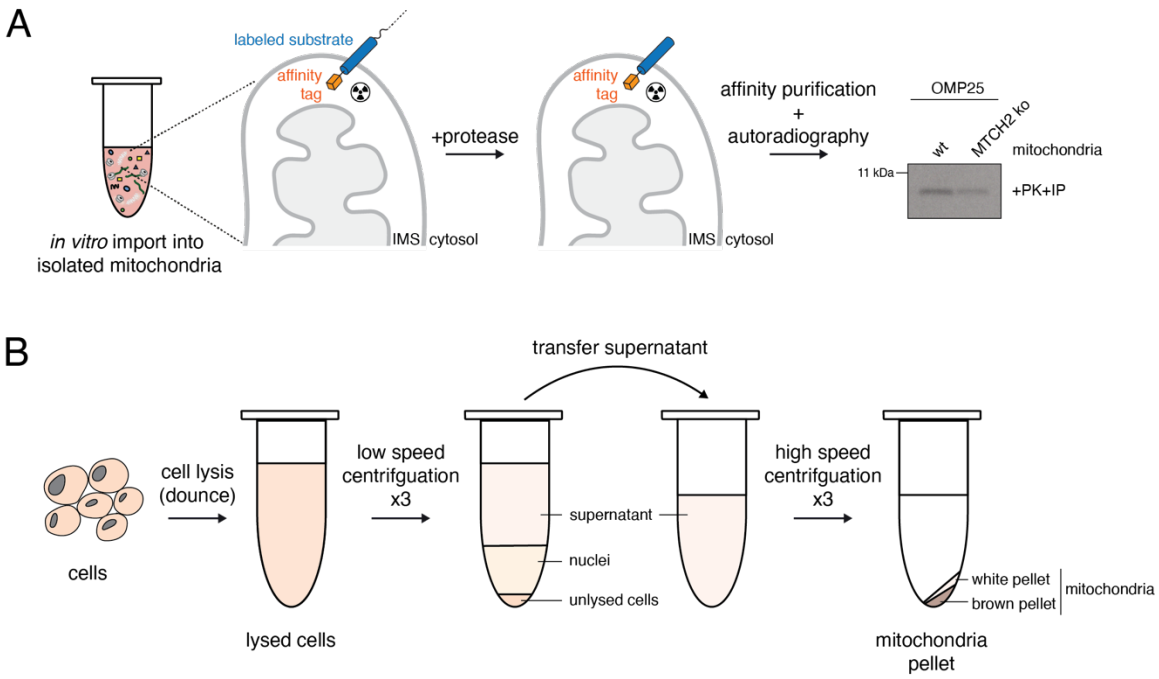

Figure 3.2. *In vitro* import assay into isolated mitochondria.

(**A**) Schematic of an *in vitro* import assay with isolated mitochondria, utilizing protease protection as a readout for membrane protein insertion. ^{35}S-methionine radiolabeled substrates are translated in rabbit reticulocyte lysate and then incubated with mitochondria isolated from human cells. Reactions are treated with protease to digest uninserted and exposed substrates, and any protected fragment is enriched through precipitation via an affinity tag. The resulting fragments are analyzed by SDS-PAGE and autoradiography as shown in this representative gel. (**B**) Schematic of mitochondrial isolation protocol. First, human cells are lysed using a Dounce homogenizer. A series of three low-speed centrifugations results in an opaque pellet of unlysed cells at the bottom, a translucent gel like layer of nuclei, and supernatant containing mitochondria, ER, and cytoplasm. A series of high-speed centrifugations of the supernatant results in a mitochondrial enriched pellet. The resuspended pellet can be used directly in import assays.

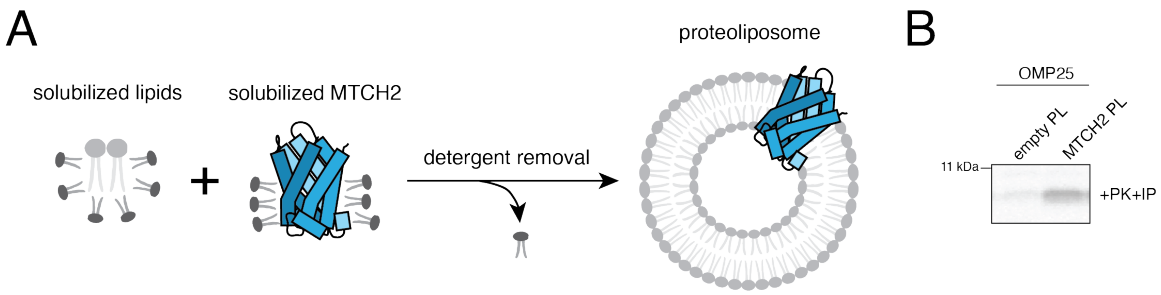

Figure 3.3. Reconstitution of MTCH2 into proteoliposomes.

(**A**) Schematic of the reconstitution of detergent purified MTCH2 into proteoliposomes (PL). (**B**) Representative insertion reaction of the mitochondrial TA protein OMP25 into reconstituted MTCH2 proteoliposomes. ^{35}S-methionine labeled OMP25 was generated in rabbit reticulocyte lysate, as described in Section 3.3.2. Following incubation with MTCH2 containing proteoliposomes and empty control liposomes, insertion was determined using a protease protection assay followed by affinity purification of the protected fragment using a C-terminal tag. The protected fragment was analyzed by SDS-PAGE and autoradiography.

3.5 Acknowledgements

Thank you to the Voorhees lab for thoughtful comments and discussion.

This work was supported by funding from: the Rothenberg Innovation Initiative (T.S.), the Merkin Institute for Translational research (T.S.), a Hevolution/AFAR new investigator award (R.M.V.), the Center for Evolution Science (T.S./R.M.V.), the Sontag Foundation (R.M.V.), the NIH's National Institute of General Medicine 1K99GM151478 (A.G.), and the Howard Hughes Medical Institute (R.M.V.).

Chapter 4

MOLECULAR MECHANISM OF MTCH2 FUNCTION AND REGULATION

4.1 Abstract

In mammals, the outer mitochondrial membrane (OMM) is composed of ~150 proteins, of which the majority contain α-helical transmembrane domains. The field's understanding of how these α-helical proteins are inserted into the OMM remains incomplete. The conserved OMM protein MTCH2 has been recently identified as an insertase capable of inserting biophysically diverse α-helical proteins into human mitochondria. However, our understanding of the molecular mechanism and function of MTCH2 requires further studies. In this study, we highlight ongoing work on investigating the functional mechanism of MTCH2 activity. Using tail-anchored (TA) proteins as a model substrate, we characterize the features of mitochondrial TA proteins that allow accurate sorting to the mitochondria, and through mutational analysis, we probe MTCH2 for a selectivity mechanism at the membrane. We also identify a region of MTCH2 that may regulate its insertion activity. Lastly, we characterize previously identified MTCH2 homologs and demonstrate that they may also be regulated under a similar mechanism. In combination, this study provides initial steps towards deciphering the role MTCH2 plays in the biogenesis and maintenance of the OMM proteome.

4.2 Introduction

The eukaryotic cell is an extremely crowded yet highly organized environment, with a myriad of subcellular compartments. The evolution of the cellular compartmentalization led to specialization and unique biochemical environments that has allowed for the emergence of the multicellular organism. However, it also introduced technical challenges as proteins now needed to localize to their respective subcellular locations. The mitochondria are key organelles as they have evolved to play critical roles in cellular stress, homeostasis, metabolism, and signaling (Nunnari and Suomalainen, 2012; Friedman and Nunnari, 2014). The mitochondria depend on extremely diverse classes of proteins to support these functions across the four sub-compartments: the outer mitochondrial membrane (OMM), the intermembrane space (IMS), the inner mitochondrial membrane (IMM), and the mitochondrial matrix (Pagliarini et al., 2008; Morgenstern et al., 2017). With the exception of a small fraction of electron transport chain subunits, the overwhelming majority of mitochondrial

proteins, approximately 99%, are nuclear encoded, and thus are translated in the cytosol and subsequently targeted and imported into the correct compartment (Neupert and Herrmann, 2007; Richter-Dennerlein et al., 2015; Becker et al., 2019; Pfanner et al., 2019; Busch et al., 2023).

Evolved from a bacterial ancestor that integrated into an archaeal host as a permanent organelle during the evolution of eukaryotes (Roger et al., 2017), the mitochondria's OMM is now responsible for the communication between the mitochondria and the rest of the cell. The OMM contains two major classes of membrane proteins, β-barrel and α-helical proteins, which rely on distinct biogenesis machinery for integration into the lipid bilayer. Conserved from the mitochondria's bacterial ancestor, β-barrel proteins are inserted into the OMM through a two-step process. They are first translocated into the IMS via the translocase of the outer mitochondrial membrane (TOM) and subsequently inserted into the OMM by the sorting and assembly machinery (SAM) complex (Kutik et al., 2008; Dukanovic and Rapaport, 2011; Höhr et al., 2015; Takeda et al., 2021; Busch et al., 2023). α-helical proteins, however, are unlikely to have been found in the bacterial ancestor's outer membrane, and thus their insertion mechanism into the OMM still remains to be elucidated.

Early studies performed in yeast have characterized the basic principles of α-helical protein integration into mitochondria and identified the mitochondrial import (MIM) complex as the main insertase for α-helical protein integration into the OMM (Becker et al., 2011; Doan et al., 2020). Furthermore, a protein with no sequence or topological similarity, pATOM36, was identified as a functional analogue of the α-helical membrane protein insertion machinery in trypanosomes (Vitali et al., 2018). And most recently, MTCH2 was shown to be an insertase for a diverse variety of OMM α-helical proteins in mammalian cells (Guna et al., 2022).

One of the major α-helical protein substrates of MTCH2 are tail-anchored (TA) proteins, characterized by a single C-terminal transmembrane domain (TMD) followed by a short soluble C-terminal domain. TA proteins targeted to the OMM and inserted by MTCH2 have low hydrophobicity TMDs and are biophysically similar to those targeted to the endoplasmic reticulum (ER) where they are inserted by the ER membrane protein complex (EMC) (Guna et al., 2018). Due to their biophysical similarity, there is thought to be some constitutive levels of mistargeting of TA proteins between the two compartments. Our recent study on the human EMC identified a selectivity filter that controls the subcellular localization of TA proteins and the accurate sorting of TA proteins between the ER and the OMM. The selectivity filter of the EMC uses charge-repulsion to reject mitochondrial TA proteins which are enriched for positive charges in the C-terminal domain (Pleiner

et al., 2023). Whether a reciprocal selection mechanism exists in the OMM is unknown. As the major insertase for mitochondrial TA proteins in the human OMM, MTCH2 is a prime candidate to serve such a selectivity function if it exists at all.

MTCH2 in humans, the MIM complex in yeast, and pATOM36 in trypanosomes represent three distinct OMM insertases. With no obvious homology to one another, these insertases appear to be members of distinct families of proteins. Given the lack of α-helical proteins in bacterial outer membranes, it is highly unlikely that the bacterial predecessor of the mitochondria contained many α-helical proteins in the outer membrane. Thus, the emergence of the α-helical OMM proteome and the machinery responsible for the biogenesis of these proteins must have evolved after the integration of the mitochondria as an organelle.

In metazoans, the mitochondria adopted increasingly multi-functional roles in the cell including regulating key aspects of apoptosis, innate immunity, and mitochondrial dynamics (Ravagnan et al., 2002; Yoon et al., 2003; Seth et al., 2005; Gabaldón and Huynen, 2007; Saotome et al., 2008). These processes need to be strictly regulated to avoid disastrous consequences for the cell, such as immature cell death in the case of poorly regulated apoptosis. Thus, the evolution of an OMM insertase for tighter control of the OMM proteome would have been necessary. Deciphering the role MTCH2 plays in the biogenesis and maintenance of the OMM proteome is key in understanding how the mitochondria, its proteome, and functions have evolved.

In this chapter, we describe our search for a selectivity mechanism for mitochondrial TA proteins in the OMM and the characterization of metazoan and protist MTCH2 homologs. First, we study the features of mitochondrial TA proteins that allow for correct sorting to the mitochondria. Second, we probe MTCH2 through mutational experiments to search for the molecular basis of the mitochondrial selectivity. Third, we hypothesize that MTCH2 may be under regulation and demonstrate that said regulation is nucleotide independent. Finally, we demonstrate that the MTCH2 homologs are able to function as OMM insertases and may have a conserved regulation mechanism to human MTCH2.

4.3 Results

Selectivity at the mitochondria

TA proteins with low hydrophobicity TMDs are either targeted to the ER, where they are inserted by the EMC (Guna et al., 2018), or to the OMM, where they are inserted by MTCH2 (Guna et al., 2022).

We wondered whether ER-destined TA proteins that misinsert into the OMM, do so in a MTCH2 dependent manner. To investigate this, we employed an established split GFP reporter assay to specifically assess the integration of TA proteins into the OMM (Figure 4.1A; Guna et al. 2022). As was previously reported, we reproducibly showed that MTCH2 is indeed responsible for the integration of mitochondrial TA proteins (RHOT2 and MAVS) into the OMM (Figure 4.1B; Guna et al. 2022). Notably, an ER-destined TA protein, squalene synthase (SQS), demonstrated minimal OMM integration. However, the very little misinsertion that does occur appeared to be MTCH2 dependent (Figure 4.1B).

As previously described, some mitochondrial TA proteins are known to dual localize to the ER and can be misinserted by the EMC (Guna et al., 2022; McKenna et al., 2022; Pleiner et al., 2023). Increasing the cytosolic pool of mitochondrial TA proteins, induced by depleting the EMC via knockdown of EMC2, increased integration of these proteins into the OMM (Figure 4.1B). Interestingly, we also noted a decreased integration of SQS into the OMM following EMC depletion (Figure 4.1B), suggesting that even with the increased cytosolic pool of SQS, selectivity at the mitochondria limits its misintegration and the existence of a robust quality control mechanism in the cytosol.

Mitochondrial selectivity of positive charges and their positions

Mitochondrial TA proteins are enriched for positive charges in their C-terminal domains. To investigate whether the OMM is selective for these positive charges, we mutated the positively charged amino acid residues in the C-terminal domains of various TA proteins to observe the effect of charge on integration into the OMM. We selected three mitochondrial TA proteins (MAVS, RHOT2, and OMP25), created charge-swap mutants to generate a series of mutants with increasing amounts of negative charge within its C-terminal domain, and utilizing the split GFP reporter assay assessed their OMM integration. We found that while all mutants remained dependent on MTCH2 for integration to varying degrees (Figure S4.1A), the insertion efficiency of the mutants were inversely correlated with the negative charges introduced (Figure 4.1C). Even single charge swap mutations led to significant decrease in integration of all three substrates into the OMM (Figure 4.1C). For MAVS and OMP25 the combined mutations of their multiple positively charged amino acid residues into negative charges further reduced OMM integration (Figure 4.1C), emphasizing the critical role of the positive charges in the C-terminal domain of TA proteins.

Interestingly, the position of the positively charged amino acid in the C-terminal domain proved to be of significance. We individually mutated the positively charged amino acids in MAVS and OMP25 and observed that mutating the amino acid residue closest to the TMD reduced its integration into the OMM significantly more than when mutating an amino acid further away from the TMD (Figure 4.1C). This suggests that while the OMM selectivity mechanism is sensitive to the presence of positive charges in the C-terminal domain, it is even more selective regarding where they are positioned, favoring positively charged residues closer to the TMD.

We also tested a series of charge mutants of an ER-destined TA protein, SQS (Pleiner et al., 2023), to determine if increasing the number of positive charges within the C-terminal domain of SQS could increase its integration into the OMM. While making the C-terminal domain charge more positive resulted in a slight increase in OMM integration of SQS, it did not convert SQS into a mitochondrial substrate, suggesting that other selectivity mechanisms beyond simple C-terminal domain charge influence SQS's integration (Figure 4.1D). Interestingly, the SQS mutant with a single mutation right after the TMD (+1x mutant) showed comparable OMM insertion rates to the SQS mutant with three mutations (+3 mutant), and was only surpassed by the SQS mutant with four mutations (+4 mutant) which included the same mutation right after the TMD (Figure 4.1D). Moreover, comparing the two SQS mutants with a single mutation revealed that the mutant with a less drastic mutation (S>K) closer to the TMD (+1x mutant) integrated more effectively into the OMM, compared to the more drastic charge swap (D>R) mutation further away from the TMD (+1 mutant) (Figure 4.1D). This observation parallels our findings with the mitochondrial TA proteins and reinforces the idea that selectivity at the OMM is sensitive to the position of the positive charges relative to the TMD.

Finally, we also assessed the integration of the mitochondrial TA protein mutants into the ER, to determine whether the decrease in OMM integration was simply due to an increase in ER integration. Utilizing the split GFP reporter system to specifically query the integration into the ER (Figure S1B; Pleiner et al., 2023), the charge mutants for MAVS and RHOT2 were tested for insertion into the ER. We show that indeed the charge mutants with more negatively charged C-terminal domains integrate into the ER more efficiently. Moreover, for MAVS, the opposite trend to integration into the OMM is observed, where the more negatively charged the C-terminal domain becomes, the more ER integration is observed (Figure S4.1B). This raises an important question: are these mutants unable to integrate into the OMM because they are successfully integrating into the ER, or are they integrating into the ER due to their inability to integrate into the OMM? To address this, we depleted EMC by

performing a knockdown of EMC2 to reduce integration into the ER (Figure S4.1C). The lack of significant increase in OMM integration following EMC knockdown for most of the mutants suggests that their low integration into the OMM is not a result of increased integration into the ER, but rather indicates that the OMM actively selects against these mutants. The rejection from entering the OMM likely results in an increased pool of substrates in the cytosol, consequently increasing the integration of these mutants into the ER.

MTCH2's hydrophilic vestibule does not act as a selectivity filter

Our recent study on the EMC identified a charge-based selectivity filter that contributes to the accurate sorting of TA proteins between the ER and the OMM. Thus, we were interested in how the reciprocal selection operates, specifically, whether a similar mechanism functions at the OMM that governs the selectivity of mitochondrial TA proteins. We focus on MTCH2 as the major insertase of mitochondrial TA proteins. To investigate whether MTCH2 possesses a charge-based selectivity filter analogous to that of the EMC, we examined the AlphaFold2 predicted structural model of MTCH2 (Figure 4.2A). This model revealed that the hydrophilic vestibule of MTCH2 is lined with polar and charged residues. Of significance, at the entrance of the hydrophilic vestibule, where we hypothesize a substrate to dwell as it interacts with MTCH2, we identified patches of negative charges (Figure 4.2A). It should be noted that the negatively charged entrance of MTCH2 is not as prominent as the positively charged selectivity filter observed in the EMC (Pleiner et al., 2023), and it is also not the most conserved region within the MTCH2 model (Figure S4.2A).

To assess the role of these negatively charged patches, we systematically introduced mutations to all of the negatively charged residues that face the hydrophilic vestibule (Figure 4.2B). We then tested the ability of these mutants to rescue the knockout phenotype of MTCH2 using the split GFP reporter system to assess OMM integration. If MTCH2 indeed functioned as a charge-based selectivity filter like the EMC, we would anticipate that mutating these residues would reduce insertion of the mitochondrial TA proteins, MAVS and RHOT2. Contrary to predictions, most mutations had little to no effect. Some mutations showed substrate dependent effects. For example, the mutations E112S and D209A affected MAVS more than RHOT2. However, the full charge swap mutations of these positions, E112R and D209R, had little effect on OMM integration of both substrates, suggesting that the effect of reduced insertion activity of the E112S and D209A mutants are not due to the amino acid charge at these positions. Furthermore, mutating E123 and E127 resulted instead in increased protein integration into the OMM (Figure 4.2C). These two residues are positioned further inside the

hydrophilic cavity and may not be involved in substrate selectivity. Together, this suggests that MTCH2 may not have a similar charge-based selectivity filter as the EMC.

We also tested a combination of substrate charge mutants with MTCH2 charge mutants in a split GFP reporter assay. In the case of the EMC, flipping the charges in both the EMC and the substrate rescued the decreased insertion phenotype resulting from one or the other mutant. However, we found that no MTCH2 mutation that decreased insertion when paired with wildtype (WT) MAVS was able to counter and increase insertion into the OMM with any of the charge mutants of MAVS (Figure 4.2D). Instead, only mutations such as E123R and E127R, which increase insertion of even the WT MAVS construct, also showed increased integration into the OMM of the charge mutants (Figure 4.2D). These observations further implicating that MTCH2 does not have a charge-based selectivity mechanism similar to that of the EMC.

MTCH2 activity might be regulated

To tackle the question of how MTCH2 inserts its substrates into the OMM, a broad mutational panel of MTCH2 was performed to identify key residues for MTCH2 function. Including previous mutational studies (Guna et al., 2022), we identified three mutations that stood out as significantly increasing MTCH2 activity: K25E, Y235A, and V238D (Figure 4.3A). The triple mutant combining all three mutations displayed an additive effect with further increased MTCH2 insertion activity (Figure 4.3B). To further explore these mutations, we tested the insertion activity of the individual mutants, as well as the triple mutant, alongside a mutant that causes decreased MTCH2 activity (D189A), on a panel of substrates (Figure 4.3C). While V238D showed varying increase in insertion activity depending on the substrate; at similar expression levels K25E, Y235A, and the triple mutant were all effective in increasing OMM integration of most substrates (Figure 4.3C, S4.3A). This indicates that the MTCH2 mutants, in particular K25E and Y235A, do seem to generally increase MTCH2 activity and may be disrupting a regulatory mechanism. A number of substrates, TOM70 and TSPO, notably do not show any increased integration into the OMM (Figure 4.3C). This may indicate that these substrates are tightly regulated and do not accumulate over endogenous levels, and consequently even with increased insertion mediated by MTCH2, the quality control pathways associated with these substrates efficiently turnover the excess proteins. Mutations that increase the activity of insertases are almost unheard of and suggest that MTCH2's insertion activity may be under a regulatory mechanism.

MTCH2 regulation is not nucleotide dependent

While the regulatory mechanism underlying MTCH2 activity remains to be determined, studies on the SLC25 family of proteins, that MTCH2 is a member of, may provide an insight. Previous studies on the SLC25 family member UCP1, a proton transporter in the IMM, demonstrated that its proton leak activity is inhibited by nucleotide binding (Lee et al., 2015; Jones et al., 2023; Kang & Chen, 2023). Given that MTCH2 is a member of this SLC25 family, we compared the structures of MTCH2 and UCP1, focusing on where the nucleotide binds in UCP1 and the position of the mutations which increased MTCH2 activity (Figure S4.3B). From the similarities in their structures and position of the amino acid residues, we hypothesized that MTCH2 may also possibly bind nucleotides to regulate its activity.

To test this hypothesis, a thermal unfolding assay was employed to assess the thermostability of MTCH2 in the presence of various nucleotides. For this GFP-MTCH2 was incubated in increasing temperatures, followed by a high-speed centrifugation to pellet any unfolded and aggregated protein. The supernatant containing the soluble GFP-MTCH2 was sampled and GFP fluorescence was measured as a proxy for how much GFP-MTCH2 remained folded and in solution. When measuring GFP-MTCH2 alone, the normalized GFP fluorescence dropped to 0.5, where 50% of the GFP-MTCH2 remains folded and soluble, at 65˚C. Loss of detectable GFP fluorescence above background, indicating 100% of the GFP-MTCH2 is unfolded, was observed at 80˚C (Figure 4.3D). We then tested the effect of adding ATP and GTP and found no difference in GFP-MTCH2 unfolding (Figure 4.3D, S4.3C), suggesting that there is no difference in GFP-MTCH2 thermostability and nucleotide binding is unlikely. Intriguingly, we identified a non-hydrolyzable form of GTP, GDPNP, that increased the thermostability of GFP-MTCH2 (Figure 4.3D).

With this peculiar result, we then wanted to test whether GDPNP has any effect on MTCH2's insertion activity. To test this, we performed an insertion assay with an *in vitro* translated substrate into MTCH2 reconstituted proteoliposomes incubated with GDPNP (Figure 4.3E, S4.3D). Unfortunately, we saw no difference in insertion efficiency with or without GDPNP (Figure 4.3E). These findings collectively suggest that the regulation of MTCH2 activity is unlike UCP1 regulation and is not nucleotide dependent.

MTCH2 homologs are conserved across metazoans and are OMM insertases

Searches for homologs of OMM insertases have identified MTCH2-related proteins distributed across all metazoan species and closely related protists within the holozoan clade (Figure 4.4A; Guna et al., 2022; Stevens PhD Thesis, 2023). They all share similar features to human MTCH2, namely the absence of a sixth TMD compared to the SLC25 family, and they also share the same topology with the N-terminus facing the cytosol and C-terminus facing the IMS (Stevens PhD Thesis, 2024). While most species only have a single MTCH gene, humans and closely related metazoan species also express a MTCH1 paralog.

The paralog MTCH1 is predicted to be very similar in structure to MTCH2, and thus has been hypothesized to also functions as an OMM insertase. To test this, a split GFP reporter assay was performed to query for substrate insertion into the OMM either in a MTCH2 knockout background or with a MTCH1 knockdown. As previously demonstrated, the MTCH2 knockout decreased the insertion of MTCH2 dependent substrates, MAVS and OMP25, but did not affect the MTCH2 independent substrate TIM9A (Figure 4.4B). Similarly, the MTCH1 knockdown decreased the integration into the OMM of MAVS and OMP25, but not TIM9A. Significantly, both the MTCH2 knockout and MTCH1 knockdown phenotypes of reduced insertion could be rescued by overexpressing a rescue MTCH1 or MTCH2 construct (Figure 4.4B). This demonstrates that indeed both MTCH1 and MTCH2 can function as OMM insertases and can compensate for one another.

To assess the activity of the MTCH2 homologs from other organisms, the split GFP reporter assay was performed to test their ability to rescue the MTCH2 knockout phenotype in human cells. We observe the strongest rescue phenotype with human MTCH2 for both MAVS and OMP25, except for the *C. owczarzaki* rescue of MAVS (Figure 4.4C). *X. tropicalis* showed comparable rescue for both substrates, while *D. melanogaster* and *N. vectensis* showed reduced rescue phenotypes (Figure 4.4C). All homologs were able to at least partially rescue the knockout phenotype, demonstrating that homologs from a variety of different organisms are able to insert mitochondrial TA proteins into the OMM of human cells.

MTCH2 regulation is a conserved functional mechanism

We wanted to investigate whether the hypothesized regulatory mechanism behind human MTCH2 activity was also a conserved feature of these homologs. For this we mutated human MTCH1 and the

MTCH2 homologs at the corresponding positions K25 and Y235 of human MTCH2 for increased activity and D189 for decreased activity. For the MTCH1 mutants (K103E, Y326A, and D263A) we overexpressed the mutants and monitored the insertion of substrates into the OMM using the split GFP reporter assay. The MTCH1 mutants showed the same increase in activity with K103E and Y326A and decrease in activity with D263A, as we saw with MTCH2 and its mutants (Figure 4.5A).

We next assessed the MTCH2 homologs from other organisms and their mutations in their ability to rescue the MTCH2 knockout phenotype. *X. tropicalis*, the closest species to humans, showed the same trend as human MTCH2 with both the K25E and Y230A mutants increasing MTCH2 activity (Figure 4.5B). While the more distant *D. melanogaster* and *N. vectensis* only showed increased MTCH activity with their K38E and K39E mutants respectively but not their Y241A and Y247A mutants. Finally, *C. owczarzaki* showed no increase in activity with its K39E mutation, but instead only with the F324A mutation. While the effect on the insertion activity of each homolog varied, we were able to increase the activity of all the homologs tested. These findings suggest that the MTCH2 homologs may share similar regulatory mechanisms that modulate its activity.

4.4 Discussion

These results are a part of ongoing work to dissect TA protein insertion into the OMM and determine the molecular mechanism by which MTCH2 achieves this. Our findings here are in agreement with previous work that enrichment of positive charges in the C-termini of TA proteins is a signal for integration into the OMM (Isenmann et al., 1998; Horie et al., 2002; Borgese et al., 2007). We have further shown that not only is the presence of said positively charged residues but their positions relative to the TMD is critical in their ability to localize to the mitochondria. For many TA proteins, the soluble C-terminal domains are functionally dispensable and may have evolved to primarily facilitate accurate sorting. However, the precise mechanism by which the positive charges specify mitochondrial localization is still unclear.

In previous work, we have shown the molecular logic behind the enrichment of positive charge in the C-terminal domain of mitochondrial TA proteins serving as a flag for discrimination by the EMC at the ER (Pleiner et al., 2023). This formulated the idea that limited misinsertion of mitochondrial TA proteins at the ER arose from the combined evolution of mitochondrial TA protein's positively charged C-termini and the positively charged hydrophilic vestibule of the EMC. One possible theory that resulted from this is that TA proteins are initially targeted to the ER and those rejected by the

charge selectivity filter of the EMC are then targeted to the other organelles including the mitochondria. However, our data presented here does not agree with this. When insertion to the ER was knocked down, the integration into the OMM of mitochondrial TA proteins did not significantly increase. We were also unable to direct an ER destined TA protein, SQS, to integrate better into the OMM. To fully understand the mechanics of protein localization and protein homeostasis, further details on which protein imposes the selectivity and how it enforces its selection is necessary.

We hypothesized that as the major OMM insertase, MTCH2 could be said protein that acted as a selectivity filter for mitochondrial TA proteins. However, our initial screening of MTCH2 for a charge-based selectivity filter analogous to the EMC failed to identify any such feature. In this study we mutated each of the negatively charged residues facing the hydrophilic vestibule on MTCH2 individually. What was observed was that most mutations had little to no effect, while some even resulted in increased insertion of MTCH2 substrates. This raises the question of whether these patches of negatively charged residues play a tiny role in charge repulsion even if not the main selectivity filter or if they play any role at all in MTCH2 function. The patches of negatively charged residues are in a region of low sequence conservation for MTCH2. Nevertheless, while the region is not strictly conserved at the amino acid sequence, the MTCH2 homologs that were identified all have a similar structural fold in the membrane, in addition to having negatively charged patches on the cytosolic side in the vicinity of the entrance to the hydrophilic vestibule. Thus, this may be a conserved feature which may act as a charge filter that simply is not observable on the amino acid sequence level. As only individual amino acids have been mutated and tested, it would be of interest to mutate multiple residues together and study the negatively charged patch in its entirety.

Nevertheless, it should be noted that the negatively charged patches at the entrance of MTCH2 are not as prominent as the positively charged selectivity filter observed in the EMC. Additionally, no single mutant disrupts the insertion activity as much as some did for the EMC (Pleiner et al., 2023), suggesting that the two insertases may operate through different mechanisms for the recognition and insertion of their target proteins. Furthermore, we observe that the mitochondria, and its insertion machineries, including MTCH2, is more sensitive and selective against the position of the positive charge within the C-termini of TA proteins. This is in contrast to the EMC that does not seem to care about the position of the charges but instead is discriminating the substrates simply by overall charge in the C-termini (Pleiner et al., 2023). Put together, the selectivity by MTCH2, if any, is likely not based on a simple charge repulsion filter. One possible explanation for this is that the substrate charge

selection is simply not happening at MTCH2 but at steps prior to its hand-off to MTCH2, such as the targeting of the substrates to the mitochondria, a process that is not well understood. This is an avenue of pursuit that would be interesting to follow up on.

In line with this idea, the ER-destined TA protein SQS was mutated to have a more positively charged C-terminal domain, as opposed to its negatively charged wildtype counterpart, but still failed to integrate efficiently into the OMM. There are a number of possibilities as to why we fail to see OMM integration of SQS. The first is simply that it does integrate into the OMM, however, as it does not belong in the OMM, quality control machineries quickly turn over the mislocalized SQS. The second is that the mutations introduced into the C-termini have created a mitochondrial targeting sequence and the protein is getting translocated into the matrix, while the current assay can only read out GFP conjugation in the IMS. Finally, the third is that there are additional factors that impose the selection criteria for mitochondrial integration, and they select for features beyond C-terminal charge that SQS does not fit. It is prudent to determine which of these is the likely explanation to understand the selection mechanism occurring at the mitochondria. To test the first explanation of a fast turnover of SQS in the OMM, inhibitors to the quality control pathways, such as an E3 ligase inhibitor, could be used to see if the mislocalized SQS can be stabilized. To evaluate the second possibility, we can perform an *in vitro* insertion assay into isolated mitochondria to assess whether there is any import at all. The final possibility will require an exploratory approach into investigating selectivity in targeting pathways to the mitochondria. Genetic CRISPR screens and proteomic studies will aid in the initial identification of such targeting factors and should then be followed-up with a biochemical dissection of how they exert their selection.

While the molecular mechanism of substrate selectivity and the MTCH2 insertion mechanism are both unclear, we have made key observations that provide initial ideas that MTCH2 may be regulated in performing this key function. The hyperactive mutants reported to increase the activity of an insertase is unheard of, as mutations in insertases usually disrupt the insertion activity, and could be an indication that MTCH2's insertion activity may be under a regulatory mechanism (Pleiner et al., 2020; Miller-Vedam et al., 2020; O'Donnell et al., 2020; Pleiner et al., 2023). The need for regulating MTCH2 activity is not a surprise, given prior studies from our lab showing that MTCH2 mutants with increased insertion activity can increase cellular sensitivity to apoptosis (Guna et al., 2022). Additionally, it has been previously reported in literature that modulating MTCH2 impacts lipid accumulation in both mice and *C. elegans* (Rottiers et al., 2017), and that MTCH2 is implicated in

starvation-induced mitochondrial hyperfusion (Labbé et al., 2021). It is possible that MTCH2 evolved from an SLC25 family member, and the regulatory mechanism of that SLC25 protein was conserved to enable regulation of MTCH2. As a mitochondrial carrier, the SLC25 family of proteins are responsible for maintaining solute flux to fulfil the needs of the metabolic pathways in which they are involved, and thus their activity must be regulated under various physiological conditions. Modulation of activity can be achieved through i) interactions with inhibitors or activators, ii) changes in gene expression at the transcriptional or translational level, and iii) changes in kinetic driving forces such as substrate concentration (Palmieri, 2013). Our MTCH2 mutants show increased activity even at similar expression levels and there is a lack of evidence of insertase activity being regulated by increase in substrate concentrations, strongly indicating that MTCH2 activity, if regulated, could be regulated via a small molecule interaction. UCP1, an SLC25 family member, has been demonstrated to be regulated through inhibition by nucleotide binding (Lee et al., 2015; Jones et al., 2023; Kang & Chen, 2023). We noted the significant resemblance of MTCH2 to UCP1 in its nucleotide binding conformation and the position of the amino acid residues in the binding pocket that increase MTCH2 activity. Nevertheless, our data does not agree with MTCH2 binding to any nucleotide nor is its activity effected by the presence or absence of nucleotide.

It would be of great interest to identify a small molecule that binds to and regulates MTCH2, and to further investigate whether the resultant change in MTCH2 activity will stimulate a response in the involved metabolic pathway by remodeling the OMM proteome. One approach to identifying the small molecule would be to utilize small molecule metabolite or drug libraries, to test for either MTCH2 binding or changes to MTCH2 insertion activity in cells. Once identified, structural characterization of MTCH2 in its small molecule bound or protein substrate bound state would enable more detailed studies of the mechanism behind the regulation of MTCH2 activity. Does the small molecule function by steric hinderance of the insertion pathway within MTCH2? Or does the small molecule interaction cause a conformation change altering substrate interaction? These studies would provide insight into how small molecule drugs could be developed to more precisely and/or potently target MTCH2 activity and provide a tool for modulating the OMM proteome.

In attempting to modulate the OMM proteome, we would need to look at the roles other insertases could be playing. MTCH1, the MTCH2 paralog, has been speculated to also function as an insertase. Here, we were able to demonstrate that MTCH1 can rescue a MTCH2 knockout phenotype in cells and that MTCH1 indeed functions as an insertase at the OMM. However, whether the MTCH1 and

MTCH2 paralogs are completely redundant or whether they play different roles in maintaining the OMM proteome is unclear. Of significant note, while we are able to generate MTCH2 knockout cells in K562 cells, we have not been able to generate MTCH1 knockout cells. Suggesting that there is a difference in the role the two paralogs play and that MTCH2 cannot fully compensate the loss of MTCH1 in K562 cells. So, what are the key differences? These differences could be in their insertion mechanism, protein activity regulation, or substrate specificity. It would be of interest to understand the physiological relationship between MTCH1 and MTCH2, and how each play their individual roles in maintaining the OMM proteome.

We have also demonstrated here that MTCH2 represents a class of metazoan OMM insertases. The metazoan MTCH2 homologs studied here all show the capability to function as an OMM insertase in a human cell line. Furthermore, mutations to the MTCH2 homologs alter their activity in much the same way as human MTCH2 activity is affected. This indicates possibly a conserved regulatory mechanism for the metazoan MTCH2 function, and more widely MTCH2's role in remodeling of the OMM proteome and regulation of the involved metabolic pathways. With the independent evolution of MTCH2 in metazoans, the MIM complex in fungi, and pATOM36 in trypanosomes, it would be of great interest to investigate whether the other OMM insertases are also under regulation. This will provide insight into understanding the necessity of the evolution of OMM insertases and the role of the OMM insertases in the evolution of the OMM proteome.

In summary, we have characterized the positively charged residues in the C-termini of mitochondrial TA proteins as a source of mitochondrial selection. Whether MTCH2 confers this substrate selectivity at the OMM will need further investigation. However, specificity is not only determined at the membrane and the mechanism by which the targeting step contributes to specificity is an area that requires further study. We have also provided insight into a regulatory mechanism of metazoan MTCH2 activity on protein insertion into the OMM. Further studies into the mechanistic details of MTCH2's protein insertion activity, and in particular the regulatory mechanism of OMM insertases, holds promise to better understand how they contribute to the proteostasis of the mitochondrial proteome.

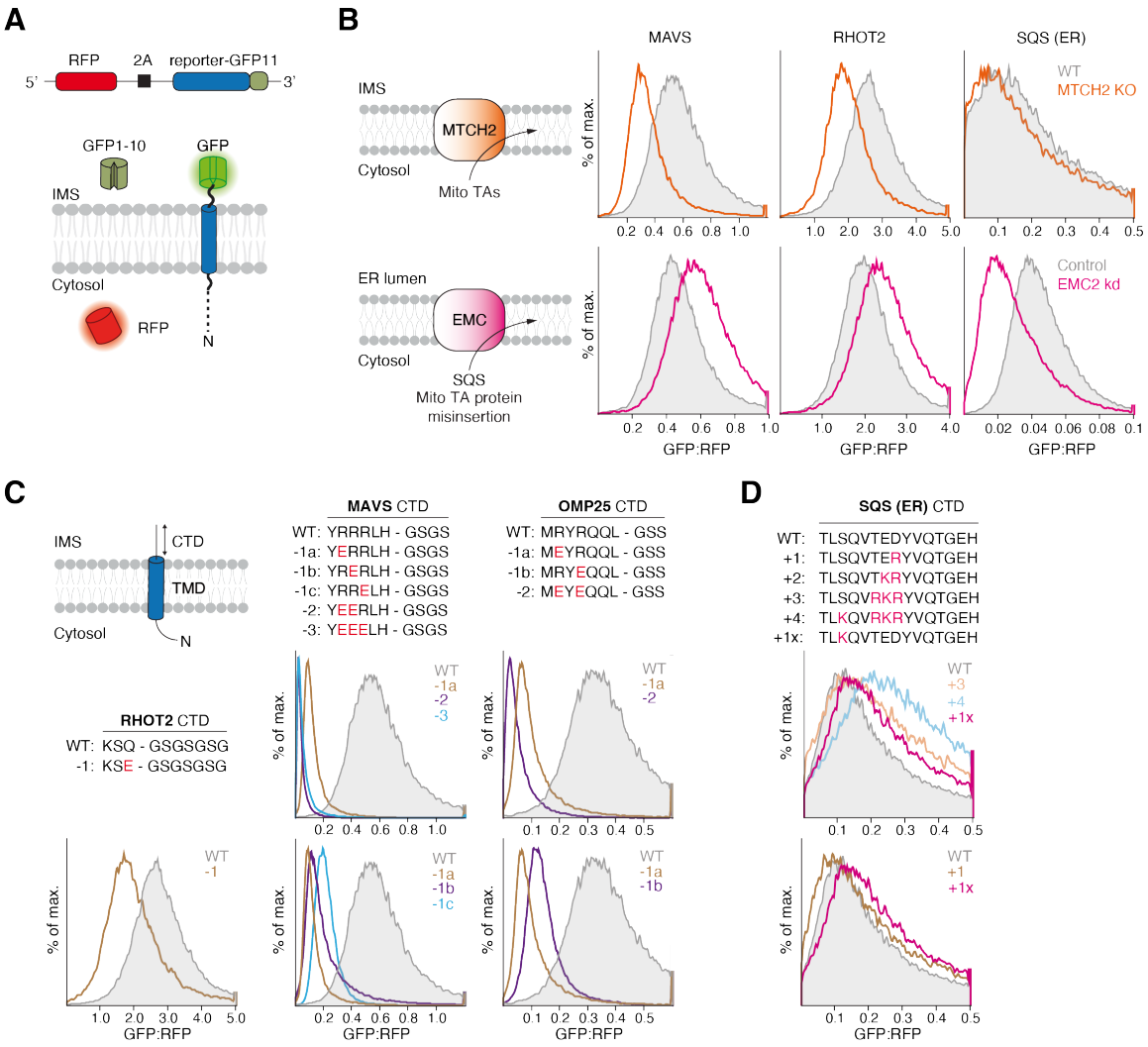

Figure 4.1. Positively charged C-terminal domains of TA proteins are critical for OMM integration.

(**A**) Schematic of the split GFP reporter system used to selectively monitor TA protein insertion into the OMM. TA proteins fused to GFP11 are expressed in K562 cells constitutively expressing GFP1-10 in the IMS, along with a translation normalization marker (RFP). Successful integration into the OMM results in GFP complementation and fluorescence. (**B**) (Left) OMM and ER insertion pathways. (Right) OMM insertion of the indicated mitochondrial (MAVS, RHOT2) and ER (SQS) TA proteins, using the split GFP system as described in (A), was assessed in MTCH2 knockout (KO) cell and in cells transduced with either a non-targeting (control) or EMC2 knockdown (kd) single guide RNA. GFP fluorescence relative to the normalization marker RFP was determined by flow

cytometry and displayed as a histogram. (**C**) Schematic of a TA proteins C-terminal domain (CTD). The C-terminus of several mitochondrial TA proteins (RHOT2, MAVS, OMP25) was mutated to introduce negatively charged residues at the indicated positions. Integration of the indicated mitochondrial TA protein mutants into the OMM was determined using the split GFP reporter system described in (A). (**D**) As in (C) monitoring OMM insertion but for the ER TA protein, SQS, where mutations introduced positively charged residues to the CTD.

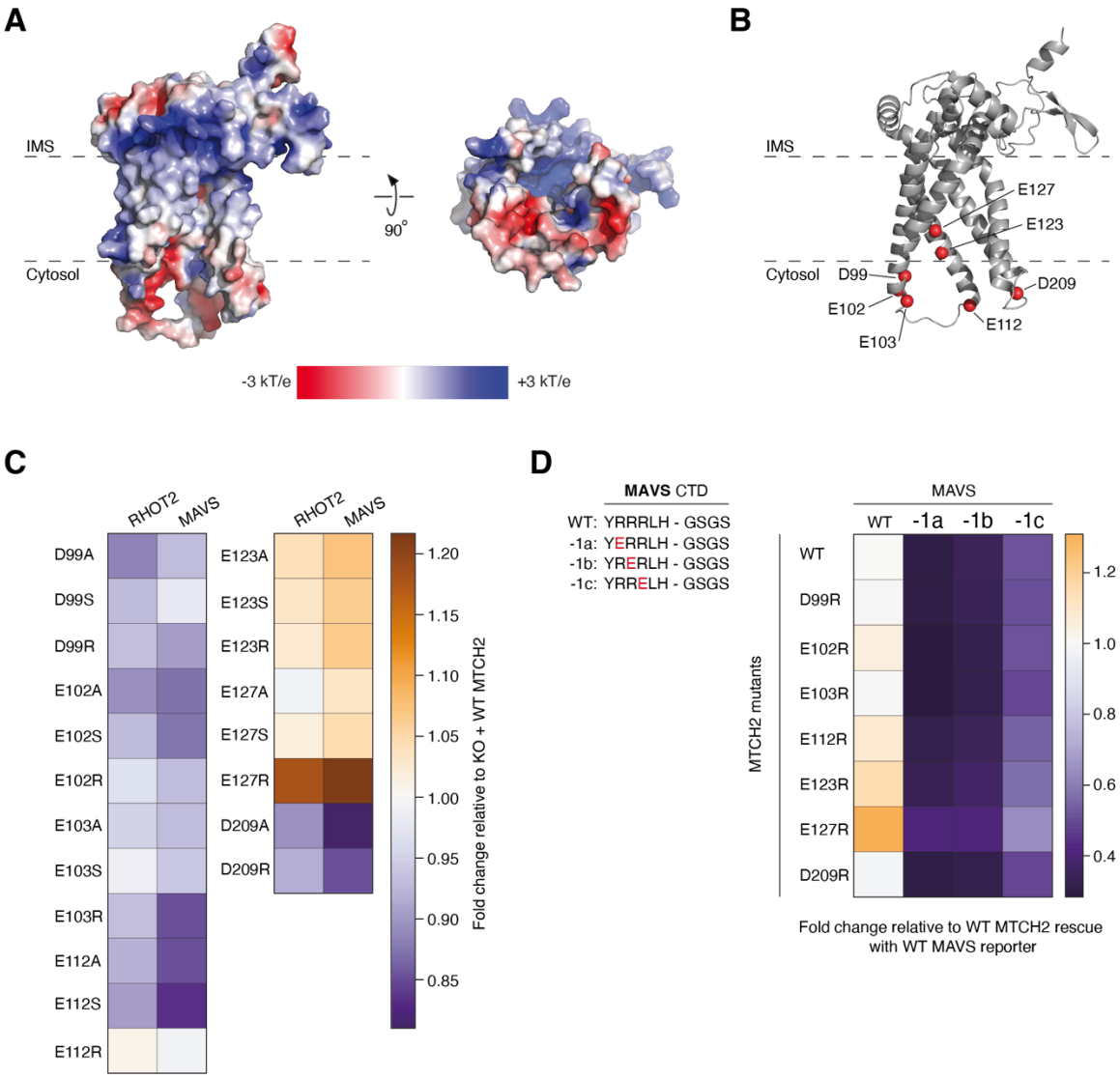

Figure 4.2. Characterization of the cytosolic residues required for selectivity by MTCH2.

(**A**) Surface representation of the electrostatic potential of the AlphaFold2 predicted model of MTCH2 ranging from -3 to +3 kT/e. (Left) A view of MTCH2 looking partially into the hydrophilic vestibule. (Right) A view of the hydrophilic vestibule of MTCH2 from the cytosol. (**B**) AlphaFold2 predicted model of MTCH2 highlighting negatively charged residues within the hydrophilic vestibule. (**C**) The effects of each MTCH2 mutant rescue, on top of a MTCH2 KO, on the insertion of MTCH2-dependent (MAVS, RHOT2) substrates was determined using the split GFP reporter assay described in Figure 4.1A. Shown is a heat map summarizing the mutant MTCH2 rescue normalized to WT MTCH2 rescue. (**D**) (Left) Schematic of MAVS CTD charge series. (Right) Same

as in (C) but a subset of MTCH2 mutants were tested against a panel of MAVS charge mutants. Depicted is a heat map of substrate insertion relative to WT MAVS insertion with WT MTCH2 rescue.

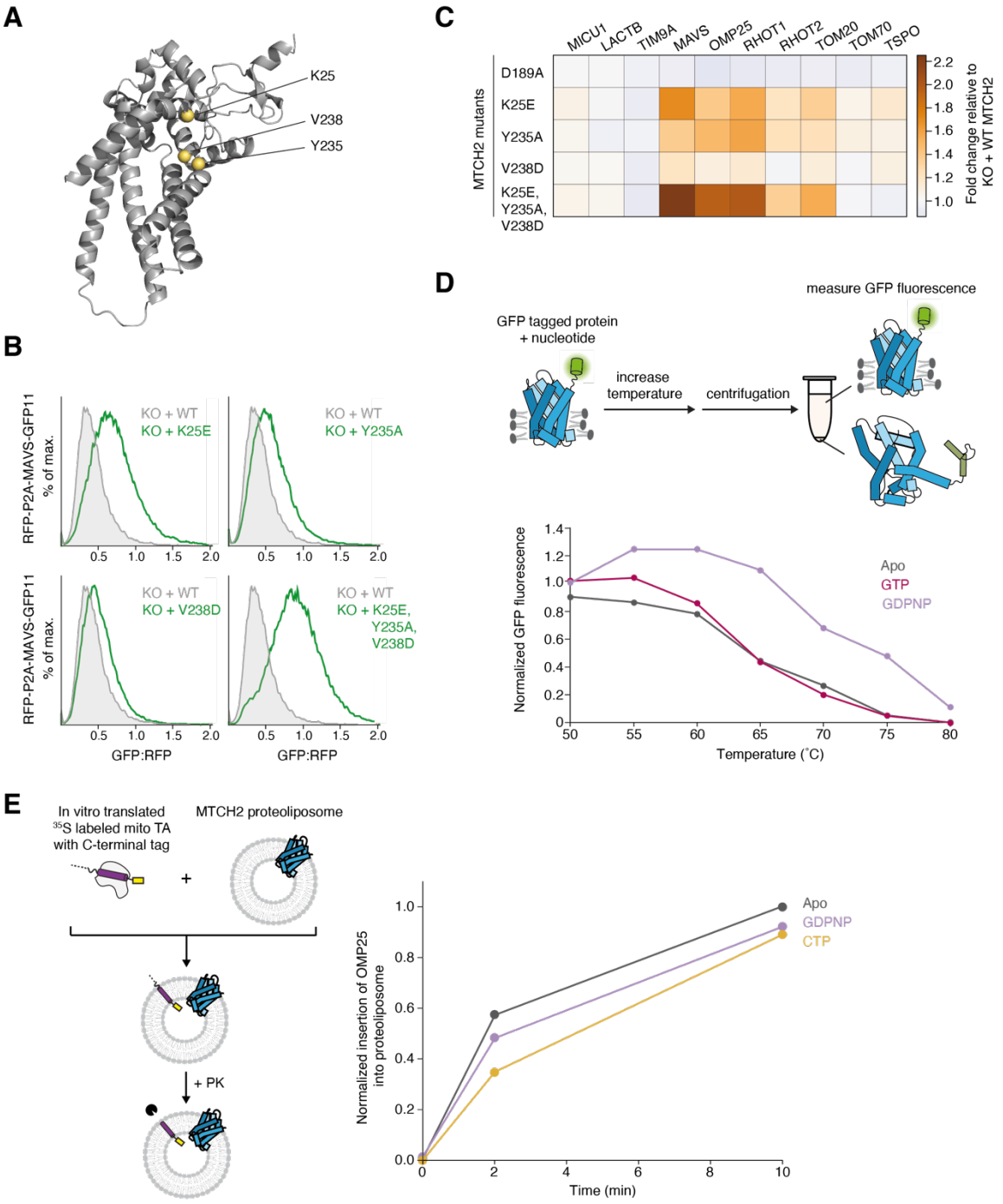

Figure 4.3. Exploring the regulatory mechanism of MTCH2.

(**A**) AlphaFold2 predicted model of MTCH2 highlighting three amino acids which increase MTCH2 insertion activity when mutated. (**B**) MTCH2 KO cells transduced with lentivirus to express either WT MTCH2 or the indicated MTCH2 mutants. OMM insertion of MAVS was assessed using the

split GFP reporter system. The GFP:RFP ratio for each mutant was determined using flow cytometry and is plotted as a histogram. (**C**) Same as in (B) but assessing a variety of MTCH2-independent (MICU1, LACTB, TIM9A) and MTCH2-dependent (MAVS, OMP25, RHOT1, RHOT2, TOM20, TOM70, TSPO) substrates. Depicted is a heat map showing the effects of the MTCH2 mutants normalized to WT MTCH2 rescue. (**D**) (Top) Schematic of thermal unfolding assay. GFP-MTCH2 is incubated at increasing temperatures, followed by centrifugation to pellet unfolded and aggregated protein. The soluble protein in the supernatant is measured for GFP fluorescence. (Bottom) The normalized GFP fluorescence of the supernatant post-centrifugation is plotted against the temperature at which GFP-MTCH2 was incubated. The addition of GDPNP but not GTP increase GFP-MTCH2 thermostability at higher temperatures. (**E**) (Left) Schematic of *in vitro* insertion assay into proteoliposomes, using protease protection of a C-terminal tag as a readout for insertion. A TA protein was *in vitro* translated in rabbit reticulocyte lysate supplemented with ^{35}S-methionine enabling detection by autoradiography. After incubating with MTCH2 reconstituted proteoliposomes, reactions were treated with proteinase K (PK). For TA proteins, the resulting protease protected fragment was affinity purified via a tag on its C-terminus, ensuring insertion into the proteoliposome in the correct orientation, and analyzed by SDS-PAGE and autoradiography. (Right) OMP25 insertion into MTCH2 reconstituted proteoliposomes was assessed at 0, 2, and 10 minutes by protease protection. Time course of insertion in the presence of GDPNP or CTP (as a nucleotide control) was quantified.

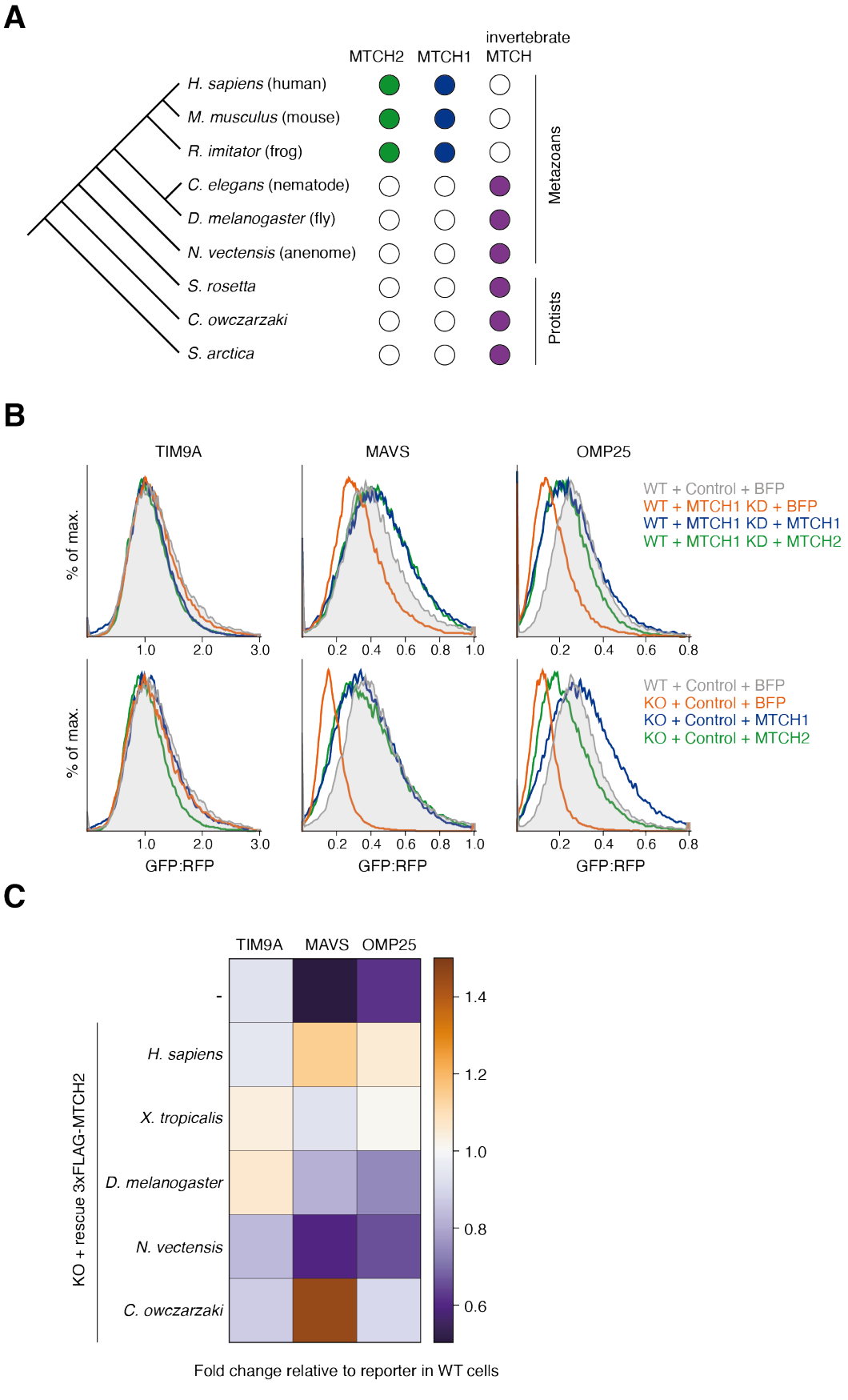
A
MTCH2
MTCH1
invertebrate MTCH
H. sapiens (human)
M. musculus (mouse)
R. imitator (frog)
C. elegans (nematode)
D. melanogaster (fly)
N. vectensis (anenome)
S. rosetta
C. owczarzaki
S. arctica
Metazoans
Protists
B
TIM9A
MAVS
OMP25
% of max.
WT + Control + BFP
WT + MTCH1 KD + BFP
WT + MTCH1 KD + MTCH1
WT + MTCH1 KD + MTCH2
KO + Control + BFP
KO + Control + MTCH1
KO + Control + MTCH2
GFP:RFP
C
TIM9A
MAVS
OMP25
-
H. sapiens
X. tropicalis
D. melanogaster
N. vectensis
C. owczarzaki
KO + rescue 3xFLAG-MTCH2
Fold change relative to reporter in WT cells

Figure 4.4. MTCH2 homologs can function as OMM insertases.

(**A**) Species tree of metazoans and closely related protists with graphical representation of MTCH2 homolog conservation. Species with only a single MTCH gene are represented as an invertebrate MTCH. (**B**) OMM insertion of MTCH2-independent (TIM9A) and MTCH2-dependent (MAVS, OMP25) substrates was assessed using the split GFP reporter system in WT cells transduced with either a non-targeting (Control) or MTCH1 kd single guide RNA, and MTCH2 KO cells transduced with a non-targeting (Control) single guide RNA. The guide RNA transduced cells were further transduced to express MTCH1 or MTCH2 rescue constructs. The GFP:RFP ratio was determined using flow cytometry and is plotted as a histogram. (**C**) MTCH2 KO cells were transduced with lentivirus to express either human MTCH2 or the indicated MTCH2 homologs. OMM insertion of MTCH2-independent (TIM9A) and MTCH2-dependent (MAVS, OMP25) substrates was assessed using the split GFP reporter system. The heat map shows the relative insertion of the substrates compared to insertion in a WT cell.

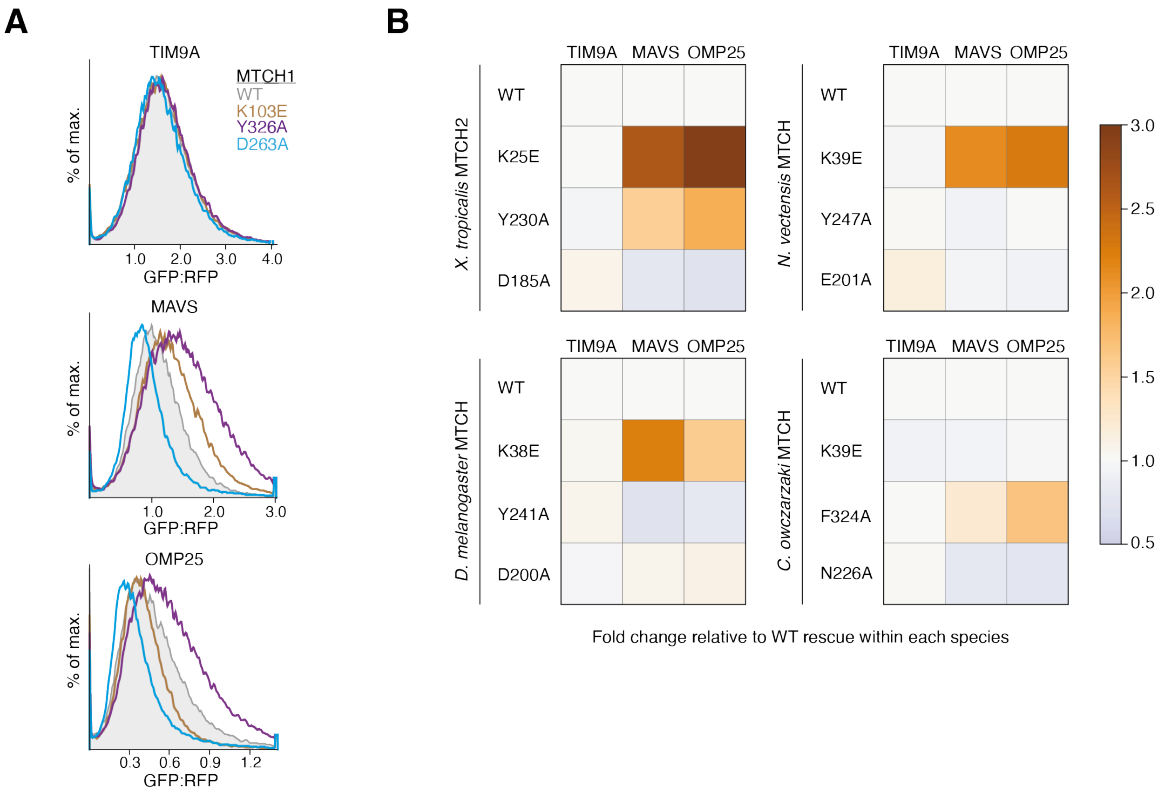

Figure 4.5. MTCH2 homologs are under the same regulatory mechanism.

(**A**) WT cells were lentivirally transduced to express either the WT or indicated mutants of MTCH1. The split GFP reporter assay was used to assess the OMM insertion of TIM9A, MAVS, and OMP25. The GFP:RFP ratio is plotted as a histogram. (**B**) As in Figure 4.4 (C) but expressing the indicated mutants of each MTCH2 homolog based on the sequence conservation shown in Figure S4.4. The heat maps depict the relative insertion normalized to the WT rescue of each MTCH2 homolog.

4.5 Materials and Methods

Plasmids and antibodies

Constructs for *in vitro* translations in rabbit reticulocyte lysate were cloned into the pSP64 vector (Promega, USA). pLG1-puro non-targeting sgRNA 3, used for cloning CRISPRi sgRNAs, was a gift from Jacob Corn (Addgene plasmid #109003). The second generation lenti-viral packaging plasmid psPAX2 (Addgene plasmid #12260) and envelope plasmid pMD2.G (Addgene #12259) were gifts from Didier Trono. The pHAGE2 lenti-viral transfer plasmid was a gift of Magnus A. Hoffmann and Pamela Bjorkman. For expression in K562 cells, a lenti-viral backbone containing a UCOE-EF-1α promoter and a 3′ WPRE element was used (Addgene #135448), which was a kind gift of Martin Kampmann and Jonathan Weissman.

Endogenous sequences used in this study for in cell reporter assays were sourced from UniProtKB/Swiss-Prot and included: SQS/FDFT1 (**Q6IAX1**), OMP25/SYNJBP (**P57105-1**), MAVS (**Q7Z434-1**), TIM9 (**Q9Y5J7-1**), RHOT1 (**Q8IXI2-1**), RHOT2 (**Q8IXI1-1**), TSPO (**P30536**), TOM20 (**Q15388**), TOM70 (**O94826**), MTCH1 (**Q9NZJ7**), MTCH2 (**Q9Y6C9**), *X. tropicalis* MTCH2 (**Q6P818**), *D. melanogaster* MTCH (**Q9V3Y4**), *N. vectensis* MTCH (**A7SSN1**), and *C. owczarzaki* MTCH (**A0A0D2WXZ**5).

The following antibodies were used in this study: rabbit polyclonal anti-MTCH2 (16888-1-AP, Proteintech, USA); mouse monoclonal anti-alpha-tubulin (T9026, Millipore-Sigma, USA). Secondary antibodies used for Western blotting were: goat anti-mouse- and anti-rabbit-HRP (#172-1011 and #170-6515, Bio-Rad, USA).

The following sgRNAs were cloned into pLG1 for CRISPRi knockdowns: non-targeting control (GGCTCGGTCCCGCGTCGTCG); EMC2 (GCCATCTTCCCAGAACCTAG); MTCH1 guide 1 (GCGGCACCGCCGCGAGCCCA); MTCH1 guide 2 (GAGCCCAGGGCGCCACTTCC)

Cell culture

K562 cells were grown in RPMI-1640 medium supplemented with 10% FBS, 100 U/mL Penicillin, and 100 µg/mL Streptomycin. Cells were maintained between 0.25 and 1.00×10^6 cells/mL. Cells were grown in a humidified incubator at 37°C and 5% CO_2. All K562 cells stable expressed dCas9-BFP-KRAB (KOX1-derived) and constitutively expressed β-strands 1-10 of GFP in the

intermembrane space via fusion to an N-terminal MICU1 signal sequence as previously described (Guna et al., 2022). MTCH2 knockout cell lines were generated using CRISPR-Cas9 as previously described (Guna et al., 2022).

Adherent HEK293T cells were grown in Dulbecco's Modified Eagle Medium (DMEM) supplemented with 10% FBS, 2 mM glutamine, 100 units/mL penicillin and 100 µg/mL streptomycin. Cells were grown in a humidified incubator at 37°C and 5% CO_2. Expi293F cells were grown in Expi293 Expression Medium in a humidified incubator at 37°C and 8% CO_2, while shaking at 125 RPM. Cells were maintained between 0.5 and 2.0 × 10^6 cells/mL.

Lentivirus production

Lentivirus was produced by co-transfecting HEK293T cells with a desired transfer plasmid and two packaging plasmids (psPAX2 and pMD2.G) with TransIT-293 transfection reagent (Mirus, USA). 48 hours post-transfection, the culture supernatant was harvested, and flash frozen in liquid nitrogen. Lentivirus was rapidly thawed right before use for transduction.

Lentivirus transduction

K562 cells were transduced with lentivirus by spinfection. Briefly, 0.25 × 10^6 cells were mixed with 50-200 µL of lentiviral supernatant, RPMI medium, and polybrene (final 8 µg/mL) in a total volume of 1 mL in a 24-well plate. The plates were spun at 1,000 ×g for 1.5 h at 30˚C. Lentiviral substrate reporter constructs for flow cytometry analysis contained an upstream UCOE-EF1α promoter, followed by RFP, a P2A site, and the substrate reporter fused to GFP11 via a Gly-Ser linker. For all mitochondrial TA proteins and their mutants, the full-length human coding regions were used. For the SQS mutants the cytosolic linker (residues 2-70) of human SEC61β was fused to the N-terminal flanking region, TMD, and complete C-terminus of human SQS/FDFT1 (residues 378-end). Charge mutations for each substrate were introduced as shown in Figure 4.1C-D. The MTCH2 rescue constructs were expressed from a lentiviral transfer plasmid with an upstream UCOE-EF1α promoter, followed by an N-terminal TagBFP-P2A, and MTCH2. In addition, where indicated MTCH2 homologs were fused to an N-terminal 3xFLAG tag. Mutations for MTCH2 were introduced as indicated in Figures 4.2B and 4.3A.

Flow cytometry analysis of reporter assay

For all experiments in K562 cells, lentiviral fluorescent reporters and MTCH2 rescue constructs were co-transduced by spinfection as described above and analyzed 72 hours post-transduction. To probe the effect on EMC2 or MTCH1 knockdown on reporter insertion, cells were additionally transduced with sgRNA expressing lentiviral vectors 8 days prior to analysis. Samples were run on an Attune NxT Flow Cytometer (Thermo Fisher Scientific, USA) and flow cytometry data was analyzed in FlowJo v10.8 Software (BD Life Sciences, USA) or EasyFlowQ.

Western blot sample preparation

To quantify rescue protein expression levels, a portion of cells for flow cytometry analysis was harvested for western blot analysis. For whole cell samples, the cells were resuspended in solubilization buffer (50 mM HEPES/KOH pH 7.5, 200 mM NaCl, 2 mM MgAc, 1 mM DTT, 1% [w/v] DDM, 1x complete EDTA-free protease inhibitor cocktail [Roche, Germany]). After 30 min of incubation on ice, the lysate was spun for 15 min at 4˚C in a tabletop centrifuge, and the supernatant was sampled for a western blot.

For membrane fraction only samples, the cells were resuspended in digitonin lysis buffer (50 mM HEPES/KOH pH 7.5, 10 mM KAc, 2 mM MgAc, 1 mM DTT, 0.01% [w/v] digitonin, and 1x complete EDTA-free protease inhibitor cocktail). Resuspended cells were then passed 12x times through a 27G x 1-1⁄4 needle (#305136; BD Biosciences, USA) on ice. Lysed cells were then spun for 15 min at 4˚C in a tabletop centrifuge to remove cellular debris. The supernatant was aspirated, and the pellet was washed in digitonin lysis buffer with 150 mM KAc. The pellet was then resuspended in solubilization buffer and prepped as described above.

MTCH2 purification from stable suspension cell lines

Stable human suspension cell lines expressing wildtype MTCH2 with an N-terminal GFP-SUMO^{Eu} under doxycycline induction were generated and grown as previously described (Guna et al., 2022). To purify a GFP tagged MTCH2, a cell line was generated expressing GFP-MTCH2 in an identical manner. MTCH2 alone or GFP-MTCH2 were purified using anti-GFP nanobody as previously described (Guna et al., 2022; Stevens et al., 2023).

Briefly, the MTCH2 cell lines were grown and induced for 24 hours with 1 µg/mL doxycycline prior to cell harvesting. Cells were harvested by centrifugation for 10 min at 3,000 xg, washed in 1xPBS, and the cell pellet was weighed. The cell pellets were resuspended in 10 mL hypotonic lysis buffer (10 mM HEPES pH 7.5, 10 mM KAc, 1.5 mM MgAc, 0.5 mM DTT, and 1x complete EDTA-free protease inhibitor cocktail) per 1 g cell pellet and incubated on ice for 10 min. The cells that swelled up were lysed in a Dounce homogenizer with 10 strokes. The NaCl concentration was adjusted to 180 mM.

Immediately after Dounce homogenization and cell membranes were pelleted by centrifugation for 10 min at 18,000 xg in an SS-34 rotor (Beckman-Coulter, USA). Supernatant was discarded and cell membranes were resuspended in membrane wash buffer (10 mM HEPES/KOH pH 7.5, 200 mM NaCl, 1.5 mM MgAc, 0.5 mM DTT) and pelleted again. The resulting pellet was resuspended at a ratio of 1 g (original cell pellet weight) to 1.6 mL solubilization buffer (50 mM HEPES/KOH pH 7.5, 200 mM NaCl, 2 mM MgAc, 1 mM DTT, 1% [w/v] DDM, 1x complete EDTA-free protease inhibitor cocktail) and incubated for 30 min at 4˚C. Lysates were cleared by centrifugation for 30 min at 4˚C at 18,000 rpm (SS-34 rotor; Beckman-Coulter, USA).

In parallel, Pierce magnetic Streptavidin beads (Thermo Fisher Scientific, USA) were equilibrated in wash buffer (solubilization buffer with 0.02175% [w/v] DDM) and then incubated with biotinylated anti-GFP nanobody, purified as previously described (Stevens et al., 2023). For the GFP-SUMO^{Eu}-MTCH2 the His_{14}–Avi–anti-GFP nanobody was utilized and for the GFP-MTCH2 the His_{14}–Avi–SUMO^{Eu}–anti-GFP nanobody was utilized (Stevens et al., 2023). Following nanobody immobilization, binding sites were blocked with free biotin for 10 min on ice. Blocked, nanobody-bound beads were then added to the cleared cell lysate for binding to detergent-solubilized GFP-tagged MTCH2 for 1 hour at 4˚C with head-over-tail mixing. The magnetic beads were collected back and washed five times with wash buffer, before resuspension in wash buffer containing SENP^{EuB} protease and incubated on ice. The GFP-SUMO^{Eu}-MTCH2 construct was resuspended with 1.2 µM SENP^{EuB} protease and incubated for 2 hours releasing a tag-less MTCH2. While the GFP-MTCH2 construct was resuspended with 0.25 µM SENP^{EuB} protease and incubated for 30 min, releasing a GFP tagged MTCH2 into solution. Eluted samples were analyzed via SDS-PAGE with Sypro Ruby stain (BioRad).

MTCH2 purified for proteoliposome reconstitution was purified from GFP-SUMO^{Eu}-MTCH2 in solubilization buffer containing 1% deoxy-BigCHAP (DBC) and wash buffer containing 0.25% DBC.

Thermal unfolding assay

1 µg of GFP-MTCH2 was mixed with 2 mM nucleotide in a final volume of 20 µL. The samples were incubated for 10 min at set constant temperatures (50-80˚C) in a thermocycler. Heated samples were then immediately spun by centrifugation at max speed for 15 min at 4˚C in a tabletop centrifuge, to pellet any unfolded and aggregated protein. The supernatant was retrieved and GFP fluorescence was recorded on a microplate reader (BioTek, USA).

Proteoliposome reconstitutions

Reconstitutions of MTCH2 into liposomes followed similar protocols to those previously described (Guna & Hegde, 2018; Guna et al., 2022; Mariappan et al., 2011). The following phospholipids were purchased from Avanti Polar Lipids: egg phosphatidyl-choline (PC), egg phosphatidyl-ethanolamine (PE), and 1,2-dioleoyl-sn-glycero-3-phosphoethanolamine-N-lissamine rhodamine B (Rh-PE). The lipids were mixed at a mass ratio of 8:1.9:0.1 PC:PE:Rh-PE, adjusted to 10 mM DTT, and dried by centrifugation under vacuum overnight. The resulting lipid film was rehydrated to a final concentration of 20 mg/mL in lipid buffer (15% glycerol, 50 mM HEPES pH 7.4) and mixed for 8 hours at 25 °C until a homogenous mixture was achieved. Rh-PE absorbance at 573 nm was used to quantify the lipid concentration after rehydration. BioBeads-SM2 (Bio-Rad, USA) were activated with methanol, washed thoroughly with distilled water, and then resuspended and stored in water in a 50% slurry. Excess water was removed from the BioBeads just before use.

For a standard 90 µL reaction, the reconstitution mix contained MTCH2 purified in DBC, 180 µg lipids, and the remaining volume made up with buffer, salts, and detergent to achieve a final concentration of 0.8% DBC, 25 mM HEPES pH 7.5, and 100 mM NaCl. The lipid:protein molar ratio used in reconstitutions was 2,000:1. The reconstitution mixture was then added to 90 µL BioBeads in a 1.5 mL Eppendorf tube and the slurry was mixed in a thermomixer for 18 hours at 4 °C. The liquid phase was separated from the BioBeads, diluted with five volumes of ice-cold water, and pelleted by centrifugation at 70,000 rpm (TLA-100.3 rotor; Beckman-Coulter, USA) for 30 min at 4˚C. The

supernatant was discarded, and the pelleted liposomes were resuspended in 18 µL of liposome resuspension buffer (50 mM HEPES pH 7.5, 100 mM KAc, 250 mM sucrose, 1 mM DTT).

Mammalian *in vitro* translation and proteoliposome insertion

In vitro translation reactions were carried out in rabbit reticulocyte lysate (RRL) with *in vitro* transcribed mRNA as described before (Sharma et al., 2010). PCR products generated from pSP64-derived plasmids contained a 5' SP6 promoter, followed by the open-reading frame, and a 3' stop codon. The 3xFLAG-OMP25-6xHis construct used here was previously described in Guna et al., 2022. Transcription reactions were carried for 1.5 hours at 37˚C and contained T1 mix (Sharma et al., 2010), SP6 polymerase (New England Biolabs, USA), RNAsin (Promega, USA), and the PCR product. The transcriptions were added directly to RRL and nascent proteins were translated for 30 min at 32˚C in the presence of radioactive ^{35}S-methionine (Revvity, USA). Nascent proteins were released from the ribosome with 1 mM puromycin. To assess for an effect of nucleotide addition on MTCH2 insertion activity, nucleotides present in the translation extract needed to be depleted by buffer exchange. Translations were buffer exchanged into RRL buffer (20 mM HEPES pH 7.5, 80 mM KAc, 2.5 mM MgAc2, 0.5 mM spermidine, 1.5 mM reduced glutathione) using a NAP-5 desalting column (Cytiva, USA). Proteoliposome insertion reactions contained 9µL buffer exchanged translation, 1 µL resuspended proteoliposomes, 1.5µL nucleotide diluted into RRL buffer, and incubated at 32°C for 0-20 minutes.

Successful post-translational insertion into proteoliposomes was monitored by a protease protection assay. Protease-accessible regions were digested by incubation with 0.25 mg/ml Proteinase K for 1 hour at 4˚C. Protease digestion reactions were quenched by the addition of 5 mM PMSF in DMSO, followed by quick transfer into boiling SDS buffer (100 mM Tris/HCl pH 8.4, 1% [w/v] SDS). The quenched reactions were diluted tenfold in IP Buffer (50 mM HEPES/KOH pH 7.5, 500 mM NaCl, 10 mM imidazole, 0.5% [v/v] Triton X-100) and incubated with NiNTA resin (QIAGEN, USA) for 1.5 hours at 4˚C for affinity purification of His-tagged protected fragments. The resin was washed three times with IP buffer and resuspended in SDS-PAGE sample buffer containing 50 mM EDTA pH 8.0 for elution of the protected fragments. Samples were analyzed by SDS-PAGE and autoradiography

Sequence analysis

MTCH2 homolog sequences were obtained by querying UniProt for sequences annotated with the PANTHER family, PTHR10780 (Mistry et al., 2021; Thomas et al., 2022). AlphaFold-predicted models were obtained from a published database (https://AlphaFold.ebi.ac.uk/) (Jumper et al., 2021). Sequence alignments were generated using MUSCLE v5 (Edgar, 2004) and the ESPript 3.0 server (https://espript.ibcp.fr, (Robert & Gouet, 2014)) was used to visualize the alignment.

4.6 Supplementary Materials

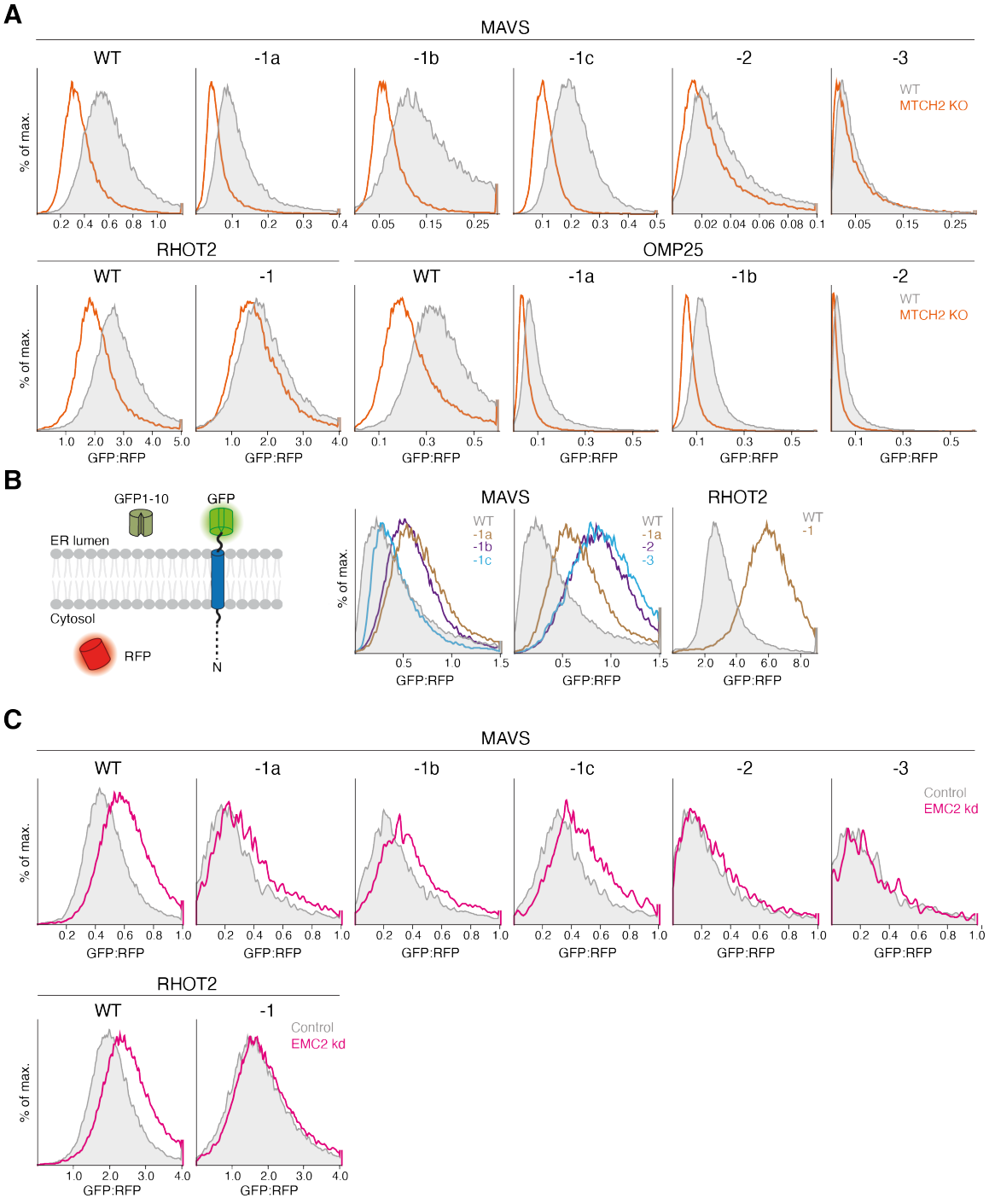

Figure S4.1. Characterizing the mitochondrial TA protein charge series' ability to insert into the mitochondria and ER.

(**A**) As in Figure 4.1C, the OMM insertion is assessed in the MTCH2 KO cells. The GFP:RFP ratio is plotted as a histogram comparing OMM insertion into WT and MTCH2 KO cells for each substrate mutant to test for MTCH2 dependence. (**B**) (Left) Schematic of the split GFP reporter system used to selectively monitor TA protein insertion into the ER. Cells are constitutively expressing GFP1-10 in the ER lumen instead of the IMS. (Right) As in Figure 4.1C but instead monitoring insertion into the ER. (**C**) As in Figure 4.1C, the OMM insertion of each substrate mutant is assessed in cells transduced with either a non-targeting (control) or EMC2 knockdown (kd) single guide RNA.

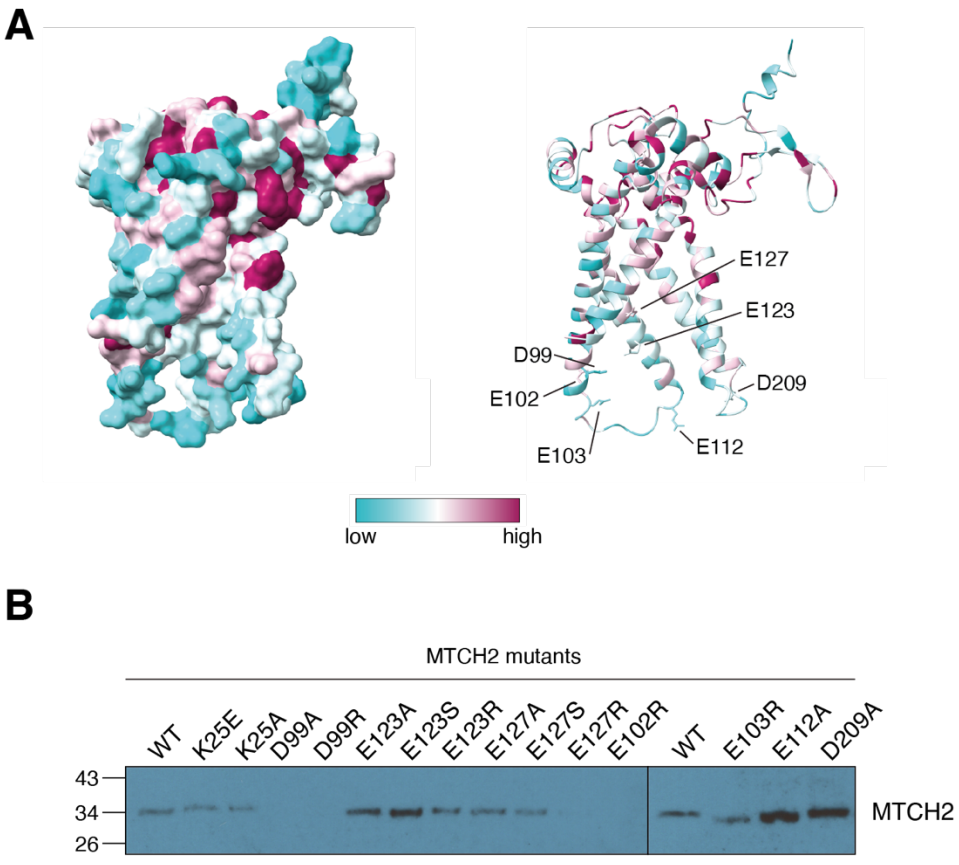

Figure S4.2. Characterization of the MTCH2 charge mutants.

(**A**) AlphaFold2 predicted model of MTCH2 colored by sequence conservation calculated from the sequence alignment shown in Figure S4.4 in ChimeraX. The model on the right highlights the negatively charged residues within the hydrophilic vestibule tested in Figure 4.2C. (**B**) Related to Figure 4.2C. The membrane fractions of MTCH2 KO cells transduced with WT or the indicated MTCH2 mutants were blotted for MTCH2 to check for their expression level.

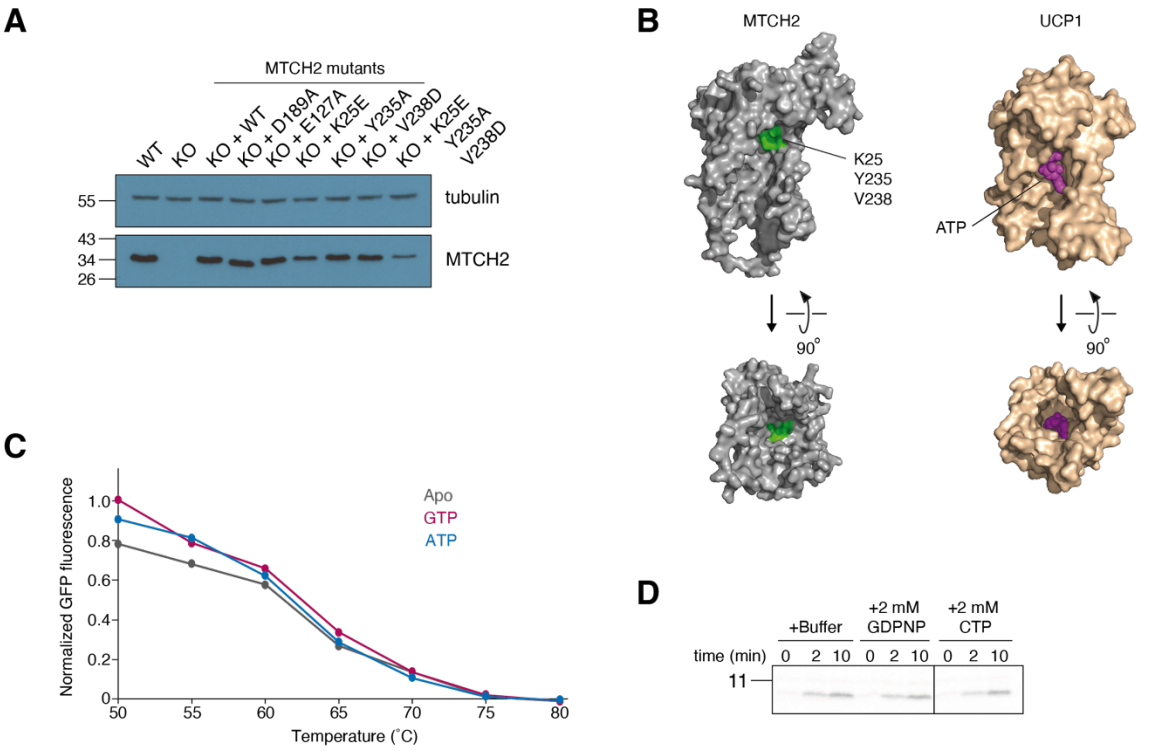

Figure S4.3. MTCH2 is not under nucleotide regulation.

(**A**) Western blot of cells from Figure 4.3C. Immunoblot of MTCH2 to check expression levels in the cell, and tubulin as a loading control. (**B**) Two views of the AlphaFold2 predicted model of MTCH2 and the ATP-bound UCP1 structure (PDB: 8HBW). In MTCH2 the three amino acids (K25, Y235, V238) which increase MTCH2 insertion activity when mutated are highlighted. In the UCP1 structure the bound ATP is colored in magenta. For clarity the nanobody and amino acids 271-307 are omitted from the UCP1 structure. On top is a side view of the two and on the bottom is a view from the cytosol towards the IMS for MTCH2, and from the IMS towards the matrix for UCP1. (**C**) As in Figure 4.3D, the normalized GFP fluorescence of the supernatant is plotted against the incubation temperature. The addition of neither ATP nor GTP increases GFP-MTCH2 thermostability at higher temperatures. (**D**) Gel quantified in Figure 4.3E. OMP25 was *in vitro* translated in the presence of ^{35}S-methionine. OMP25 was incubated with MTCH2 reconstituted proteoliposomes for 0, 2, and 10 minutes. The reactions were then treated with PK and the protease protected fragment was affinity purified. The samples were analyzed by SDS-PAGE and autoradiography.

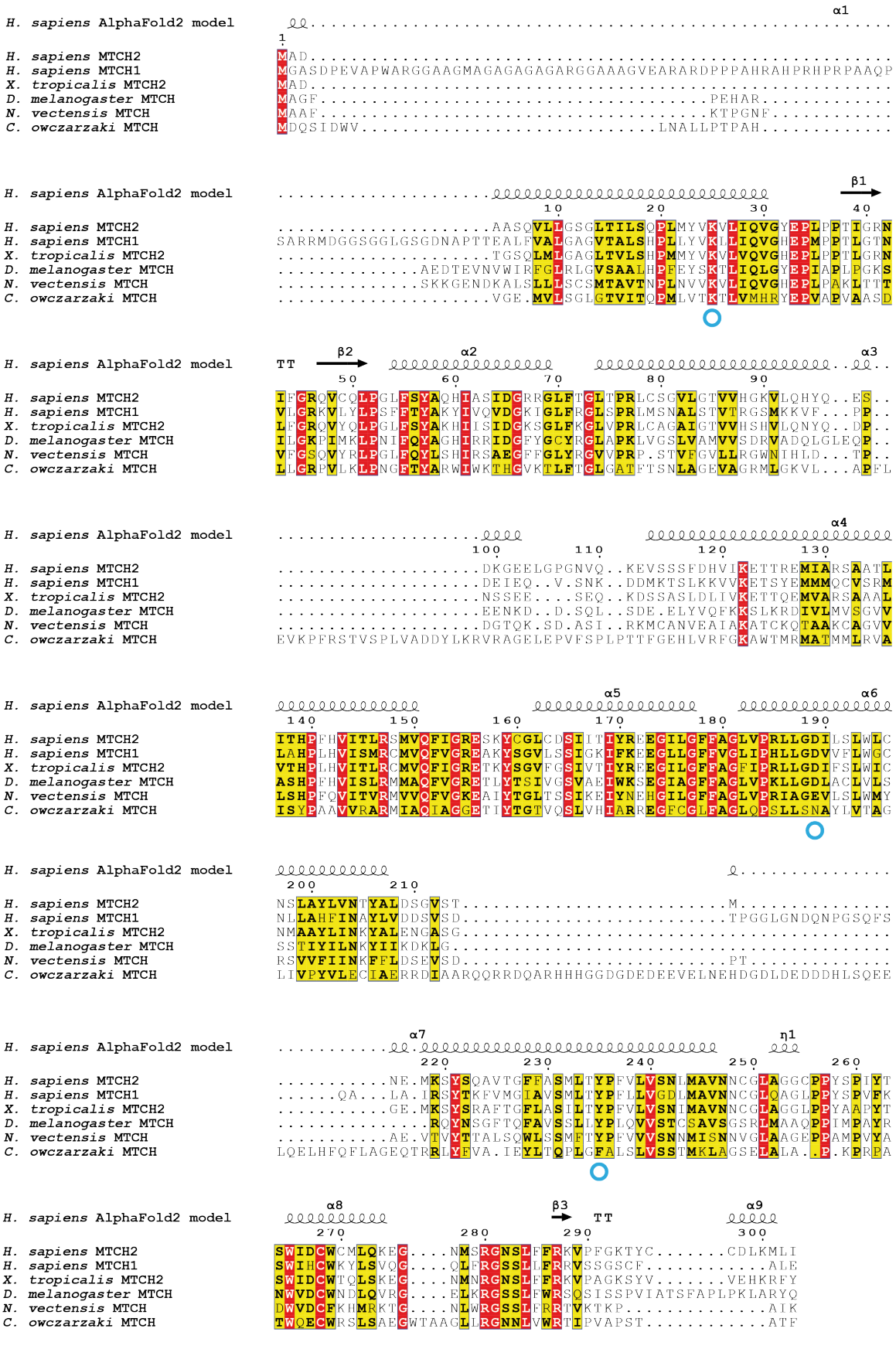
H. sapiens AlphaFold2 model
H. sapiens MTCH2
H. sapiens MTCH1
X. tropicalis MTCH2
D. melanogaster MTCH
N. vectensis MTCH
C. owczarzaki MTCH

Figure S4.4. Sequence alignment of human MTCH2 and its homologs.

Sequence alignment of MTCH2 homologs was generated in MUSCLE v5 (Edgar, 2004) and visualized using the ESPript 3.0 server (https://espript.ibcp.fr, (Robert & Gouet, 2014)). The secondary structure representation on top is based on the *H. sapiens* MTCH2 AlphaFold2 predicted model. Red columns denote 100% sequence conservation; yellow columns denote moderate conservations with similar residues bolded. The amino acid residues mutated in Figure 4.5 are indicated with a blue circle.

4.7 Acknowledgements

I would like to thank Taylor Stevens, Erini Galatis, Alina Guna, and Rebecca Voorhees for the thoughtful discussions, and their initial work that led to this study. Taylor Stevens performed the bioinformatic analysis of the MTCH2 homologs.

Chapter 5

CONCLUDING REMARKS

Research into the fundamental question of how membrane proteins are synthesized has been ongoing for decades, with significant progress made over recent years. Initially understood as a simple, linear process for membrane insertion, the field has since expanded to reveal a much more complex and multi-faceted system involving a variety of factors and pathways. Despite this progress, our current understanding remains incomplete, and many aspects of the intricate mechanisms surrounding membrane protein biogenesis are still poorly understood. Advances in technology, particularly in functional genomics, single particle cryo-electron microscopy (cryo-EM), and cryo-electron tomography (cryo-ET), have played a crucial role in accelerating the research into these processes. These tools have allowed us to examine the diverse protein biogenesis pathways in much greater detail, shedding light on how different membrane proteins are accommodated by various insertion machineries. In the past two decades, we have gained valuable insights into the functional mechanism of the Sec61 translocon guided by the structure. More recently, within the last four years, high-resolution structures of other membrane protein biogenesis machineries in the endoplasmic reticulum (ER) including the ER membrane protein complex (EMC), the multi-pass translocon (MPT), and the holo-insertase complex, and in the mitochondria including the TOM, SAM, and TIM23 complexes, have been solved. These structural advances have not only deepened our understanding of how membrane proteins are synthesized and inserted into membranes but have also raised new questions that remain to be answered. The rapid development of functional genomics tools, such as genetic CRISPR screens, have led to key discoveries of novel factors in recent years. These include the discovery of MTCH2 as an essential outer mitochondrial membrane (OMM) insertase and the BOS complex as a critical player in both the MPT and the holo-insertase complex. These findings underscore that our understanding of membrane protein biogenesis is still evolving, and we continue to identify new factors involved in the process.

Ultimately, the goal of this field is to achieve a comprehensive understanding of the entire process by which membrane proteins are synthesized and mature into their final, functional state. To fully decipher the molecular logic behind membrane protein biogenesis at each cellular membrane, it is essential to conduct detailed mechanistic studies. This will enable us to understand how the membrane proteome is established and maintained across all cellular membranes, shedding light on the

fundamental processes that govern cell function and organization. This thesis aimed to answer questions surrounding how membrane proteins are integrated to different cellular compartments and the molecular basis for the accurate sorting.

The main question, which my thesis work addressed, is delineating and understanding the mechanistic details of membrane protein biogenesis at the molecular level. Building on prior knowledge that the EMC, a novel insertase described within the last 10 years, is required for the biogenesis of several classes of membrane proteins, my work aimed to understand the molecular details of membrane protein biogenesis by the EMC. Several aspects of the EMC insertase function remained elusive: How is the post-translational TA protein targeted to the EMC handed over to the EMC? How does the EMC insert these TA proteins? And does the EMC confer any selection pressure to contribute accurate sorting of these TA proteins?

To address these questions, we leveraged our improved structure of the EMC and through site-specific crosslinking and structure-guided mutational analysis mapped the pathway of a TA protein through the EMC. Starting with the capture of the TA protein by hydrophobic loops of the EMC in the cytosol located right underneath the intramembrane hydrophilic vestibule, which we definitively identified as the insertase competent surface. We probed the effect of mutations to the EMC on the insertion of both ER and mitochondrial TA proteins, through systematic analysis of insertion assays *in vitro* and in cells. We identified positively charged residues at the entrance to the hydrophilic vestibule which uses charge repulsion to function as a selectivity filter against TAs with positively charged C-termini, such as mitochondrial TA proteins. Furthermore, in addition to TA proteins, the EMC also co-translationally inserts the first TMD of N_{exo} (N-terminus in the ER lumen) multi-pass membrane proteins, which are enriched with negative charges. Finally, we found that the EMC's selectivity filter also ensures the soluble domain of multi-pass membrane proteins with positively charged N-termini to be retained in the cytosol and adopt the correct topology. The selectivity filter at the EMC provides a biochemical basis for EMC's role in limiting TA protein mislocalisation and preventing topological errors of multi-pass membrane proteins. The EMC protects compartment integrity by enforcing the accurate sorting of TA proteins between the ER and outer mitochondrial membrane, and enforcing the 'positive-inside' rule, to limit protein misinsertion at the ER.

This work showed that the EMC imposes specificity at the ER membrane, but this is only a single aspect of the multi-faceted approach to regulating sorting specificity. It is believed that cells regulate overall fidelity of protein localization through a combination of processes including selectivity of the chaperone binding in the cytosol for correct targeting, selectivity at the insertion step (this thesis

work), and extraction of mislocalized proteins. More mechanistic studies need to be performed to define how selectivity is achieved in these other processes.

In addition to studying the molecular details of membrane protein biogenesis at the ER, my thesis work aimed to further our understanding of the biogenesis of membrane proteins at the OMM. I focused on dissecting MTCH2 as a recently identified novel OMM insertase for α-helical membrane proteins in humans. The primary objective of this work was to develop an understanding of how MTCH2 inserts TA proteins into the OMM and whether MTCH2 confers selectivity at the membrane like the EMC. We developed a set of tools to study the biogenesis of α-helical membrane proteins in the OMM of mammalian cells and used them to probe MTCH2's insertion activity. Through this work I showed that the mitochondria are highly selective for TA proteins with positively charged C-termini and specifically prefer a positive charge right after the transmembrane domain (TMD). Utilizing the AlphaFold-predicted model of MTCH2, I performed structure-based mutagenesis to see if a selectivity filter in MTCH2 existed. While I could not identify a molecular basis for selectivity, instead the possibility of MTCH2 being regulated arose from these studies. It was hypothesized that MTCH2 could have evolved from a member of the SLC25 family and retained its ability to be regulated. MTCH2 was tested for nucleotide regulation but failed to show any regulatory effect in the presence or absence of nucleotide. The evolution of MTCH2 is particularly interesting as OMM insertases in other organisms are functional paralogs that do not share any sequence or structural homology. MTCH2 homologs were identified throughout metazoans and closely related holozoan protists, and we demonstrated that they could function as an OMM insertase in human cells. Mutational analysis of the homologs also revealed that they too may be similarly regulated as human MTCH2.

This will be the basis of ongoing work on understanding the molecular mechanism of MTCH2 insertase activity, as it provides insight towards long-standing questions while opening more. How do OMM insertase carry out their function? Are OMM insertases under strict regulation, and if so what and why are they regulated? Could we target the regulation to manipulate OMM proteostasis? Future work investigating the mechanistic detail of MTCH2 insertion activity will answer these questions and help us better understand membrane protein homeostasis at the OMM.

BIBLIOGRAPHY

Abe, Y., Shodai, T., Muto, T., Mihara, K., Torii, H., Nishikawa, S., Endo, T., & Kohda, D. (2000). Structural Basis of Presequence Recognition by the Mitochondrial Protein Import Receptor Tom20. Cell, 100(5), 551–560. https://doi.org/10.1016/S0092-8674(00)80691-1

Ai, H., Shen, W., Sagi, A., Chen, P. R., & Schultz, P. G. (2011). Probing Protein–Protein Interactions with a Genetically Encoded Photo-crosslinking Amino Acid. ChemBioChem, 12(12), 1854–1857. https://doi.org/10.1002/cbic.201100194

Akopian, D., Shen, K., Zhang, X., & Shan, S. (2013). Signal Recognition Particle: An Essential Protein-Targeting Machine. Annual Review of Biochemistry, 82(Volume 82, 2013), 693–721. https://doi.org/10.1146/annurev-biochem-072711-164732

Anderson, S., Bankier, A. T., Barrell, B. G., de Bruijn, M. H. L., Coulson, A. R., Drouin, J., Eperon, I. C., Nierlich, D. P., Roe, B. A., Sanger, F., Schreier, P. H., Smith, A. J. H., Staden, R., & Young, I. G. (1981). Sequence and organization of the human mitochondrial genome. Nature, 290(5806), Article 5806. https://doi.org/10.1038/290457a0

Anghel, S. A., McGilvray, P. T., Hegde, R. S., & Keenan, R. J. (2017). Identification of Oxa1 Homologs Operating in the Eukaryotic Endoplasmic Reticulum. Cell Reports, 21(13), 3708–3716. https://doi.org/10.1016/j.celrep.2017.12.006

Bahat, A., Goldman, A., Zaltsman, Y., Khan, D. H., Halperin, C., Amzallag, E., Krupalnik, V., Mullokandov, M., Silberman, A., Erez, A., Schimmer, A. D., Hanna, J. H., & Gross, A. (2018). MTCH2-mediated mitochondrial fusion drives exit from naïve pluripotency in embryonic stem cells. Nature Communications, 9(1), 5132. https://doi.org/10.1038/s41467-018-07519-w

Bai, L., You, Q., Feng, X., Kovach, A., & Li, H. (2020). Structure of the ER membrane complex, a transmembrane-domain insertase. Nature, 584(7821), 475–478. https://doi.org/10.1038/s41586-020-2389-3

Bauer, F., Elbers, C. C., Adan, R. A., Loos, R. J., Onland-Moret, N. C., Grobbee, D. E., van Vliet-Ostaptchouk, J. V., Wijmenga, C., & van der Schouw, Y. T. (2009). Obesity genes identified in genome-wide association studies are associated with adiposity measures and potentially with nutrient-specific food preference2. The American Journal of Clinical Nutrition, 90(4), 951–959. https://doi.org/10.3945/ajcn.2009.27781

Becker, T., Pfannschmidt, S., Guiard, B., Stojanovski, D., Milenkovic, D., Kutik, S., Pfanner, N., Meisinger, C., & Wiedemann, N. (2008). Biogenesis of the Mitochondrial TOM Complex: Mim1 PROMOTES INSERTION AND ASSEMBLY OF SIGNAL-ANCHORED RECEPTORS *. Journal of Biological Chemistry, 283(1), 120–127. https://doi.org/10.1074/jbc.M706997200

Becker, T., Song, J., & Pfanner, N. (2019). Versatility of Preprotein Transfer from the Cytosol to Mitochondria. Trends in Cell Biology, 29(7), 534–548. https://doi.org/10.1016/j.tcb.2019.03.007

Becker, T., Wenz, L.-S., Krüger, V., Lehmann, W., Müller, J. M., Goroncy, L., Zufall, N., Lithgow, T., Guiard, B., Chacinska, A., Wagner, R., Meisinger, C., & Pfanner, N. (2011). The mitochondrial import protein Mim1 promotes biogenesis of multispanning outer membrane proteins. Journal of Cell Biology, 194(3), 387–395. https://doi.org/10.1083/jcb.201102044

Beilharz, T., Egan, B., Silver, P. A., Hofmann, K., & Lithgow, T. (2003). Bipartite Signals Mediate Subcellular Targeting of Tail-anchored Membrane Proteins in Saccharomyces cerevisiae *. Journal of Biological Chemistry, 278(10), 8219–8223. https://doi.org/10.1074/jbc.M212725200

Berg, B. van den, Clemons, W. M., Collinson, I., Modis, Y., Hartmann, E., Harrison, S. C., & Rapoport, T. A. (2004). X-ray structure of a protein-conducting channel. Nature, 427(6969), 36–44. https://doi.org/10.1038/nature02218

Bernhard, F., Landgraf, K., Klöting, N., Berthold, A., Büttner, P., Friebe, D., Kiess, W., Kovacs, P., Blüher, M., & Körner, A. (2013). Functional relevance of genes implicated by obesity genome-wide association study signals for human adipocyte biology. Diabetologia, 56(2), 311–322. https://doi.org/10.1007/s00125-012-2773-0

Bircham, P. W., Maass, D. R., Roberts, C. A., Kiew, P. Y., Low, Y. S., Yegambaram, M., Matthews, J., Jack, C. A., & Atkinson, P. H. (2011). Secretory pathway genes assessed by high-throughput microscopy and synthetic genetic array analysis. Molecular BioSystems, 7(9), 2589–2598. https://doi.org/10.1039/C1MB05175J

Bohnert, M., Rehling, P., Guiard, B., Herrmann, J. M., Pfanner, N., & Laan, M. van der. (2010). Cooperation of Stop-Transfer and Conservative Sorting Mechanisms in Mitochondrial Protein Transport. Current Biology, 20(13), 1227–1232. https://doi.org/10.1016/j.cub.2010.05.058

Borgese, N., Brambillasca, S., & Colombo, S. (2007). How tails guide tail-anchored proteins to their destinations. Current Opinion in Cell Biology, 19(4), 368–375. https://doi.org/10.1016/j.ceb.2007.04.019

Borgese, N., & Fasana, E. (2011). Targeting pathways of C-tail-anchored proteins. Biochimica et Biophysica Acta (BBA) - Biomembranes, 1808(3), 937–946. https://doi.org/10.1016/j.bbamem.2010.07.010

Borowska, M. T., Dominik, P. K., Anghel, S. A., Kossiakoff, A. A., & Keenan, R. J. (2015). A YidC-like Protein in the Archaeal Plasma Membrane. Structure, 23(9), 1715–1724. https://doi.org/10.1016/j.str.2015.06.025

Boyd, D., Schierle, C., & Beckwith, J. (1998). How many membrane proteins are there? Protein Science, 7(1), 201–205. https://doi.org/10.1002/pro.5560070121

Bruggisser, J., Käser, S., Mani, J., & Schneider, A. (2017). Biogenesis of a Mitochondrial Outer Membrane Protein in Trypanosoma brucei: TARGETING SIGNAL AND DEPENDENCE ON A UNIQUE BIOGENESIS FACTOR *. Journal of Biological Chemistry, 292(8), 3400–3410. https://doi.org/10.1074/jbc.M116.755983

Busch, J. D., Fielden, L. F., Pfanner, N., & Wiedemann, N. (2023). Mitochondrial protein transport: Versatility of translocases and mechanisms. Molecular Cell, 83(6), 890–910. https://doi.org/10.1016/j.molcel.2023.02.020

Buzaglo-Azriel, L., Kuperman, Y., Tsoory, M., Zaltsman, Y., Shachnai, L., Zaidman, S. L., Bassat, E., Michailovici, I., Sarver, A., Tzahor, E., Haran, M., Vernochet, C., & Gross, A. (2016). Loss of Muscle MTCH2 Increases Whole-Body Energy Utilization and Protects from Diet-Induced Obesity. Cell Reports, 14(7), 1602–1610. https://doi.org/10.1016/j.celrep.2016.01.046

Cabantous, S., Terwilliger, T. C., & Waldo, G. S. (2005). Protein tagging and detection with engineered self-assembling fragments of green fluorescent protein. Nature Biotechnology, 23(1), 102–107. https://doi.org/10.1038/nbt1044

Casañal, A., Lohkamp, B., & Emsley, P. (2020). Current developments in Coot for macromolecular model building of Electron Cryo-microscopy and Crystallographic Data. Protein Science, 29(4), 1055–1064. https://doi.org/10.1002/pro.3791

Chakrabarti, O., & Hegde, R. S. (2009). Functional Depletion of Mahogunin by Cytosolically Exposed Prion Protein Contributes to Neurodegeneration. Cell, 137(6), 1136–1147. https://doi.org/10.1016/j.cell.2009.03.042

Chen, Y., Umanah, G. K. E., Dephoure, N., Andrabi, S. A., Gygi, S. P., Dawson, T. M., Dawson, V. L., & Rutter, J. (2014). Msp1/ATAD1 maintains mitochondrial function by facilitating the degradation of mislocalized tail-anchored proteins. The EMBO Journal, 33(14), 1548–1564. https://doi.org/10.15252/embj.201487943

Chio, U. S., Cho, H., & Shan, S. (2017). Mechanisms of Tail-Anchored Membrane Protein Targeting and Insertion. Annual Review of Cell and Developmental Biology, 33(Volume 33, 2017), 417–438. https://doi.org/10.1146/annurev-cellbio-100616-060839

Chitwood, P. J., & Hegde, R. S. (2019). The Role of EMC during Membrane Protein Biogenesis. Trends in Cell Biology, 29(5), 371–384. https://doi.org/10.1016/j.tcb.2019.01.007

Chitwood, P. J., Juszkiewicz, S., Guna, A., Shao, S., & Hegde, R. S. (2018). EMC Is Required to Initiate Accurate Membrane Protein Topogenesis. Cell, 175(6), 1507-1519.e16. https://doi.org/10.1016/j.cell.2018.10.009

Christianson, J. C., Olzmann, J. A., Shaler, T. A., Sowa, M. E., Bennett, E. J., Richter, C. M., Tyler, R. E., Greenblatt, E. J., Wade Harper, J., & Kopito, R. R. (2012). Defining human ERAD networks through an integrative mapping strategy. Nature Cell Biology, 14(1), 93–105. https://doi.org/10.1038/ncb2383

Connolly, T., & Gilmore, R. (1993). GTP hydrolysis by complexes of the signal recognition particle and the signal recognition particle receptor. Journal of Cell Biology, 123(4), 799–807. https://doi.org/10.1083/jcb.123.4.799

Cory, S., & Adams, J. M. (2002). The Bcl2 family: Regulators of the cellular life-or-death switch. Nature Reviews Cancer, 2(9), 647–656. https://doi.org/10.1038/nrc883

Costello, J. L., Castro, I. G., Camões, F., Schrader, T. A., McNeall, D., Yang, J., Giannopoulou, E.-A., Gomes, S., Pogenberg, V., Bonekamp, N. A., Ribeiro, D., Wilmanns, M., Jedd, G., Islinger, M., & Schrader, M. (2017). Predicting the targeting of tail-anchored proteins to subcellular compartments in mammalian cells. Journal of Cell Science, 130(9), 1675–1687. https://doi.org/10.1242/jcs.200204

Cymer, F., von Heijne, G., & White, S. H. (2015). Mechanisms of Integral Membrane Protein Insertion and Folding. Journal of Molecular Biology, 427(5), 999–1022. https://doi.org/10.1016/j.jmb.2014.09.014

de Felipe, P., Luke, G. A., Hughes, L. E., Gani, D., Halpin, C., & Ryan, M. D. (2006). E unum pluribus: Multiple proteins from a self-processing polyprotein. Trends in Biotechnology, 24(2), 68–75. https://doi.org/10.1016/j.tibtech.2005.12.006

Diekert, K., Kispal, G., Guiard, B., & Lill, R. (1999). An internal targeting signal directing proteins into the mitochondrial intermembrane space. Proceedings of the National Academy of Sciences, 96(21), 11752–11757. https://doi.org/10.1073/pnas.96.21.11752

Dinur-Mills, M., Tal, M., & Pines, O. (2008). Dual Targeted Mitochondrial Proteins Are Characterized by Lower MTS Parameters and Total Net Charge. PLOS ONE, 3(5), e2161. https://doi.org/10.1371/journal.pone.0002161

Doan, K. N., Grevel, A., Mårtensson, C. U., Ellenrieder, L., Thornton, N., Wenz, L.-S., Opaliński, Ł., Guiard, B., Pfanner, N., & Becker, T. (2020). The Mitochondrial Import Complex MIM Functions as Main Translocase for α-Helical Outer Membrane Proteins. Cell Reports, 31(4), 107567. https://doi.org/10.1016/j.celrep.2020.107567

Dobson, L., Reményi, I., & Tusnády, G. E. (2015). The human transmembrane proteome. Biology Direct, 10(1), 31. https://doi.org/10.1186/s13062-015-0061-x

Dukanovic, J., & Rapaport, D. (2011). Multiple pathways in the integration of proteins into the mitochondrial outer membrane. Biochimica et Biophysica Acta (BBA) - Biomembranes, 1808(3), 971–980. https://doi.org/10.1016/j.bbamem.2010.06.021

Edgar, R. C. (2004). MUSCLE: Multiple sequence alignment with high accuracy and high throughput. Nucleic Acids Research, 32(5), 1792–1797. https://doi.org/10.1093/nar/gkh340

Elsässer, S. J., Ernst, R. J., Walker, O. S., & Chin, J. W. (2016). Genetic code expansion in stable cell lines enables encoded chromatin modification. Nature Methods, 13(2), 158–164. https://doi.org/10.1038/nmeth.3701

Emsley, P., Lohkamp, B., Scott, W. G., & Cowtan, K. (2010). Features and development of Coot. Acta Crystallographica Section D: Biological Crystallography, 66(4), 486–501. https://doi.org/10.1107/S0907444910007493

Enquist, K., Fransson, M., Boekel, C., Bengtsson, I., Geiger, K., Lang, L., Pettersson, A., Johansson, S., von Heijne, G., & Nilsson, I. (2009). Membrane-integration Characteristics of Two ABC Transporters, CFTR and P-glycoprotein. Journal of Molecular Biology, 387(5), 1153–1164. https://doi.org/10.1016/j.jmb.2009.02.035

Favaloro, V., Spasic, M., Schwappach, B., & Dobberstein, B. (2008). Distinct targeting pathways for the membrane insertion of tail-anchored (TA) proteins. Journal of Cell Science, 121(11), 1832–1840. https://doi.org/10.1242/jcs.020321

Feng, S., Sekine, S., Pessino, V., Li, H., Leonetti, M. D., & Huang, B. (2017). Improved split fluorescent proteins for endogenous protein labeling. Nature Communications, 8, 370. https://doi.org/10.1038/s41467-017-00494-8

Feng, S., Varshney, A., Coto Villa, D., Modavi, C., Kohler, J., Farah, F., Zhou, S., Ali, N., Müller, J. D., Van Hoven, M. K., & Huang, B. (2019). Bright split red fluorescent proteins for the visualization of endogenous proteins and synapses. Communications Biology, 2(1), Article 1. https://doi.org/10.1038/s42003-019-0589-x

Fischer, J. A., Monroe, T. O., Pesce, L. L., Sawicki, K. T., Quattrocelli, M., Bauer, R., Kearns, S. D., Wolf, M. J., Puckelwartz, M. J., & McNally, E. M. (2023). Opposing effects of genetic variation in MTCH2 for obesity versus heart failure. Human Molecular Genetics, 32(1), 15–29. https://doi.org/10.1093/hmg/ddac176

Fresenius, H. L., & Wohlever, M. L. (2021). Reconstitution of Msp1 Extraction Activity with Fully Purified Components. Journal of Visualized Experiments : JoVE, 174, 10.3791/62928. https://doi.org/10.3791/62928

Friedman, J. R., & Nunnari, J. (2014). Mitochondrial form and function. Nature, 505(7483), Article 7483. https://doi.org/10.1038/nature12985

Fry, M. Y., Saladi, S. M., Cunha, A., & Clemons Jr, W. M. (2021). Sequence-based features that are determinant for tail-anchored membrane protein sorting in eukaryotes. Traffic, 22(9), 306–318. https://doi.org/10.1111/tra.12809

Gabaldón, T., & Huynen, M. A. (2004). Shaping the mitochondrial proteome. Biochimica et Biophysica Acta (BBA) - Bioenergetics, 1659(2), 212–220. https://doi.org/10.1016/j.bbabio.2004.07.011

Gabaldón, T., & Huynen, M. A. (2007). From Endosymbiont to Host-Controlled Organelle: The Hijacking of Mitochondrial Protein Synthesis and Metabolism. PLOS Computational Biology, 3(11), e219. https://doi.org/10.1371/journal.pcbi.0030219

Geetha, T. S., Lingappa, L., Jain, A. R., Govindan, H., Mandloi, N., Murugan, S., Gupta, R., & Vedam, R. (2018). A novel splice variant in EMC1 is associated with cerebellar atrophy, visual impairment, psychomotor retardation with epilepsy. Molecular Genetics & Genomic Medicine, 6(2), 282–287. https://doi.org/10.1002/mgg3.352

Gomkale, R., Linden, A., Neumann, P., Schendzielorz, A. B., Stoldt, S., Dybkov, O., Kilisch, M., Schulz, C., Cruz-Zaragoza, L. D., Schwappach, B., Ficner, R., Jakobs, S., Urlaub, H., & Rehling, P. (2021). Mapping protein interactions in the active TOM-TIM23 supercomplex. Nature Communications, 12(1), 5715. https://doi.org/10.1038/s41467-021-26016-1

Görlich, D., & Rapoport, T. A. (1993). Protein translocation into proteoliposomes reconstituted from purified components of the endoplasmic reticulum membrane. Cell, 75(4), 615–630. https://doi.org/10.1016/0092-8674(93)90483-7

Götzke, H., Kilisch, M., Martínez-Carranza, M., Sograte-Idrissi, S., Rajavel, A., Schlichthaerle, T., Engels, N., Jungmann, R., Stenmark, P., Opazo, F., & Frey, S. (2019). The ALFA-tag is a highly versatile tool for nanobody-based bioscience applications. Nature Communications, 10(1), 4403. https://doi.org/10.1038/s41467-019-12301-7

Gray, M. W., Burger, G., & Lang, B. F. (1999). Mitochondrial Evolution. Science, 283(5407), 1476–1481. https://doi.org/10.1126/science.283.5407.1476

Grinberg, M., Schwarz, M., Zaltsman, Y., Eini, T., Niv, H., Pietrokovski, S., & Gross, A. (2005). Mitochondrial Carrier Homolog 2 Is a Target of tBID in Cells Signaled To Die by Tumor Necrosis Factor Alpha. Molecular and Cellular Biology. https://doi.org/10.1128/MCB.25.11.4579-4590.2005

Guna, A., Hazu, M., Tomaleri, G. P., & Voorhees, R. M. (2023). A TAle of Two Pathways: Tail-Anchored Protein Insertion at the Endoplasmic Reticulum. Cold Spring Harbor Perspectives in Biology, 15(3), a041252. https://doi.org/10.1101/cshperspect.a041252

Guna, A., & Hegde, R. S. (2018). Transmembrane Domain Recognition during Membrane Protein Biogenesis and Quality Control. Current Biology, 28(8), R498–R511. https://doi.org/10.1016/j.cub.2018.02.004

Guna, A., Stevens, T. A., Inglis, A. J., Replogle, J. M., Esantsi, T. K., Muthukumar, G., Shaffer, K. C. L., Wang, M. L., Pogson, A. N., Jones, J. J., Lomenick, B., Chou, T.-F., Weissman, J. S., & Voorhees, R. M. (2022). MTCH2 is a mitochondrial outer membrane protein insertase. Science, 378(6617), 317–322. https://doi.org/10.1126/science.add1856

Guna, A., Volkmar, N., Christianson, J. C., & Hegde, R. S. (2018). The ER membrane protein complex is a transmembrane domain insertase. Science, 359(6374), 470–473. https://doi.org/10.1126/science.aao3099

Halic, M., & Beckmann, R. (2005). The signal recognition particle and its interactions during protein targeting. Current Opinion in Structural Biology, 15(1), 116–125. https://doi.org/10.1016/j.sbi.2005.01.013

Harel, T., Yesil, G., Bayram, Y., Coban-Akdemir, Z., Charng, W.-L., Karaca, E., Al Asmari, A., Eldomery, M. K., Hunter, J. V., Jhangiani, S. N., Rosenfeld, J. A., Pehlivan, D., El-Hattab, A. W., Saleh, M. A., LeDuc, C. A., Muzny, D., Boerwinkle, E., Gibbs, R. A., Chung, W. K., … Lupski, J. R. (2016). Monoallelic and Biallelic Variants in EMC1 Identified in Individuals with Global Developmental Delay, Hypotonia, Scoliosis, and Cerebellar Atrophy. The American Journal of Human Genetics, 98(3), 562–570. https://doi.org/10.1016/j.ajhg.2016.01.011

Hartmann, E., Rapoport, T. A., & Lodish, H. F. (1989). Predicting the orientation of eukaryotic membrane-spanning proteins. Proceedings of the National Academy of Sciences, 86(15), 5786–5790. https://doi.org/10.1073/pnas.86.15.5786

Hegde, R. S., & Keenan, R. J. (2011). Tail-anchored membrane protein insertion into the endoplasmic reticulum. Nature Reviews Molecular Cell Biology, 12(12), 787–798. https://doi.org/10.1038/nrm3226

Hegde, R. S., & Keenan, R. J. (2022). The mechanisms of integral membrane protein biogenesis. Nature Reviews Molecular Cell Biology, 23(2), 107–124. https://doi.org/10.1038/s41580-021-00413-2

Hegde, R. S., & Ploegh, H. L. (2010). Quality and quantity control at the endoplasmic reticulum. Current Opinion in Cell Biology, 22(4), 437–446. https://doi.org/10.1016/j.ceb.2010.05.005

Höhr, A. I. C., Straub, S. P., Warscheid, B., Becker, T., & Wiedemann, N. (2015). Assembly of β-barrel proteins in the mitochondrial outer membrane. Biochimica et Biophysica Acta (BBA) - Molecular Cell Research, 1853(1), 74–88. https://doi.org/10.1016/j.bbamcr.2014.10.006

Horie, C., Suzuki, H., Sakaguchi, M., & Mihara, K. (2002). Characterization of Signal That Directs C-Tail–anchored Proteins to Mammalian Mitochondrial Outer Membrane. Molecular Biology of the Cell, 13(5), 1615–1625. https://doi.org/10.1091/mbc.01-12-0570

Horlbeck, M. A., Gilbert, L. A., Villalta, J. E., Adamson, B., Pak, R. A., Chen, Y., Fields, A. P., Park, C. Y., Corn, J. E., Kampmann, M., & Weissman, J. S. (2016). Compact and highly active next-generation libraries for CRISPR-mediated gene repression and activation. eLife, 5, e19760. https://doi.org/10.7554/eLife.19760

Hung, V., Zou, P., Rhee, H.-W., Udeshi, N. D., Cracan, V., Svinkina, T., Carr, S. A., Mootha, V. K., & Ting, A. Y. (2014). Proteomic Mapping of the Human Mitochondrial Intermembrane Space in Live Cells via Ratiometric APEX Tagging. Molecular Cell, 55(2), 332–341. https://doi.org/10.1016/j.molcel.2014.06.003

Inglis, A. J., Page, K. R., Guna, A., & Voorhees, R. M. (2020). Differential Modes of Orphan Subunit Recognition for the WRB/CAML Complex. Cell Reports, 30(11), 3691-3698.e5. https://doi.org/10.1016/j.celrep.2020.02.084

Isenmann, S., Khew-Goodall, Y., Gamble, J., Vadas, M., & Wattenberg, B. W. (1998). A Splice-Isoform of Vesicle-associated Membrane Protein-1 (VAMP-1) Contains a Mitochondrial Targeting Signal. Molecular Biology of the Cell, 9(7), 1649–1660. https://doi.org/10.1091/mbc.9.7.1649

Jomaa, A., Gamerdinger, M., Hsieh, H.-H., Wallisch, A., Chandrasekaran, V., Ulusoy, Z., Scaiola, A., Hegde, R. S., Shan, S., Ban, N., & Deuerling, E. (2022). Mechanism of signal sequence handover from NAC to SRP on ribosomes during ER-protein targeting. Science, 375(6583), 839–844. https://doi.org/10.1126/science.abl6459

Jones, S. A., Gogoi, P., J. Ruprecht, J., S. King, M., Lee, Y., Zögg, T., Pardon, E., Chand, D., Steimle, S., M. Copeman, D., A. Cotrim, C., Steyaert, J., G. Crichton, P., Moiseenkova-Bell, V., & R. S. Kunji, E. (2023). Structural basis of purine nucleotide inhibition of human uncoupling protein 1. Science Advances. https://doi.org/10.1126/sciadv.adh4251

Jonikas, M. C., Collins, S. R., Denic, V., Oh, E., Quan, E. M., Schmid, V., Weibezahn, J., Schwappach, B., Walter, P., Weissman, J. S., & Schuldiner, M. (2009). Comprehensive Characterization of Genes Required for Protein Folding in the Endoplasmic Reticulum. Science, 323(5922), 1693–1697. https://doi.org/10.1126/science.1167983

Jores, T., Klinger, A., Groß, L. E., Kawano, S., Flinner, N., Duchardt-Ferner, E., Wöhnert, J., Kalbacher, H., Endo, T., Schleiff, E., & Rapaport, D. (2016). Characterization of the targeting signal in mitochondrial β-barrel proteins. Nature Communications, 7(1), 12036. https://doi.org/10.1038/ncomms12036

Jost, M., Chen, Y., Gilbert, L. A., Horlbeck, M. A., Krenning, L., Menchon, G., Rai, A., Cho, M. Y., Stern, J. J., Prota, A. E., Kampmann, M., Akhmanova, A., Steinmetz, M. O., Tanenbaum, M. E., & Weissman, J. S. (2017). Combined CRISPRi/a-Based Chemical Genetic Screens Reveal that Rigosertib Is a Microtubule-Destabilizing Agent. Molecular Cell, 68(1), 210-223.e6. https://doi.org/10.1016/j.molcel.2017.09.012

Jumper, J., Evans, R., Pritzel, A., Green, T., Figurnov, M., Ronneberger, O., Tunyasuvunakool, K., Bates, R., Žídek, A., Potapenko, A., Bridgland, A., Meyer, C., Kohl, S. A. A., Ballard, A. J., Cowie, A., Romera-Paredes, B., Nikolov, S., Jain, R., Adler, J., … Hassabis, D. (2021). Highly accurate protein structure prediction with AlphaFold. Nature, 596(7873), 583–589. https://doi.org/10.1038/s41586-021-03819-2

Juszkiewicz, S., & Hegde, R. S. (2018). Quality Control of Orphaned Proteins. Molecular Cell, 71(3), 443–457. https://doi.org/10.1016/j.molcel.2018.07.001

Kalbfleisch, T., Cambon, A., & Wattenberg, B. W. (2007). A Bioinformatics Approach to Identifying Tail-Anchored Proteins in the Human Genome. Traffic, 8(12), 1687–1694. https://doi.org/10.1111/j.1600-0854.2007.00661.x

Kang, J., Guan, R.-C., Zhao, Y., & Chen, Y. (2020). Obesity-related loci in TMEM18, CDKAL1 and FAIM2 are associated with obesity and type 2 diabetes in Chinese Han patients. BMC Medical Genetics, 21(1), 65. https://doi.org/10.1186/s12881-020-00999-y

Kang, Y., & Chen, L. (2023). Structural basis for the binding of DNP and purine nucleotides onto UCP1. Nature, 620(7972), 226–231. https://doi.org/10.1038/s41586-023-06332-w

Keenan, R. J., Freymann, D. M., Stroud, R. M., & Walter, P. (2001). The Signal Recognition Particle. Annual Review of Biochemistry, 70(Volume 70, 2001), 755–775. https://doi.org/10.1146/annurev.biochem.70.1.755

Kirchhofer, A., Helma, J., Schmidthals, K., Frauer, C., Cui, S., Karcher, A., Pellis, M., Muyldermans, S., Casas-Delucchi, C. S., Cardoso, M. C., Leonhardt, H., Hopfner, K.-P., & Rothbauer, U. (2010). Modulation of protein properties in living cells using nanobodies. Nature Structural & Molecular Biology, 17(1), 133–138. https://doi.org/10.1038/nsmb.1727

Kohno, T., Mohan, S., Goto, T., Morita, C., Nakano, T., Hong, W., Sangco, J. C. E., Morimatsu, S., & Sano, K. (2002). A new improved method for the concentration of HIV-1 infective particles. Journal of Virological Methods, 106(2), 167–173. https://doi.org/10.1016/S0166-0934(02)00162-3

Kong, X., Xing, X., Zhang, X., Hong, J., & Yang, W. (2019). Sexual Dimorphism of a Genetic Risk Score for Obesity and Related Traits among Chinese Patients with Type 2 Diabetes. Obesity Facts, 12(3), 328–343. https://doi.org/10.1159/000500490

Krogh, A., Larsson, B., von Heijne, G., & Sonnhammer, E. L. L. (2001). Predicting transmembrane protein topology with a hidden markov model: Application to complete genomes1. Journal of Molecular Biology, 305(3), 567–580. https://doi.org/10.1006/jmbi.2000.4315

Krüger, V., Becker, T., Becker, L., Montilla-Martinez, M., Ellenrieder, L., Vögtle, F.-N., Meyer, H. E., Ryan, M. T., Wiedemann, N., Warscheid, B., Pfanner, N., Wagner, R., & Meisinger, C. (2017). Identification of new channels by systematic analysis of the mitochondrial outer membrane. Journal of Cell Biology, 216(11), 3485–3495. https://doi.org/10.1083/jcb.201706043

Kumazaki, K., Chiba, S., Takemoto, M., Furukawa, A., Nishiyama, K., Sugano, Y., Mori, T., Dohmae, N., Hirata, K., Nakada-Nakura, Y., Maturana, A. D., Tanaka, Y., Mori, H., Sugita, Y., Arisaka, F., Ito, K., Ishitani, R., Tsukazaki, T., & Nureki, O. (2014). Structural basis of Sec-independent membrane protein insertion by YidC. Nature, 509(7501), 516–520. https://doi.org/10.1038/nature13167

Kuroda, R., Ikenoue, T., Honsho, M., Tsujimoto, S., Mitoma, J., & Ito, A. (1998). Charged Amino Acids at the Carboxyl-Terminal Portions Determine the Intracellular Locations of Two Isoforms of Cytochromeb 5*. Journal of Biological Chemistry, 273(47), 31097–31102. https://doi.org/10.1074/jbc.273.47.31097

Kutay, U., Hartmann, E., & Rapoport, T. A. (1993). A class of membrane proteins with a C-terminal anchor. Trends in Cell Biology, 3(3), 72–75. https://doi.org/10.1016/0962-8924(93)90066-A

Kutik, S., Stojanovski, D., Becker, L., Becker, T., Meinecke, M., Krüger, V., Prinz, C., Meisinger, C., Guiard, B., Wagner, R., Pfanner, N., & Wiedemann, N. (2008). Dissecting membrane insertion of mitochondrial beta-barrel proteins. Cell, 132(6), 1011–1024. https://doi.org/10.1016/j.cell.2008.01.028

Labbé, K., Mookerjee, S., Le Vasseur, M., Gibbs, E., Lerner, C., & Nunnari, J. (2021). The modified mitochondrial outer membrane carrier MTCH2 links mitochondrial fusion to lipogenesis. Journal of Cell Biology, 220(11), e202103122. https://doi.org/10.1083/jcb.202103122

Lahiri, S., Chao, J. T., Tavassoli, S., Wong, A. K. O., Choudhary, V., Young, B. P., Loewen, C. J. R., & Prinz, W. A. (2014). A conserved endoplasmic reticulum membrane protein complex (EMC) facilitates phospholipid transfer from the ER to mitochondria. PLoS Biology, 12(10), e1001969. https://doi.org/10.1371/journal.pbio.1001969

Lakshminarayan, R., Phillips, B. P., Binnian, I. L., Gomez-Navarro, N., Escudero-Urquijo, N., Warren, A. J., & Miller, E. A. (2020). Pre-emptive Quality Control of a Misfolded Membrane Protein by Ribosome-Driven Effects. Current Biology, 30(5), 854-864.e5. https://doi.org/10.1016/j.cub.2019.12.060

Landgraf, K., Strobach, A., Kiess, W., & Körner, A. (2016). Loss of mtch2 function impairs early development of liver, intestine and visceral adipocytes in zebrafish larvae. FEBS Letters, 590(17), 2852–2861. https://doi.org/10.1002/1873-3468.12330

Laskowski, P. R., Pluhackova, K., Haase, M., Lang, B. M., Nagler, G., Kuhn, A., & Müller, D. J. (2021). Monitoring the binding and insertion of a single transmembrane protein by an insertase. Nature Communications, 12(1), 7082. https://doi.org/10.1038/s41467-021-27315-3

Le Vasseur, M., Friedman, J., Jost, M., Xu, J., Yamada, J., Kampmann, M., Horlbeck, M. A., Salemi, M. R., Phinney, B. S., Weissman, J. S., & Nunnari, J. (2021). Genome-wide CRISPRi screening identifies OCIAD1 as a prohibitin client and regulatory determinant of

mitochondrial Complex III assembly in human cells. eLife, 10, e67624. https://doi.org/10.7554/eLife.67624

Lee, J.-Y., & Lee, H.-H. (2018). A new chemical complex can rapidly concentrate lentivirus and significantly enhance gene transduction. Cytotechnology, 70(1), 193–201. https://doi.org/10.1007/s10616-017-0133-0

Lee, Y., Willers, C., Kunji, E. R. S., & Crichton, P. G. (2015). Uncoupling protein 1 binds one nucleotide per monomer and is stabilized by tightly bound cardiolipin. Proceedings of the National Academy of Sciences, 112(22), 6973–6978. https://doi.org/10.1073/pnas.1503833112

Liebschner, D., Afonine, P. V., Baker, M. L., Bunkóczi, G., Chen, V. B., Croll, T. I., Hintze, B., Hung, L.-W., Jain, S., McCoy, A. J., Moriarty, N. W., Oeffner, R. D., Poon, B. K., Prisant, M. G., Read, R. J., Richardson, J. S., Richardson, D. C., Sammito, M. D., Sobolev, O. V., … Adams, P. D. (2019). Macromolecular structure determination using X-rays, neutrons and electrons: Recent developments in Phenix. Acta Crystallographica Section D: Structural Biology, 75(10), 861–877. https://doi.org/10.1107/S2059798319011471

Liu, L., Spurrier, J., Butt, T. R., & Strickler, J. E. (2008). Enhanced protein expression in the baculovirus/insect cell system using engineered SUMO fusions. Protein Expression and Purification, 62(1), 21–28. https://doi.org/10.1016/j.pep.2008.07.010

Louie, R. J., Guo, J., Rodgers, J. W., White, R., Shah, N. A., Pagant, S., Kim, P., Livstone, M., Dolinski, K., McKinney, B. A., Hong, J., Sorscher, E. J., Bryan, J., Miller, E. A., & Hartman, J. L. (2012). A yeast phenomic model for the gene interaction network modulating CFTR-ΔF508 protein biogenesis. Genome Medicine, 4(12), 103. https://doi.org/10.1186/gm404

Louwers, Y. V., Rayner, N. W., Herrera, B. M., Stolk, L., Groves, C. J., Barber, T. M., Uitterlinden, A. G., Franks, S., Laven, J. S. E., & McCarthy, M. I. (2014). BMI-Associated Alleles Do Not Constitute Risk Alleles for Polycystic Ovary Syndrome Independently of BMI: A Case-Control Study. PLOS ONE, 9(1), e87335. https://doi.org/10.1371/journal.pone.0087335

Mariappan, M., Li, X., Stefanovic, S., Sharma, A., Mateja, A., Keenan, R. J., & Hegde, R. S. (2010). A ribosome-associating factor chaperones tail-anchored membrane proteins. Nature, 466(7310), 1120–1124. https://doi.org/10.1038/nature09296

Mariappan, M., Mateja, A., Dobosz, M., Bove, E., Hegde, R. S., & Keenan, R. J. (2011). The mechanism of membrane-associated steps in tail-anchored protein insertion. Nature, 477(7362), 61–66. https://doi.org/10.1038/nature10362

Marinko, J. T., Huang, H., Penn, W. D., Capra, J. A., Schlebach, J. P., & Sanders, C. R. (2019). Folding and Misfolding of Human Membrane Proteins in Health and Disease: From Single Molecules to Cellular Proteostasis. Chemical Reviews, 119(9), 5537–5606. https://doi.org/10.1021/acs.chemrev.8b00532

Maryanovich, M., Zaltsman, Y., Ruggiero, A., Goldman, A., Shachnai, L., Zaidman, S. L., Porat, Z., Golan, K., Lapidot, T., & Gross, A. (2015). An MTCH2 pathway repressing mitochondria metabolism regulates haematopoietic stem cell fate. Nature Communications, 6(1), 7901. https://doi.org/10.1038/ncomms8901

Mastronarde, D. N. (2005). Automated electron microscope tomography using robust prediction of specimen movements. Journal of Structural Biology, 152(1), 36–51. https://doi.org/10.1016/j.jsb.2005.07.007

McDowell, M. A., Heimes, M., Fiorentino, F., Mehmood, S., Farkas, Á., Coy-Vergara, J., Wu, D., Bolla, J. R., Schmid, V., Heinze, R., Wild, K., Flemming, D., Pfeffer, S., Schwappach, B., Robinson, C. V., & Sinning, I. (2020). Structural Basis of Tail-Anchored Membrane Protein Biogenesis by the GET Insertase Complex. Molecular Cell, 80(1), 72-86.e7. https://doi.org/10.1016/j.molcel.2020.08.012

McGilvray, P. T., Anghel, S. A., Sundaram, A., Zhong, F., Trnka, M. J., Fuller, J. R., Hu, H., Burlingame, A. L., & Keenan, R. J. (2020). An ER translocon for multi-pass membrane protein biogenesis. eLife, 9, e56889. https://doi.org/10.7554/eLife.56889

McKenna, M. J., Adams, B. M., Chu, V., Paulo, J. A., & Shao, S. (2022). ATP13A1 prevents ERAD of folding-competent mislocalized and misoriented proteins. Molecular Cell, 82(22), 4277-4289.e10. https://doi.org/10.1016/j.molcel.2022.09.035

McKenna, M. J., Sim, S. I., Ordureau, A., Wei, L., Harper, J. W., Shao, S., & Park, E. (2020). The endoplasmic reticulum P5A-ATPase is a transmembrane helix dislocase. Science, 369(6511), eabc5809. https://doi.org/10.1126/science.abc5809

Meusser, B., Hirsch, C., Jarosch, E., & Sommer, T. (2005). ERAD: The long road to destruction. Nature Cell Biology, 7(8), 766–772. https://doi.org/10.1038/ncb0805-766

Miller-Vedam, L. E., Bräuning, B., Popova, K. D., Schirle Oakdale, N. T., Bonnar, J. L., Prabu, J. R., Boydston, E. A., Sevillano, N., Shurtleff, M. J., Stroud, R. M., Craik, C. S., Schulman, B. A., Frost, A., & Weissman, J. S. (2020). Structural and mechanistic basis of the EMC-dependent biogenesis of distinct transmembrane clients. eLife, 9, e62611. https://doi.org/10.7554/eLife.62611

Mirdita, M., Schütze, K., Moriwaki, Y., Heo, L., Ovchinnikov, S., & Steinegger, M. (2022). ColabFold: Making protein folding accessible to all. Nature Methods, 19(6), 679–682. https://doi.org/10.1038/s41592-022-01488-1

Mistry, J., Chuguransky, S., Williams, L., Qureshi, M., Salazar, G. A., Sonnhammer, E. L. L., Tosatto, S. C. E., Paladin, L., Raj, S., Richardson, L. J., Finn, R. D., & Bateman, A. (2021). Pfam: The protein families database in 2021. Nucleic Acids Research, 49(D1), D412–D419. https://doi.org/10.1093/nar/gkaa913

Mokranjac, D., & Neupert, W. (2007). Protein Import Into Isolated Mitochondria. In D. Leister & J. M. Herrmann (Eds.), Mitochondria: Practical Protocols (pp. 277–286). Humana Press. https://doi.org/10.1007/978-1-59745-365-3_20

Morgenstern, M., Stiller, S. B., Lübbert, P., Peikert, C. D., Dannenmaier, S., Drepper, F., Weill, U., Höß, P., Feuerstein, R., Gebert, M., Bohnert, M., van der Laan, M., Schuldiner, M., Schütze, C., Oeljeklaus, S., Pfanner, N., Wiedemann, N., & Warscheid, B. (2017). Definition of a High-Confidence Mitochondrial Proteome at Quantitative Scale. Cell Reports, 19(13), 2836–2852. https://doi.org/10.1016/j.celrep.2017.06.014

Mozdy, A. D., McCaffery, J. M., & Shaw, J. M. (2000). Dnm1p Gtpase-Mediated Mitochondrial Fission Is a Multi-Step Process Requiring the Novel Integral Membrane Component Fis1p. Journal of Cell Biology, 151(2), 367–380. https://doi.org/10.1083/jcb.151.2.367

Murschall, L. M., Peker, E., MacVicar, T., Langer, T., & Riemer, J. (2021). Protein Import Assay into Mitochondria Isolated from Human Cells. Bio-Protocol, 11(12), e4057. https://doi.org/10.21769/BioProtoc.4057

Neupert, W., & Herrmann, J. M. (2007). Translocation of Proteins into Mitochondria. Annual Review of Biochemistry, 76(1), 723–749. https://doi.org/10.1146/annurev.biochem.76.052705.163409

Ng, D. P., Poulsen, B. E., & Deber, C. M. (2012). Membrane protein misassembly in disease. Biochimica et Biophysica Acta (BBA) - Biomembranes, 1818(4), 1115–1122. https://doi.org/10.1016/j.bbamem.2011.07.046

Nicolaus, F., Metola, A., Mermans, D., Liljenström, A., Krč, A., Abdullahi, S. M., Zimmer, M., Miller III, T. F., & von Heijne, G. (2021). Residue-by-residue analysis of cotranslational membrane protein integration in vivo. eLife, 10, e64302. https://doi.org/10.7554/eLife.64302

Nunnari, J., & Suomalainen, A. (2012). Mitochondria: In Sickness and in Health. Cell, 148(6), 1145–1159. https://doi.org/10.1016/j.cell.2012.02.035

O'Donnell, J. P., Phillips, B. P., Yagita, Y., Juszkiewicz, S., Wagner, A., Malinverni, D., Keenan, R. J., Miller, E. A., & Hegde, R. S. (2020). The architecture of EMC reveals a path for membrane protein insertion. eLife, 9, e57887. https://doi.org/10.7554/eLife.57887

Okreglak, V., & Walter, P. (2014). The conserved AAA-ATPase Msp1 confers organelle specificity to tail-anchored proteins. Proceedings of the National Academy of Sciences, 111(22), 8019–8024. https://doi.org/10.1073/pnas.1405755111

Ott, M., & Herrmann, J. M. (2010). Co-translational membrane insertion of mitochondrially encoded proteins. Biochimica et Biophysica Acta (BBA) - Molecular Cell Research, 1803(6), 767–775. https://doi.org/10.1016/j.bbamcr.2009.11.010

Overington, J. P., Al-Lazikani, B., & Hopkins, A. L. (2006). How many drug targets are there? Nature Reviews Drug Discovery, 5(12), 993–996. https://doi.org/10.1038/nrd2199

Page, K. R., Nguyen, V. N., Pleiner, T., Tomaleri, G. P., Wang, M. L., Guna, A., Hazu, M., Wang, T.-Y., Chou, T.-F., & Voorhees, R. M. (2024). Role of a holo-insertase complex in the biogenesis of biophysically diverse ER membrane proteins. Molecular Cell, 84(17), 3302-3319.e11. https://doi.org/10.1016/j.molcel.2024.08.005

Pagliarini, D. J., Calvo, S. E., Chang, B., Sheth, S. A., Vafai, S. B., Ong, S.-E., Walford, G. A., Sugiana, C., Boneh, A., Chen, W. K., Hill, D. E., Vidal, M., Evans, J. G., Thorburn, D. R., Carr, S. A., & Mootha, V. K. (2008). A Mitochondrial Protein Compendium Elucidates Complex I Disease Biology. Cell, 134(1), 112–123. https://doi.org/10.1016/j.cell.2008.06.016

Palmieri, F. (2013). The mitochondrial transporter family SLC25: Identification, properties and physiopathology. Molecular Aspects of Medicine, 34(2), 465–484. https://doi.org/10.1016/j.mam.2012.05.005

Park, E., & Rapoport, T. A. (2012). Mechanisms of Sec61/SecY-Mediated Protein Translocation Across Membranes. Annual Review of Biophysics, 41(Volume 41, 2012), 21–40. https://doi.org/10.1146/annurev-biophys-050511-102312

Pettersen, E. F., Goddard, T. D., Huang, C. C., Couch, G. S., Greenblatt, D. M., Meng, E. C., & Ferrin, T. E. (2004). UCSF Chimera—A visualization system for exploratory research and analysis. Journal of Computational Chemistry, 25(13), 1605–1612. https://doi.org/10.1002/jcc.20084

Pfanner, N., Warscheid, B., & Wiedemann, N. (2019). Mitochondrial proteins: From biogenesis to functional networks. Nature Reviews Molecular Cell Biology, 20(5), 267–284. https://doi.org/10.1038/s41580-018-0092-0

Pleiner, T., Bates, M., & Görlich, D. (2017). A toolbox of anti–mouse and anti–rabbit IgG secondary nanobodies. Journal of Cell Biology, 217(3), 1143–1154. https://doi.org/10.1083/jcb.201709115

Pleiner, T., Bates, M., Trakhanov, S., Lee, C.-T., Schliep, J. E., Chug, H., Böhning, M., Stark, H., Urlaub, H., & Görlich, D. (2015). Nanobodies: Site-specific labeling for super-resolution imaging, rapid epitope-mapping and native protein complex isolation. eLife, 4, e11349. https://doi.org/10.7554/eLife.11349

Pleiner, T., Hazu, M., Pinton Tomaleri, G., Nguyen, V. N., Januszyk, K., & Voorhees, R. M. (2023). A selectivity filter in the ER membrane protein complex limits protein misinsertion at the ER. The Journal of Cell Biology, 222(8), e202212007. https://doi.org/10.1083/jcb.202212007

Pleiner, T., Hazu, M., Tomaleri, G. P., Januszyk, K., Oania, R. S., Sweredoski, M. J., Moradian, A., Guna, A., & Voorhees, R. M. (2021). WNK1 is an assembly factor for the human ER membrane protein complex. Molecular Cell, 81(13), 2693-2704.e12. https://doi.org/10.1016/j.molcel.2021.04.013

Pleiner, T., Tomaleri, G. P., Januszyk, K., Inglis, A. J., Hazu, M., & Voorhees, R. M. (2020). Structural basis for membrane insertion by the human ER membrane protein complex. Science, 369(6502), 433–436. https://doi.org/10.1126/science.abb5008

Punjani, A., Rubinstein, J. L., Fleet, D. J., & Brubaker, M. A. (2017). cryoSPARC: Algorithms for rapid unsupervised cryo-EM structure determination. Nature Methods, 14(3), 290–296. https://doi.org/10.1038/nmeth.4169

Raemy, E., Montessuit, S., Pierredon, S., van Kampen, A. H., Vaz, F. M., & Martinou, J.-C. (2016). Cardiolipin or MTCH2 can serve as tBID receptors during apoptosis. Cell Death & Differentiation, 23(7), 1165–1174. https://doi.org/10.1038/cdd.2015.166

Rao, M., Okreglak, V., Chio, U. S., Cho, H., Walter, P., & Shan, S. (2016). Multiple selection filters ensure accurate tail-anchored membrane protein targeting. eLife, 5, e21301. https://doi.org/10.7554/eLife.21301

Rapoport, T. A., Li, L., & Park, E. (2017). Structural and Mechanistic Insights into Protein Translocation. Annual Review of Cell and Developmental Biology, 33(Volume 33, 2017), 369–390. https://doi.org/10.1146/annurev-cellbio-100616-060439

Rask-Andersen, M., Masuram, S., & Schiöth, H. B. (2014). The Druggable Genome: Evaluation of Drug Targets in Clinical Trials Suggests Major Shifts in Molecular Class and Indication.

Annual Review of Pharmacology and Toxicology, 54(Volume 54, 2014), 9–26. https://doi.org/10.1146/annurev-pharmtox-011613-135943

Rath, S., Sharma, R., Gupta, R., Ast, T., Chan, C., Durham, T. J., Goodman, R. P., Grabarek, Z., Haas, M. E., Hung, W. H. W., Joshi, P. R., Jourdain, A. A., Kim, S. H., Kotrys, A. V., Lam, S. S., McCoy, J. G., Meisel, J. D., Miranda, M., Panda, A., … Mootha, V. K. (2021). MitoCarta3.0: An updated mitochondrial proteome now with sub-organelle localization and pathway annotations. Nucleic Acids Research, 49(D1), D1541–D1547. https://doi.org/10.1093/nar/gkaa1011

Ravagnan, L., Roumier, T., & Kroemer, G. (2002). Mitochondria, the killer organelles and their weapons. Journal of Cellular Physiology, 192(2), 131–137. https://doi.org/10.1002/jcp.10111

Rehling, P., Model, K., Brandner, K., Kovermann, P., Sickmann, A., Meyer, H. E., Kühlbrandt, W., Wagner, R., Truscott, K. N., & Pfanner, N. (2003). Protein Insertion into the Mitochondrial Inner Membrane by a Twin-Pore Translocase. Science, 299(5613), 1747–1751. https://doi.org/10.1126/science.1080945

Richard, M., Boulin, T., Robert, V. J. P., Richmond, J. E., & Bessereau, J.-L. (2013). Biosynthesis of ionotropic acetylcholine receptors requires the evolutionarily conserved ER membrane complex. Proceedings of the National Academy of Sciences, 110(11), E1055–E1063. https://doi.org/10.1073/pnas.1216154110

Richter-Dennerlein, R., Dennerlein, S., & Rehling, P. (2015). Integrating mitochondrial translation into the cellular context. Nature Reviews Molecular Cell Biology, 16(10), 586–592. https://doi.org/10.1038/nrm4051

Richter-Dennerlein, R., Korwitz, A., Haag, M., Tatsuta, T., Dargazanli, S., Baker, M., Decker, T., Lamkemeyer, T., Rugarli, E. I., & Langer, T. (2014). DNAJC19, a Mitochondrial Cochaperone Associated with Cardiomyopathy, Forms a Complex with Prohibitins to Regulate Cardiolipin Remodeling. Cell Metabolism, 20(1), 158–171. https://doi.org/10.1016/j.cmet.2014.04.016

Robert, X., & Gouet, P. (2014). Deciphering key features in protein structures with the new ENDscript server. Nucleic Acids Research, 42(W1), W320–W324. https://doi.org/10.1093/nar/gku316

Roger, A. J., Muñoz-Gómez, S. A., & Kamikawa, R. (2017). The Origin and Diversification of Mitochondria. Current Biology, 27(21), R1177–R1192. https://doi.org/10.1016/j.cub.2017.09.015

Rottiers, V., Francisco, A., Platov, M., Zaltsman, Y., Ruggiero, A., Lee, S. S., Gross, A., & Libert, S. (2017). MTCH2 is a conserved regulator of lipid homeostasis. Obesity, 25(3), 616–625. https://doi.org/10.1002/oby.21751

Ruprecht, J. J., & Kunji, E. R. S. (2020). The SLC25 Mitochondrial Carrier Family: Structure and Mechanism. Trends in Biochemical Sciences, 45(3), 244–258. https://doi.org/10.1016/j.tibs.2019.11.001

Sanders, C. R., & Myers, J. K. (2004). Disease-Related Misassembly of Membrane Proteins. Annual Review of Biophysics, 33(Volume 33, 2004), 25–51. https://doi.org/10.1146/annurev.biophys.33.110502.140348

Saotome, M., Safiulina, D., Szabadkai, G., Das, S., Fransson, Å., Aspenstrom, P., Rizzuto, R., & Hajnóczky, G. (2008). Bidirectional Ca2+-dependent control of mitochondrial dynamics by the Miro GTPase. Proceedings of the National Academy of Sciences of the United States of America, 105(52), 20728–20733. https://doi.org/10.1073/pnas.0808953105

Satoh, T., Ohba, A., Liu, Z., Inagaki, T., & Satoh, A. K. (2015). dPob/EMC is essential for biosynthesis of rhodopsin and other multi-pass membrane proteins in Drosophila photoreceptors. eLife, 4, e06306. https://doi.org/10.7554/eLife.06306

Schmid, P. M., Heid, I., Buechler, C., Steege, A., Resch, M., Birner, C., Endemann, D. H., Riegger, G. A., & Luchner, A. (2012). Expression of fourteen novel obesity-related genes in zucker diabetic fatty rats. Cardiovascular Diabetology, 11(1), 48. https://doi.org/10.1186/1475-2840-11-48

Schuldiner, M., Collins, S. R., Thompson, N. J., Denic, V., Bhamidipati, A., Punna, T., Ihmels, J., Andrews, B., Boone, C., Greenblatt, J. F., Weissman, J. S., & Krogan, N. J. (2005). Exploration of the Function and Organization of the Yeast Early Secretory Pathway through an Epistatic Miniarray Profile. Cell, 123(3), 507–519. https://doi.org/10.1016/j.cell.2005.08.031

Schuldiner, M., Metz, J., Schmid, V., Denic, V., Rakwalska, M., Schmitt, H. D., Schwappach, B., & Weissman, J. S. (2008). The GET Complex Mediates Insertion of Tail-Anchored Proteins into the ER Membrane. Cell, 134(4), 634–645. https://doi.org/10.1016/j.cell.2008.06.025

Seth, R. B., Sun, L., Ea, C.-K., & Chen, Z. J. (2005). Identification and Characterization of MAVS, a Mitochondrial Antiviral Signaling Protein that Activates NF-κB and IRF3. Cell, 122(5), 669–682. https://doi.org/10.1016/j.cell.2005.08.012

Shan, S., & Walter, P. (2005). Co-translational protein targeting by the signal recognition particle. FEBS Letters, 579(4), 921–926. https://doi.org/10.1016/j.febslet.2004.11.049

Shao, D. D., Straussberg, R., Ahmed, H., Khan, A., Tian, S., Hill, R. S., Smith, R. S., Majmundar, A. J., Ameziane, N., Neil, J. E., Yang, E., Tenaiji, A. A., Jamuar, S. S., Schlaeger, T. M., Al-Saffar, M., Hovel, I., Al-Shamsi, A., Basel-Salmon, L., Amir, A. Z., … Walsh, C. A. (2021). A recurrent, homozygous EMC10 frameshift variant is associated with a syndrome of developmental delay with variable seizures and dysmorphic features. Genetics in Medicine, 23(6), 1158–1162. https://doi.org/10.1038/s41436-021-01097-x

Shao, S., & Hegde, R. S. (2011a). A Calmodulin-Dependent Translocation Pathway for Small Secretory Proteins. Cell, 147(7), 1576–1588. https://doi.org/10.1016/j.cell.2011.11.048

Shao, S., & Hegde, R. S. (2011b). Membrane Protein Insertion at the Endoplasmic Reticulum. Annual Review of Cell and Developmental Biology, 27(Volume 27, 2011), 25–56. https://doi.org/10.1146/annurev-cellbio-092910-154125

Shao, S., Rodrigo-Brenni, M. C., Kivlen, M. H., & Hegde, R. S. (2017). Mechanistic basis for a molecular triage reaction. Science, 355(6322), 298–302. https://doi.org/10.1126/science.aah6130

Sharma, A., Mariappan, M., Appathurai, S., & Hegde, R. S. (2010). In Vitro Dissection of Protein Translocation into the Mammalian Endoplasmic Reticulum. In A. Economou (Ed.), Protein Secretion: Methods and Protocols (pp. 339–363). Humana Press. https://doi.org/10.1007/978-1-60327-412-8_20

Shurtleff, M. J., Itzhak, D. N., Hussmann, J. A., Schirle Oakdale, N. T., Costa, E. A., Jonikas, M., Weibezahn, J., Popova, K. D., Jan, C. H., Sinitcyn, P., Vembar, S. S., Hernandez, H., Cox, J., Burlingame, A. L., Brodsky, J. L., Frost, A., Borner, G. H., & Weissman, J. S. (2018). The ER membrane protein complex interacts cotranslationally to enable biogenesis of multipass membrane proteins. eLife, 7, e37018. https://doi.org/10.7554/eLife.37018

Sievers, F., Wilm, A., Dineen, D., Gibson, T. J., Karplus, K., Li, W., Lopez, R., McWilliam, H., Remmert, M., Söding, J., Thompson, J. D., & Higgins, D. G. (2011). Fast, scalable generation of high-quality protein multiple sequence alignments using Clustal Omega. Molecular Systems Biology, 7(1), 539. https://doi.org/10.1038/msb.2011.75

Sirrenberg, C., Bauer, M. F., Guiard, B., Neupert, W., & Brunner, M. (1996). Import of carrier proteins into the mitochondrial inner membrane mediated by Tim22. Nature, 384(6609), 582–585. https://doi.org/10.1038/384582a0

Soman, R., Yuan, J., Kuhn, A., & Dalbey, R. E. (2014). Polarity and Charge of the Periplasmic Loop Determine the YidC and Sec Translocase Requirement for the M13 Procoat Lep

Protein *. Journal of Biological Chemistry, 289(2), 1023–1032. https://doi.org/10.1074/jbc.M113.522250

Sommer, M. S., & Schleiff, E. (2014). Protein Targeting and Transport as a Necessary Consequence of Increased Cellular Complexity. Cold Spring Harbor Perspectives in Biology, 6(8), a016055. https://doi.org/10.1101/cshperspect.a016055

Stefanovic, S., & Hegde, R. S. (2007). Identification of a Targeting Factor for Posttranslational Membrane Protein Insertion into the ER. Cell, 128(6), 1147–1159. https://doi.org/10.1016/j.cell.2007.01.036

Stevens, T. A., Tomaleri, G. P., Hazu, M., Wei, S., Nguyen, V. N., DeKalb, C., Voorhees, R. M., & Pleiner, T. (2023). A nanobody-based strategy for rapid and scalable purification of native human protein complexes (p. 2023.03.09.531980). bioRxiv. https://doi.org/10.1101/2023.03.09.531980

Stevens, T. A., Tomaleri, G. P., Hazu, M., Wei, S., Nguyen, V. N., DeKalb, C., Voorhees, R. M., & Pleiner, T. (2024). A nanobody-based strategy for rapid and scalable purification of human protein complexes. Nature Protocols, 19(1), 127–158. https://doi.org/10.1038/s41596-023-00904-w

Stiller, S. B., Höpker, J., Oeljeklaus, S., Schütze, C., Schrempp, S. G., Vent-Schmidt, J., Horvath, S. E., Frazier, A. E., Gebert, N., van der Laan, M., Bohnert, M., Warscheid, B., Pfanner, N., & Wiedemann, N. (2016). Mitochondrial OXA Translocase Plays a Major Role in Biogenesis of Inner-Membrane Proteins. Cell Metabolism, 23(5), 901–908. https://doi.org/10.1016/j.cmet.2016.04.005

Takeda, H., Tsutsumi, A., Nishizawa, T., Lindau, C., Busto, J. V., Wenz, L.-S., Ellenrieder, L., Imai, K., Straub, S. P., Mossmann, W., Qiu, J., Yamamori, Y., Tomii, K., Suzuki, J., Murata, T., Ogasawara, S., Nureki, O., Becker, T., Pfanner, N., … Endo, T. (2021). Mitochondrial sorting and assembly machinery operates by β-barrel switching. Nature, 590(7844), 163–169. https://doi.org/10.1038/s41586-020-03113-7

Takeuchi, F., Yamamoto, K., Katsuya, T., Nabika, T., Sugiyama, T., Fujioka, A., Isono, M., Ohnaka, K., Fujisawa, T., Nakashima, E., Ikegami, H., Nakamura, J., Yamori, Y., Yamaguchi, S., Kobayashi, S., Ogihara, T., Takayanagi, R., & Kato, N. (2011). Association of genetic variants for susceptibility to obesity with type 2 diabetes in Japanese individuals. Diabetologia, 54(6), 1350–1359. https://doi.org/10.1007/s00125-011-2086-8

Tamura, R., Jiang, F., Xie, J., & Kamiyama, D. (2021). Multiplexed labeling of cellular proteins with split fluorescent protein tags. Communications Biology, 4(1), Article 1. https://doi.org/10.1038/s42003-021-01780-4

Thomas, P. D., Ebert, D., Muruganujan, A., Mushayahama, T., Albou, L.-P., & Mi, H. (2022). PANTHER: Making genome-scale phylogenetics accessible to all. Protein Science, 31(1), 8–22. https://doi.org/10.1002/pro.4218

Timmis, J. N., Ayliffe, M. A., Huang, C. Y., & Martin, W. (2004). Endosymbiotic gene transfer: Organelle genomes forge eukaryotic chromosomes. Nature Reviews Genetics, 5(2), Article 2. https://doi.org/10.1038/nrg1271

Trueman, S. F., Mandon, E. C., & Gilmore, R. (2012). A gating motif in the translocation channel sets the hydrophobicity threshold for signal sequence function. Journal of Cell Biology, 199(6), 907–918. https://doi.org/10.1083/jcb.201207163

The UniProt Consortium. (2017). UniProt: The universal protein knowledgebase. Nucleic Acids Research, 45(D1), D158–D169. https://doi.org/10.1093/nar/gkw1099

Vera Rodriguez, A., Frey, S., & Görlich, D. (2019). Engineered SUMO/protease system identifies Pdr6 as a bidirectional nuclear transport receptor. Journal of Cell Biology, 218(6), 2006–2020. https://doi.org/10.1083/jcb.201812091

Vitali, D. G., Drwesh, L., Cichocki, B. A., Kolb, A., & Rapaport, D. (2020). The Biogenesis of Mitochondrial Outer Membrane Proteins Show Variable Dependence on Import Factors. iScience, 23(1), 100779. https://doi.org/10.1016/j.isci.2019.100779

Vitali, D. G., Käser, S., Kolb, A., Dimmer, K. S., Schneider, A., & Rapaport, D. (2018). Independent evolution of functionally exchangeable mitochondrial outer membrane import complexes. eLife, 7, e34488. https://doi.org/10.7554/eLife.34488

Vögtle, F.-N., Wortelkamp, S., Zahedi, R. P., Becker, D., Leidhold, C., Gevaert, K., Kellermann, J., Voos, W., Sickmann, A., Pfanner, N., & Meisinger, C. (2009). Global Analysis of the Mitochondrial N-Proteome Identifies a Processing Peptidase Critical for Protein Stability. Cell, 139(2), 428–439. https://doi.org/10.1016/j.cell.2009.07.045

Volkmar, N., & Christianson, J. C. (2020). Squaring the EMC – how promoting membrane protein biogenesis impacts cellular functions and organismal homeostasis. Journal of Cell Science, 133(8), jcs243519. https://doi.org/10.1242/jcs.243519

Volkmar, N., Thezenas, M.-L., Louie, S. M., Juszkiewicz, S., Nomura, D. K., Hegde, R. S., Kessler, B. M., & Christianson, J. C. (2019). The ER membrane protein complex promotes biogenesis

of sterol-related enzymes maintaining cholesterol homeostasis. Journal of Cell Science, 132(2), jcs223453. https://doi.org/10.1242/jcs.223453

von Heijne, G. (1986). The distribution of positively charged residues in bacterial inner membrane proteins correlates with the trans-membrane topology. The EMBO Journal, 5(11), 3021–3027. https://doi.org/10.1002/j.1460-2075.1986.tb04601.x

Von Heijne, G. (2007). The membrane protein universe: What's out there and why bother? Journal of Internal Medicine, 261(6), 543–557. https://doi.org/10.1111/j.1365-2796.2007.01792.x

Voorhees, R. M., Fernández, I. S., Scheres, S. H. W., & Hegde, R. S. (2014). Structure of the Mammalian Ribosome-Sec61 Complex to 3.4 Å Resolution. Cell, 157(7), 1632–1643. https://doi.org/10.1016/j.cell.2014.05.024

Wallin, E., & von Heijne, G. (1995). Properties of N-terminal tails in G-protein coupled receptors: A statistical study. Protein Engineering, Design and Selection, 8(7), 693–698. https://doi.org/10.1093/protein/8.7.693

Walter, P., & Blobel, G. (1981). Translocation of proteins across the endoplasmic reticulum III. Signal recognition protein (SRP) causes signal sequence-dependent and site-specific arrest of chain elongation that is released by microsomal membranes. Journal of Cell Biology, 91(2), 557–561. https://doi.org/10.1083/jcb.91.2.557

Walter, P., & Blobel, G. (1983). [6] Preparation of microsomal membranes for cotranslational protein translocation. In Methods in Enzymology (Vol. 96, pp. 84–93). Academic Press. https://doi.org/10.1016/S0076-6879(83)96010-X

Walter, P., Ibrahimi, I., & Blobel, G. (1981). Translocation of proteins across the endoplasmic reticulum. I. Signal recognition protein (SRP) binds to in-vitro-assembled polysomes synthesizing secretory protein. Journal of Cell Biology, 91(2), 545–550. https://doi.org/10.1083/jcb.91.2.545

Wattenberg, B., & Lithgow, T. (2001). Targeting of C-Terminal (Tail)-Anchored Proteins: Understanding how Cytoplasmic Activities are Anchored to Intracellular Membranes. Traffic, 2(1), 66–71. https://doi.org/10.1034/j.1600-0854.2001.20108.x

Weckbecker, D., & Herrmann, J. M. (2013). Methods to Study the Biogenesis of Membrane Proteins in Yeast Mitochondria. In D. Rapaport & J. M. Herrmann (Eds.), Membrane Biogenesis: Methods and Protocols (pp. 307–322). Humana Press. https://doi.org/10.1007/978-1-62703-487-6_20

White, S. H., & Wimley, W. C. (1999). MEMBRANE PROTEIN FOLDING AND STABILITY: Physical Principles. Annual Review of Biophysics, 28(Volume 28, 1999), 319–365. https://doi.org/10.1146/annurev.biophys.28.1.319

Wideman, J. G. (2015). The ubiquitous and ancient ER membrane protein complex (EMC): Tether or not? (4:624). F1000Research. https://doi.org/10.12688/f1000research.6944.2

Wu, X., Siggel, M., Ovchinnikov, S., Mi, W., Svetlov, V., Nudler, E., Liao, M., Hummer, G., & Rapoport, T. A. (2020). Structural basis of ER-associated protein degradation mediated by the Hrd1 ubiquitin ligase complex. Science, 368(6489), eaaz2449. https://doi.org/10.1126/science.aaz2449

Yanagisawa, T., Ishii, R., Fukunaga, R., Kobayashi, T., Sakamoto, K., & Yokoyama, S. (2008). Multistep Engineering of Pyrrolysyl-tRNA Synthetase to Genetically Encode Nε-(o-Azidobenzyloxycarbonyl) lysine for Site-Specific Protein Modification. Chemistry & Biology, 15(11), 1187–1197. https://doi.org/10.1016/j.chembiol.2008.10.004

Yanagitani, K., Juszkiewicz, S., & Hegde, R. S. (2017). UBE2O is a quality control factor for orphans of multiprotein complexes. Science, 357(6350), 472–475. https://doi.org/10.1126/science.aan0178

Yoon, Y., Krueger, E. W., Oswald, B. J., & McNiven, M. A. (2003). The Mitochondrial Protein hFis1 Regulates Mitochondrial Fission in Mammalian Cells through an Interaction with the Dynamin-Like Protein DLP1. Molecular and Cellular Biology, 23(15), 5409–5420. https://doi.org/10.1128/MCB.23.15.5409-5420.2003

Zaltsman, Y., Shachnai, L., Yivgi-Ohana, N., Schwarz, M., Maryanovich, M., Houtkooper, R. H., Vaz, F. M., De Leonardis, F., Fiermonte, G., Palmieri, F., Gillissen, B., Daniel, P. T., Jimenez, E., Walsh, S., Koehler, C. M., Roy, S. S., Walter, L., Hajnóczky, G., & Gross, A. (2010). MTCH2/MIMP is a major facilitator of tBID recruitment to mitochondria. Nature Cell Biology, 12(6), 553–562. https://doi.org/10.1038/ncb2057